Development of a Co-Dispersion Binder for the Three-Dimensional Printing Process to Facilitate Handling of Ceramic Casting Shells in the Green State

by

Richard Li-Chao Yu

B.S. Mechanical Engineering, 1992
University of California, Berkeley, CA

Submitted to the
Department of Mechanical Engineering
in Partial Fulfillment of the Requirements
for the Degree of

Master of Science in Mechanical Engineering

at the

Massachusetts Institute of Technology

May, 1994

Signature of Author_____
Department of Mechanical Engineering
May, 1994

Certified by_____
Emanuel M. Sachs
Associate Professor, Mechanical Engineering
Thesis Supervisor

Accepted by_____
Ain A. Sonin
Chairman, Graduate Committee

Development of a Co-Dispersion Binder for the Three Dimensional Printing Process to Facilitate Handling of Ceramic Casting Shells in the Green State

by

Richard Li-Chao Yu

Submitted to the Department of Mechanical Engineering
in partial fulfillment of the requirements for the degree of
Master of Science in Mechanical Engineering
May, 1994

Abstract

Three Dimensional Printing, a rapid prototyping technology, fabricates ceramic casting shells directly from 3-D CAD models. To create a shell, loose alumina powder in thin layers is joined by selectively depositing a colloidal silica binder. Firing fuses the silica to the alumina, and subsequent processing removes the unbound powder from the casting cavity. In some instances, it may be advantageous to perform powder removal before firing. This requires higher green strength than what is obtainable with the current binder.

An alternative binder consisting of 18 vol.% colloidal silica co-dispersed with 10 vol.% acrylic emulsion in an aqueous medium was developed. The polymeric component imparts higher green strength to the part (3.6 vs. 0.4 MPa), yet decomposes during firing to minimize interference with the fusion of silica to alumina. The reduction of fired strength in samples printed with co-dispersions was less than 10%.

Through designed experiments, performance of the co-dispersion was quantified by additional criteria such as shrinkage, warping, and binder stability. Average linear shrinkage in parts printed with co-dispersions was 0.05% after firing at 900°C. A simple model for warping, based on elastic response of a plate to free thermal strain, predicts that flat plates tend to warp into a paraboloid after firing. The experimental results correlated well with this prediction.

Thesis Supervisor: Dr. Emanuel M. Sachs
Title: Associate Professor of Mechanical Engineering

Dedication

This is for my parents Peter and Angel, my brother Leon, and my grandmother Womin. Thank you for supporting and believing in me every step of the way.

Acknowledgments

The author gratefully acknowledges the support of the National Science Foundation under the Strategic Manufacturing Initiative and the support of ARPA. The support from the members of the of the 3D Printing Consortium (United Technologies, Howmet, Johnson & Johnson, Boeing, AMP, Proctor and Gamble, Sandia National Labs, Hasbro, Ashland Chemical, and Draper Labs) is also gratefully acknowledged. The author also wishes to thank the MIT Leader for Manufacturing Program.

Ely Sachs, thank you for your guidance in the past years. You always found time in your busy schedule for my questions and problems.

Thank you, Mike Cima, for helping me stumble through that black magic known as material science. Your advice has been invaluable.

To all of the 3DP'ers past and present, thank you for creating this wonderful technology. In particular, I wish to thank:

Jain Charnnarong for the team effort on shrinkage and warping. Start working on your thesis now!

Jim Bredt for putting up with my never ending questions and for harassing me in my final hours of thesis writing.

Jim Serdy for the late night print sessions. Break a leg, Jim!

Dave Brancazio for telling everyone what not to do in the lab. Good luck with the house search, Dave.

Tim Anderson for knowing every conceivable UNIX command and program and the non-sequitur comments.

Steve Michaels for complaining about the proto machine. Live long and prosper!

Alain Curodeau and Tailin Fan for our rap session in 35-336.

Chris Shutts for the sanity checks at Flat Top Johnny's. When are you going to get that free cue?

Satbir Khanuja and Jae Yee for teaching me how to destroy every piece of equipment in Building 12.

John Lee for the 3DP figures and for being the only other guy in the lab from California. Too bad you went to Stanford.

Tom Nowak, thanks for the reality checks and the procrastination sessions.

To Jon Tom, your friendship has made Boston more bearable, but just a little bit!

My deepest thanks goes to Lauren Lao. I wouldn't have made it without your support and understanding.

Contents

List of Figures

List of Tables

Chapter 1

Three Dimensional Printing

1.1 Overview

To remain competitive in today's global community, manufacturers must constantly improve their development process by reducing time to market and increasing flexibility of manufacturing processes. A new technology that addresses these issues and aids in streamlining the product development cycle is Three Dimensional Printing (3D Printing or 3DP®).

One of a group of manufacturing processes collectively known as Rapid Prototyping, Three Dimensional Printing fabricates parts directly from computer models. A "slicing" algorithm first generates two-dimensional layers from a 3-D CAD model. To create these slices, regions in a thin layer of fine powder are selectively joined together by the deposition of a binder via a rastering ink-jet printhead. The powder bed, which rests on a moving piston, lowers so that a fresh layer of powder can be spread and printed. Sequential layers laminate to form the solid object. A heat treatment bonds and strengthens the printed regions. Subsequent processing removes the unbound powder from the fabricated part. Figure 1.1 illustrates these steps.

1.1.1 Current Applications

Three Dimensional Printing works with ceramics, metals, polymers, and biological substances. The most frequently used system is aluminum oxide powder with colloidal sil-

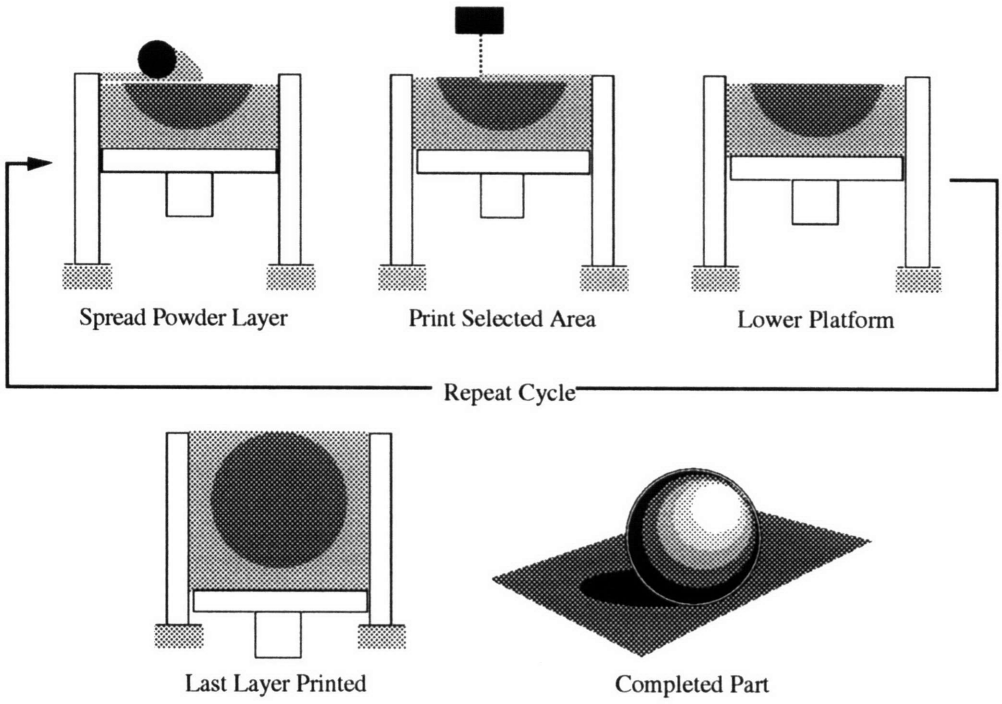

Figure 1.1: The Three Dimensional Printing Process Cycle

ica binder.

Due to its additive nature, 3D Printing can produce parts with complex curvatures, unsupported overhangs, internal features, and cross-directional voids. No specific tooling is required. The process is ideally suited for direct fabrication of metal tooling for injection molding, porous ceramic pre-forms for metal-matrix composites, and ceramic shells for metal castings. A shell made by 3D Printing and a casting from an identical shell are shown in Figure 1.2.

1.2 Green Strength

The alumina/silica material system requires high temperature firing to fuse the silica to the alumina. Before firing, only a weak network of gelled silica particles holds a part together. The green strength, defined as the modulus of rupture in this state, is on the order of 0.4 MPa. This makes unfired parts fragile and difficult to handle.

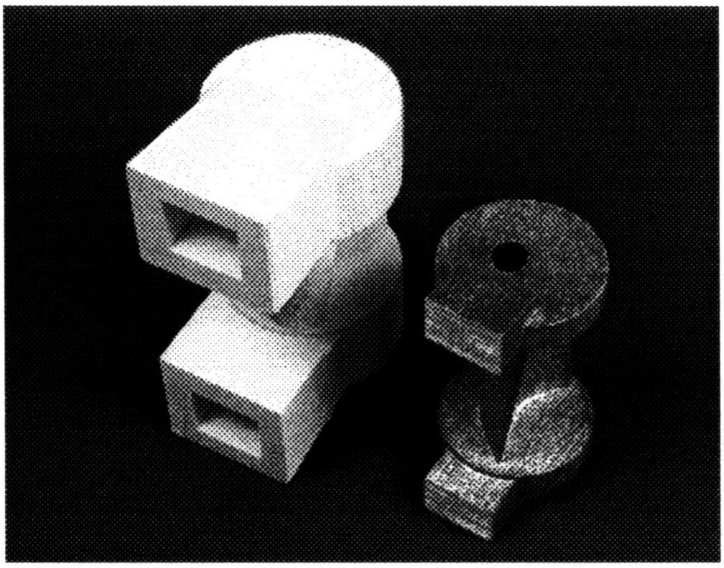

Figure 1.2: Shell produced by 3D Printing with the Resulting Casting

Low green strength complicates removal of the printed part from the powder bed and the removal of loose powder from the internal cavities. As a result, the part is fired while encased in a large amount of unprinted powder. This increases cycle time in the furnace.

Recycling of the unprinted powder is also a concern. The powder requires reprocessing after firing, adding time and cost to the process. Increasing the green strength allows removal of unprinted powder from parts before firing.

There are other applications of 3D Printing where high green strength is not only desirable, but necessary. One example is the printing of pre-forms for metal matrix composite applications, which is discussed in Appendix A.

This thesis presents the development of a binder system to achieve higher green strength in ceramic parts produced by Three Dimensional Printing.

1.3 Development Approach

Three Dimensional Printing also make metal parts using an acrylic latex emulsion binder. This latex provides good green strength, but thermally decomposes at elevated tem-

peratures. Therefore it is unsuitable as the only binder in a casting shell. The motivation for this research is to combine the low-temperature strength of latexes with the high-temperature characteristics of silica to create a new binder system.

Two possible strategies were devised. The first technique prints parts with latex and subsequently infiltrates them with colloidal silica. The second approach prints a co-dispersion of the two binders. These methods are referred to as "infiltration" and "co-dispersion".

The performance of infiltration and co-dispersion were rated by the following criteria with the current silica binder as baseline:

1. Improvement in green strength
2. Effect on fired strength
3. Stability, which means the binder will remain dispersed for a reasonable period of time.
4. Printability, which involves stability of the binder jet, binder/powder interaction, and filtration considerations.
5. Ease of powder removal
6. Dimensional control, which includes warping, drooping, and shrinkage of parts.

Chapter 2

Infiltration Studies

The ink-jet printhead used in Three Dimensional Printing works with several different binders. For example, metal tooling for injection molding are printed with Rhoplex® HA-16, tradename for a self-crosslinking acrylic polymer emulsion produced by the Rohm and Hass Company (Philadelphia, PA). Since these parts can be readily handled after drying, they must be stronger than unfired parts printed with colloidal silica. Crosslinking at 160°C imparts additional water resistance to these parts for post processing. A printing and post processing strategy was devised to utilize these properties of Rhoplex.

2.1 Process Concepts and Technique

Alumina parts can be printed with Rhoplex binder and removed from the powder bed before firing. After heating to the crosslinking temperature (160°C), the shells should be strong enough to be handled. The unprinted powder in the internal cavities can also be removed at this point.

To produce the refractory characteristics required for a metal casting shell, silica is introduced after powder removal. Dipping a dried shell into colloidal silica allows infiltration via capillary action. Firing at high temperature causes silica to soften and fuse to the alumina particles. The shell is then ready for metal pouring. A flowchart of the process is shown in Figure 2.1.

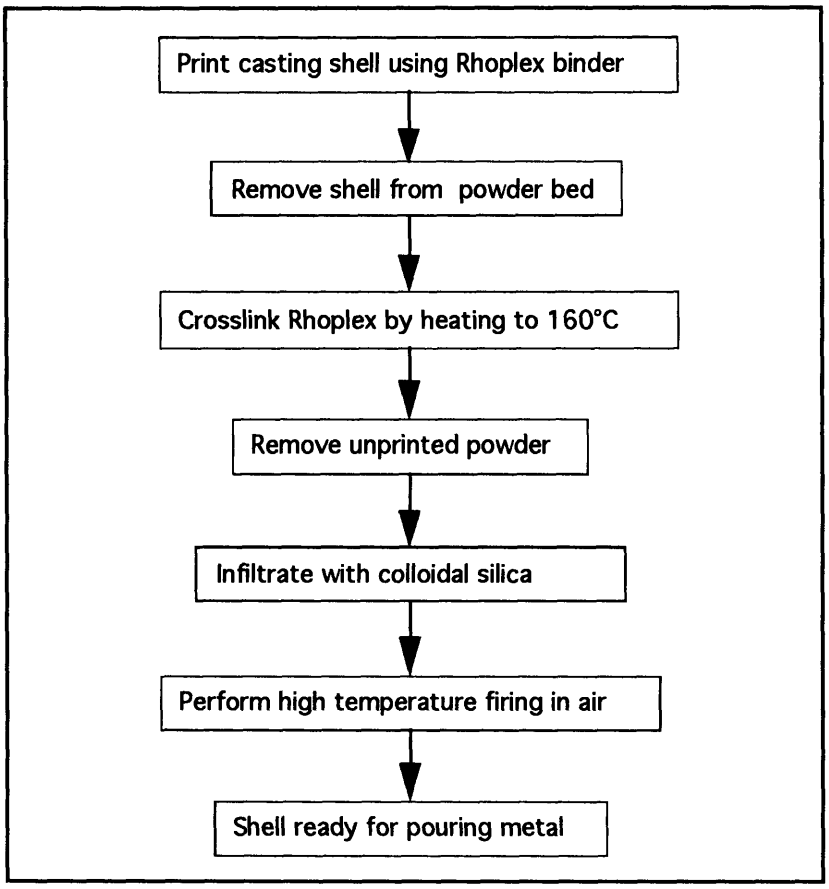

Figure 2.1: Flowchart of the steps in the Infiltration Process

After infiltration, both polymer and silica are present at the necks, or the points of contact between alumina particles. Questions remained as to the physical configuration of the necks. One hypothesis suggests an inner region of acrylic polymers surrounded by a layer of silica. A less likely possibility is a homogeneous distribution of polymer and silica particles. This can happen only if the infiltrant silica somehow dissolves and mixes with the crosslinked Rhoplex. Figure 2.2 depicts simplified schematics for both kinds of necks.

Consisting mostly of hydrocarbons, the Rhoplex polymer decomposes into CO_X gases and water vapor at temperature above 300°C. This is also referred to as burnout, and is an integral part of powder metallurgy and powder injection molding. We hoped that during the firing of an infiltrated part, Rhoplex will decompose. When the temperature passes 750°C, silica begins to soften and to fill the voids left by burnout. The shell strengthens as

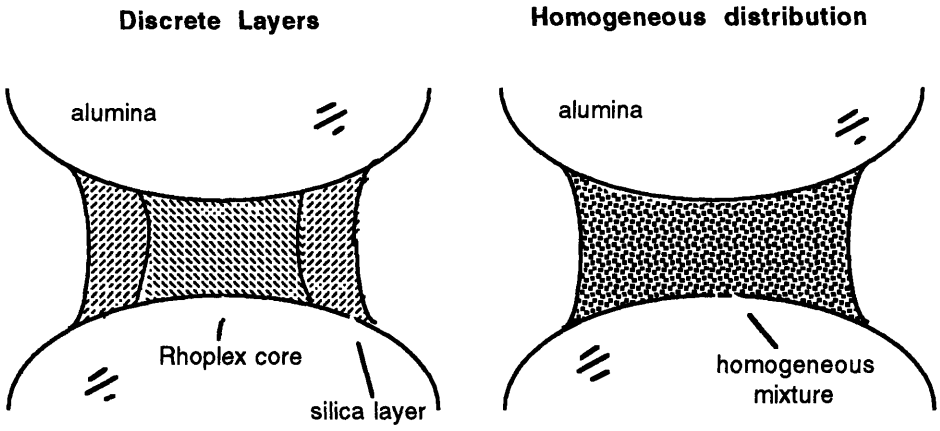

Figure 2.2: Two Possible Configurations for Necks After Infiltration.

the silica softens and fuses to the alumina particles.

2.2 Microscopic Examination

While infiltration is simple in theory, many issues remained. Burnout of the polymer might not be complete, and non-organic impurities can also be created. Impurities may affect the fusing of silica to alumina. In addition, unfilled voids in the necks may adversely affect the strength of the bond between silica and alumina. To address these issues, the necks of infiltrated parts were examined.

2.2.1 Sample Preparation

Stock Rhoplex® HA-16 contains 45.5% solids and has a viscosity of 600 centipoise. Diluting 1:1 by weight with distilled water decreases the viscosity to a point that is acceptable for 3D Printing. Experience with metal parts showed that the addition of 1% by weight (wt.%) of tetramethylammonium hydroxide ($[CH_3]_4NOH$), a base and humectant, aids in the stability of the binder stream. Samples were printed with this formulation, which is the "Standard" binder for printing metal parts.

While several type of alumina (Al_2O_3) powder have been used in 3D Printing, the

Table 2.1: Composition of the "Standard" Binder for Metal Parts

Binder Components	Proportion
stock Rhoplex HA-16	49.5 weight%
distilled water	49.5 weight%
TMAH	1.0 weight%

most common is Norton 7920 from the Norton Company (Waltham, MA). This is an electronic grade (99+% pure) powder with platelet shaped particles that are 28 μm wide on average. It is chemically produced, readily available, and relatively inexpensive. Another powder is Alunabeads CB-A30S, a spherical alumina powder produced by Showadenko (Japan) and distributed by ICD Group Inc. (Lyndhurst, NJ). This powder is not normally used in the production of shells because it is much more expensive than the 7920.

Past work showed that necks in spherical powders are more observable than those in platelet-shaped powders, since the particles only make point contact with each other. The platelet powder, on the other hand, forms irregularly shaped contact surfaces [Lauder 1992]. To facilitate locating and examining necks, the spherical powder was selected.

A file was generated to print test bars nominally 1.0" long and 0.125" by 0.125" in cross section. The bars were made on the older, or proto, 3D Printing machine using 0.007" for both line-to-line separation and layer thickness. The printhead scanned at 65 in/sec and the binder flowrate was 1.2 ml/min. These are the standard machine parameters for printing ceramic shells. Figure 2.3 below is a schematic of the proto machine.

After crosslinking at 160°C and cooling to room temperature, some of the bars were infiltrated by dipping. The infiltrant was Nyacol 9950, an aqueous silica dispersion containing 50 wt.% of 100 nm silica particles (Nyacol Products Inc., Ashland, MA). Driven by capillary forces, the dispersion wicks into the test bars and fills the pores. These samples were dried and fired at 750°C, 900°C, and 1100°C for 2 hours.

To provide a basis of comparison, similar bars were printed using the "Standard" silica binder. This binder consists of Nyacol 9950 diluted with distilled water to a specific

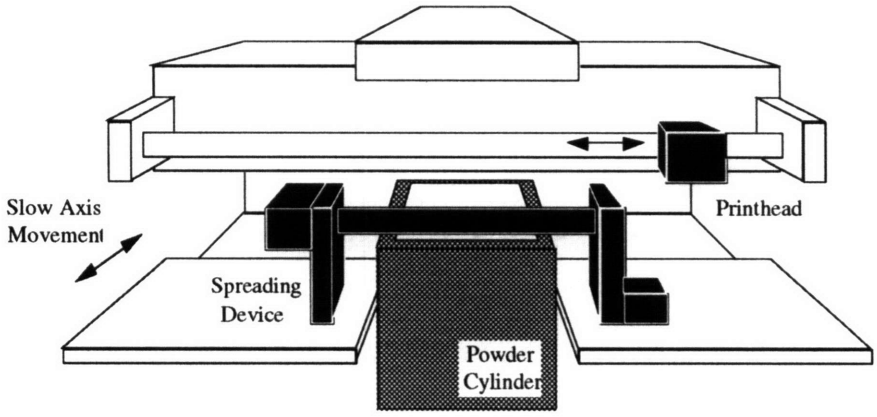

Figure 2.3: Layout of the Proto-3D Printing Machine

gravity of 1.21. Tetramethylammonium hydroxide (TMAH) is added to increase the pH of to 10, since aqueous suspensions of colloidal silica are most stable in the >pH 8.5 range [Iler 1979]. These bars were also fired at 750°C, 900°C, and 1100°C.

Breaking the bars revealed the necks in the internal regions. After mounting and gold coating, the samples were examined in a scanning electron microscope.

2.2.2 Observations

The following figures are high magnification micrographs of the observed necks. Figure 2.4 below shows typical interparticle necks formed by Rhoplex after crosslinking. They are smooth and narrow, with an average diameter of 5 μm. A higher magnification view of a neck is shown in Figure 2.5.

These micrographs indicate that necks formed by Rhoplex are solid, with no visible porosity. So it is unlikely that infiltration with silica will produce the homogeneous neck depicted in Figure 2.2, which the following micrographs confirm. The brighter areas in the infiltrated sample are silica deposits that have formed a ring around the Rhoplex (see Figure 2.6). A close-up view of a Rhoplex neck enclosed in silica is shown in Figure 2.7. The surface exhibits cracking that is typical of a dried gel. Compare the appearance of this neck to that of the pure Rhoplex.

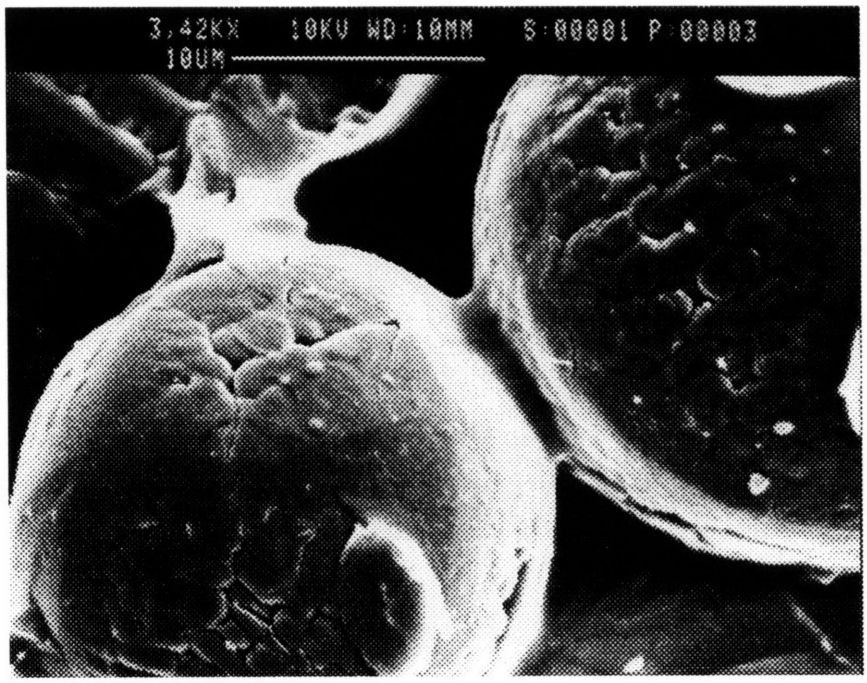

Figure 2.4: Micrograph of Necks in Crosslinked Rhoplex Test bars

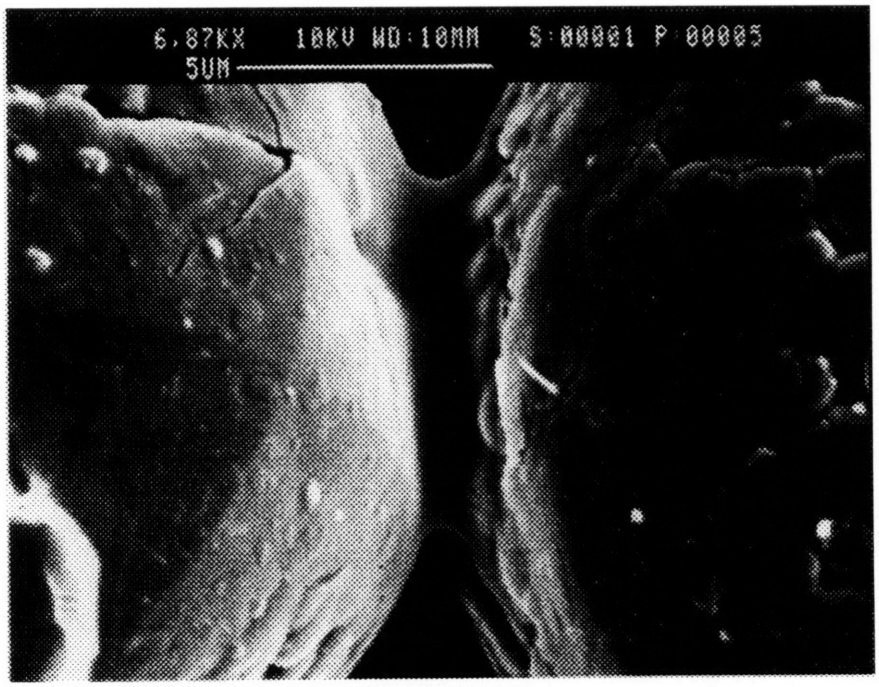

Figure 2.5: Closeup of a Crosslinked Rhoplex Neck

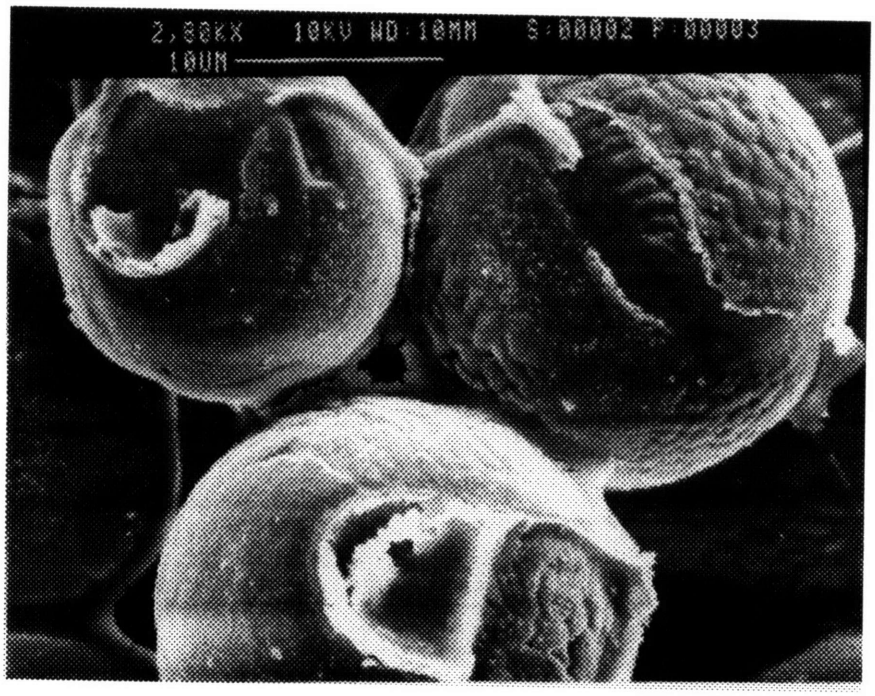

Figure 2.6: Necks printed with Rhoplex and infiltrated with Nyacol 9950 colloidal silica after drying at room temperature.

According to the hypothesis, the necks in fired bars should be filled with silica. This was not the case. While polymer did leave the necks, silica did not migrate into the resulting voids (Figure 2.8). The areas of the alumina particles that were in contact with Rhoplex are no longer wetted by silica. The silica has a contact angle greater than 90° on the alumina surface, an indicator of poor wetting. This is demonstrated by Figure 2.9, where an annulus of silica forms after firing at 750°C. The inner area of the neck, where polymer had been, appears to be bare alumina.

Compared to the infiltrated parts, the neck in a sample printed with silica look solid after firing. The silica exhibits good wetting on alumina and did not form "rings". The fracture surface of necks has no large voids. Micrographs of this sample are shown in Figure 2.10 and Figure 2.11.

Examination revealed the same trend in samples fired at higher temperatures.

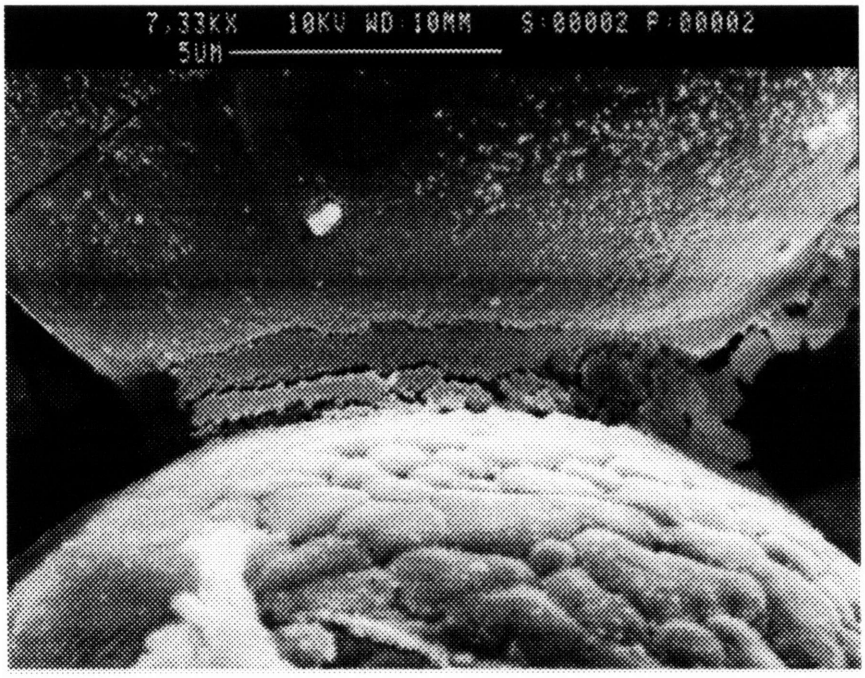

Figure 2.7: A Rhoplex neck enclosed in dried silica. Notice the cracking that is typical in a dried gel

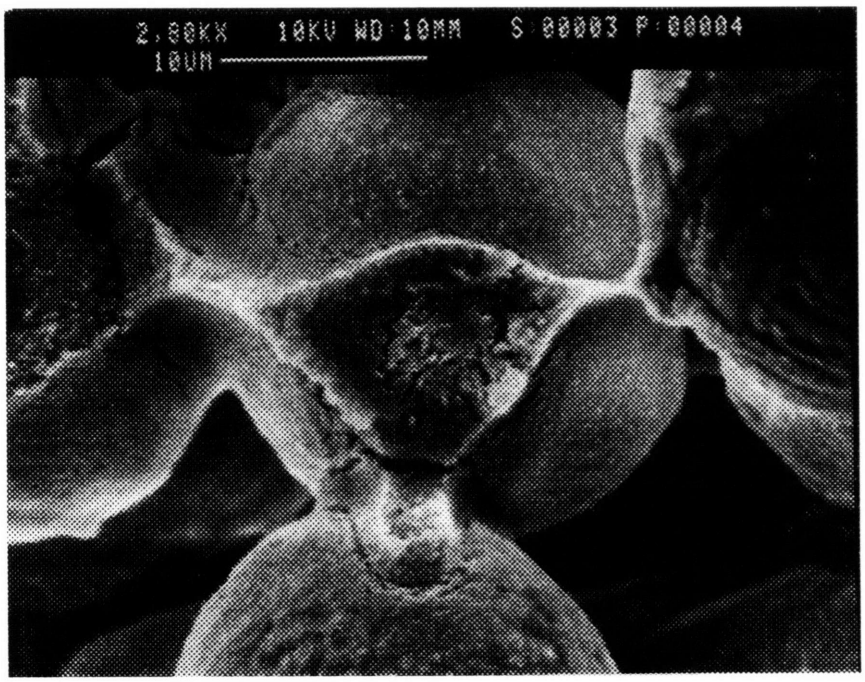

Figure 2.8: A fracture surface of a neck in an infiltrated test bar after firing at 750°C. Notice the porosities in the center of the surface, indicating that silica had not filled in the space left by Rhoplex.

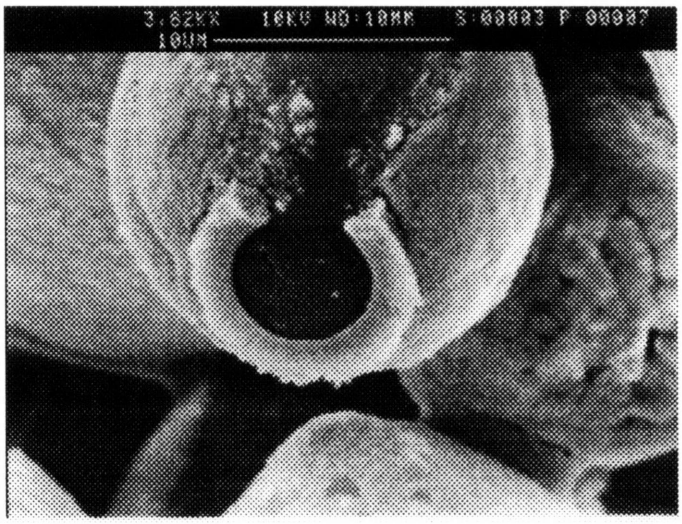

Figure 2.9: A "ring" of silica, after Rhoplex has decomposed by firing at 750°C

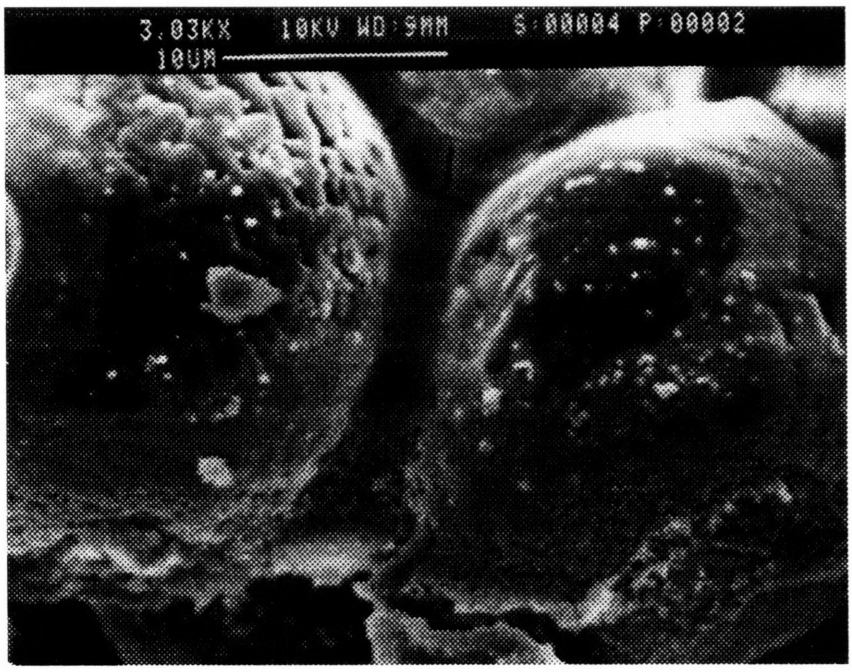

Figure 2.10: Necks in a sample printed with silica binder, fired at 750°C. The necks are well formed and exhibit good wetting of silica on alumina.

Figure 2.12 and Figure 2.13 are micrographs of infiltrated bars that were fired at 900°C. The silica is still not wetting alumina, and the necks lack intimate bonding. The micrograph

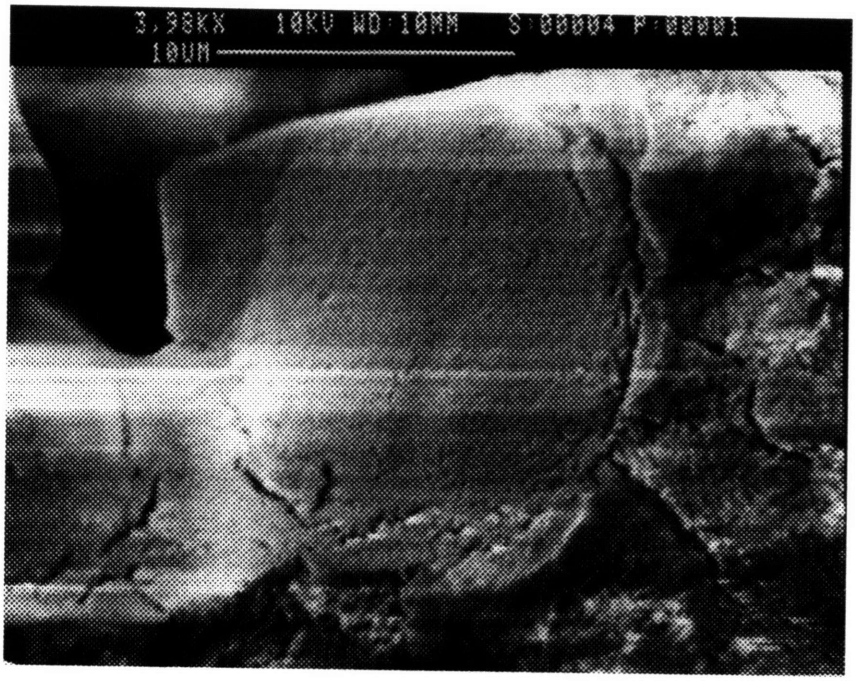

Figure 2.11: Fracture surface of a neck in a sample printed with silica binder. The neck is solid with silica.

of samples printed with silica binder and fired to 900°C shows silica covering and wetting the alumina spheres perfectly (Figure 2.14).

The adverse effects caused by Rhoplex persist even after firing at 1100°C, as visible in Figure 2.15. The silica still does not appear to be fused to the alumina spheres, and the contact angle is much greater than 90°. In fact, the silica is separated from the alumina particles. This lack of cohesiveness at the microscopic level can lead to reduced strength in the bulk, which is supported by the following quantitative testing.

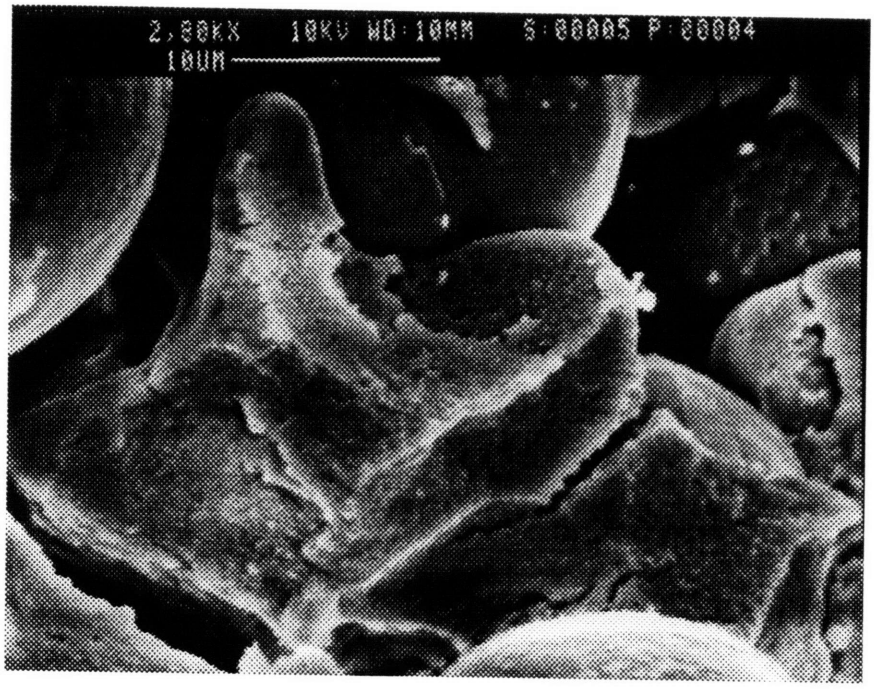

Figure 2.12: Neck in an infiltrated sample after firing at 900°C

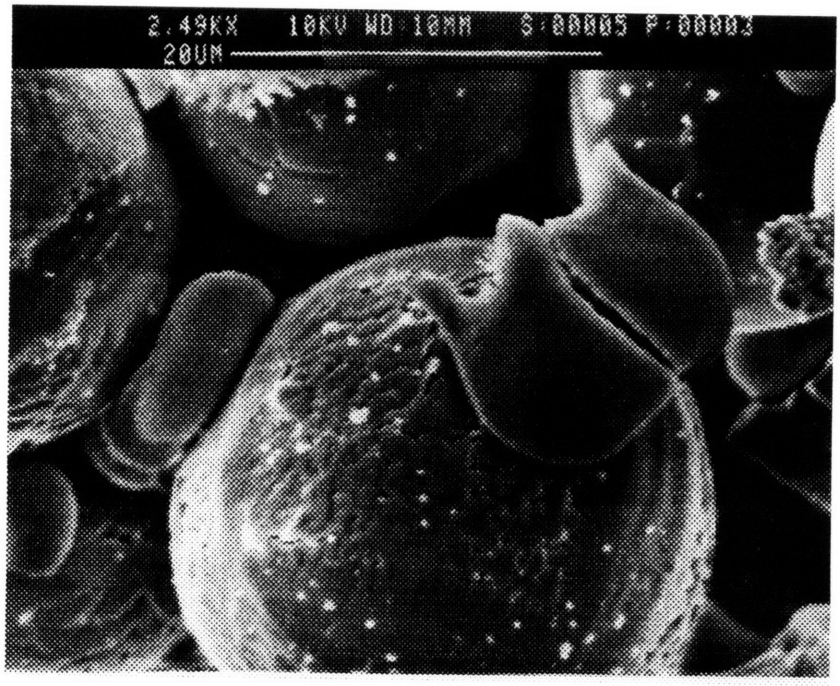

Figure 2.13: Silica "blob" showing poor wetting in infiltrated sample fired at 900°C

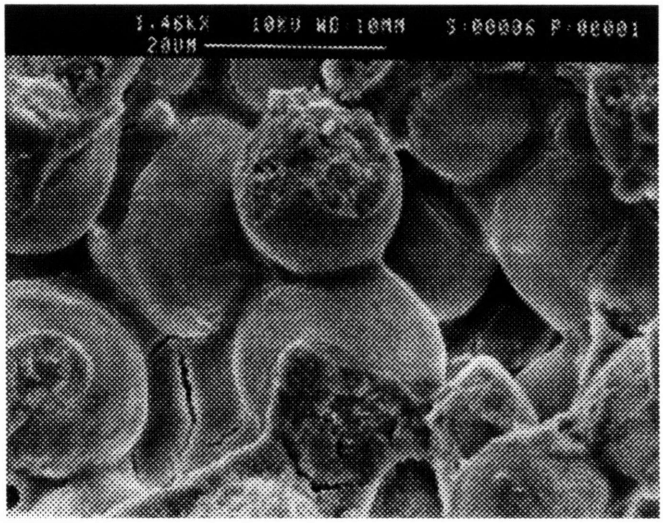

Figure 2.14: Neck in a sample printed with silica binder and fired to 900°C

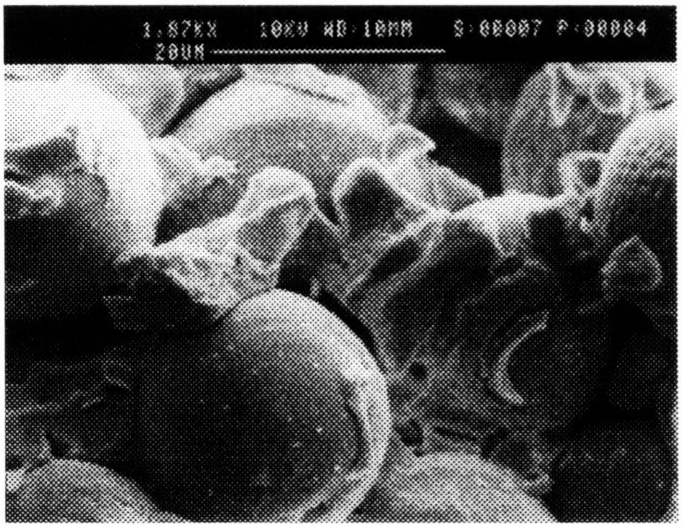

Figure 2.15: Sample made by infiltration and fired to 1100°C

2.3 Strength Measurements

After microscopic examination revealed that polymers can affect the wetting characteristics of silica on alumina, data on the strength of these samples was collected. In addition to quantifying the effect of the wetting phenomenon, these tests also measured the improvement in green strength.

Using a dispersion of smaller diameter silica particles to infiltrate may be beneficial, since it has been shown that less binder is needed to reach maximum strength with smaller particles [Rusher 1975]. Additional test bars were printed and infiltrated with Nyacol 830, another colloidal silica from Nyacol Products Inc. This aqueous dispersion has particles that are 8 nm in diameter. The smaller particle size will hopefully promote movement of silica into voids left by the decomposed polymer.

2.3.1 Measurement Procedure

In general, the brittleness of ceramics limit their strength in tension to low and unpredictable values. Their fracture properties are dictated by the largest surface flaws, which act as stress raisers. Therefore the strength of ceramics is usually characterized by bend testing [Richerson 1982]. A three or four-point bend test is used to measure the maximum tensile stress at failure. This value of this stress, also known as the cross-breaking strength or the modulus of rupture (MOR), defines the flexural strength of the sample. MOR from a three-point bend test is usually higher than that of a four-point bend test, since the probability of a large surface flaw being directly under the load in a three-point bend test is much lower than the probability of a flaw being in the loaded area of a four-point bend test [Esterman 1990].

The more conservative four-point bend test was used due to the limited number of samples. Figure 2.16 illustrates the four-point bending apparatus. Test bars (1" by 0.125" by 0.125") are placed on the lower support points, which are 0.750" apart. The upper plate, with loading points 0.250" from each of the lower supports, is aligned and placed on the

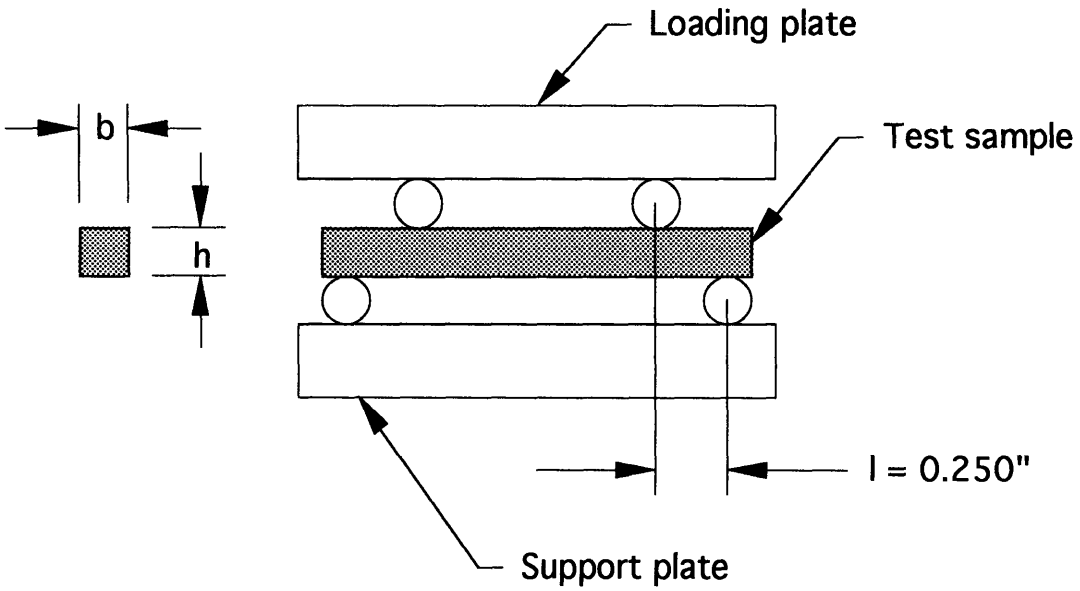

Figure 2.16: Sketch of four-point bend test apparatus

sample.

While an Instron testing machine could be used to load the sample, a much simpler method was devised. Adding water to a beaker attached to the top plate increases the load until the test bar breaks. Given the nature of the material and the limited number of samples, this technique provides equally valid results with a minimum of complication.

2.3.2 Strength Results

Analysis of the results from the four-point bend test is straightforward. A Mettler Electronic Balance measures the mass of the load that fractured the bar. The force applied ($kg \cdot m/sec^2$ or N) is calculated by multiplying the mass (gm) by the gravitational acceleration constant (9.81 m/sec^2). Modelling the test bar as a beam under two point load with simple supports, the maximum stress is described by:

$$\sigma_{max} = \frac{3Fl}{bh^2} \tag{2.1}$$

where

σ_{max} = maximum stress (2.2)

F = load at fracture (2.3)

l = distrance between load point to nearest support point (2.4)

h = thickness of sample (2.5)

b = width of sample (2.6)

Statistical analysis of the data, given the limited sample size and the degree of scatter, is meaningful. For samples with more than one data point, a simple averaging was performed. Although these results are not as reliable as those quoted in other studies of ceramics, they are sufficient to point out important trends in the infiltration technique. Table 2.2 lists the average MOR (MPa) for all of the samples. Where applicable, the MOR is given as

$$\text{mean}(x) \pm \text{SDOM}(x), N \tag{2.7}$$

where SDOM is the standard deviation of the mean defined as $\frac{\sigma}{\sqrt{N}}$, and N is the number of samples.

Table 2.2: MOR of infiltration samples made with 30 μm spherical powder

Firing Temps	**Infiltrated w/9950 13 vol.% silica in fired bar**	**Infiltrated w/830 8 vol.% silica in fired bar**	**Printed with Standard silica binder 11 vol.% silica in fired bar**
crosslinked	5.4 MPa, N=1	5.4 MPa, N=1	N/A
750°C	0.2 MPa, N=1	0.7 MPa, N=1	2.5±0.2 MPa, N=2
900°C	0.6±0.0 MPa, N=2	1.2 MPa, N=1	3.3±0.2 MPa N=2
1100°C	1.2±0.2 MPa, N=2	N/A	6.8±0.0 MPa N=2

From handling the test bars during the microscopic examination, it was obvious that samples printed with Rhoplex had much higher green strength than bars printed with silica. This observation is supported by measurements, which shows that bars printed with Rhoplex has an MOR of 5.4 MPa. The strength of bars printed with silica could not be measured in the green state, since they virtually disintegrate when touched.

The fired strength has two clear trends. First, strength increases with firing temperature, regardless of how the bar was made (i.e. infiltration or directly printing with silica). Secondly, comparison of infiltrated and silica-printed samples fired at the same temperature reveals that the infiltrated samples are always weaker. For example, bars fired at 900°C suffer a sixfold reduction in strength because of infiltration.

Finally, the strength of test bars infiltrated with Nyacol 830 (smaller particle size), although higher that of bars infiltrated with Nyacol 9950, was still lower than the strength of bars printed with silica.

2.4 Conclusions on Infiltration

SEM examinations showed that even after firing, the interparticle necks of bars made by infiltration were different from the necks of bars printed with silica. Silica in the infiltrated samples neither wets the surface of alumina particles nor fills the voids left by decomposed polymer. This produces "blobs" and "rings" of silica that are not fused to the alumina particles. This lack of bonding at the microscopic level degrades the bulk strength properties of ceramic parts.

Composed of only hydrocarbon polymers, Rhoplex® HA-16 should fully decompose into gaseous oxides of carbon (CO_x) and water vapor (H_2O) when heated in an oxidizing environment. With the presence of silica (SiO_2) and alumina (Al_2O_3), however, the decomposition reaction may produce by-products such as silicon carbide (SiC), aluminum carbide (Al_4C_3), and pure carbon. Since these residual compounds are refractory, they will remain in the necks after burnout. Their presence may contribute to the lack of cohesive-

ness in the necks by preventing silica from wetting the surface of alumina particles. A possible solution is to reduce the ratio of Rhoplex to silica to minimize residue.

Looking at the micrographs of the bars made by infiltration, it is clear that silica is not filling the voids in the necks. In addition to poor wetting, another factor may be the physical distance that silica must travel. The average diameter of a Rhoplex neck is 5 μm. Assuming that the polymer disappears completely during burnout, the silica must migrate across 2.5 μm to fill the void. Reducing the amount of Rhoplex may also alleviate this phenomenon by shrinking the necks.

Migration of silica was be enhanced by infiltrating with Nyacol 830. The 8 nm silica particles of this dispersion are more mobile than the 100 nm particles of Nyacol 9950. Although this is reflected in the measured strength of the 830 bars, the bars directly printed with silica were still much stronger.

Although printing ceramic part with Rhoplex® HA-16 acrylic emulsion produces a significant increase in green strength, the resulting reduction in fired strength is unacceptable. This marks the end of the infiltration study, and we turn our attention to printing co-dispersions.

Chapter 3

Co-Dispersions

Two binders currently used in Three Dimensional Printing are aqueous dispersions of colloidal silica (Si_2O) and acrylic polymer emulsions. Colloidal silica, used in the printing of ceramic casting shells, is incorporated into the end product and is therefore chosen for its refractory properties. Parts printed with this binder do not strengthen until they are fired at high temperatures (>750°C). On the other hand, metal parts are printed with emulsions because they require high green strength and must survive being handled in the green state. Combining the properties of both binders may produce casting shells that have high green strength.

In the last chapter, we found that the green strength of ceramic parts is dramatically improved by printing them with an acrylic emulsion and subsequently infiltrating with silica. The downside of this technique is that the fired strength declines to an unacceptable level. This is due to the combined effect of:

1. separation of polymer and silica into discrete regions in the interparticle necks
2. poor wetting of silica on alumina caused by residue from decomposition
3. long migration paths for silica to fill the voids left by decomposition
4. lack of control over the proportion of polymer to silica

An alternative strategy, which addresses these issues, is to print a binder containing a co-dispersion of colloidal silica and polymeric sols.

3.1 Process Concept and Technique

Co-dispersions create new binders for printing ceramic shells by combining colloidal silica with polymeric emulsion. A co-dispersed binder addresses many of the issues raised by the infiltration technique. Since the polymer and the silica are pre-mixed and simultaneously delivered to the powder bed, the interparticle necks will contain a more homogeneous mixture. This reduces the size of the voids that are left when the polymer decomposes, which also shortens the distance that the silica must migrate in order to fill these voids. Pre-mixing the two materials also permits exact control over the ratio of polymer to silica. The amount of polymer in the necks can be reduced to minimize the production of residue and the impact on the wetting characteristics of silica.

The printing process is straightforward. First, a co-dispersed binder is formulated. A ceramic part is printed using the co-dispersion and alumina (Al_2O_3) powder. The part is removed from the powder bed in the green state. After crosslinking the polymer by heating to 160°C, the unprinted powder can be removed. The polymer thermally decomposes in the course of the subsequent high temperature firing (>750°C), which also fuses the silica to the alumina powder. A flowchart of the process is shown in Figure 3.1. In essence, the co-dispersion procedure differs from the infiltration technique only in the manner that the two binder components are delivered.

3.2 Overview of the Printhead

At this point, we need to describe the technology used in 3D Printing to deliver the binder. Borrowed from commercial ink-jet printing applications, the printhead operates by the continuous-drop method (the other is drop-on-demand, and is currently being tested for 3D Printing). In this system, the pressurized ink (or binder) continuously jets out of a small diameter nozzle or orifice. The jet is broken up into evenly sized and regularly spaced droplets by mechanical stimulation via a piezoelectric element. The train of droplets passes through a charging cell, which imparts a charge to each droplet. A set of high voltage plates

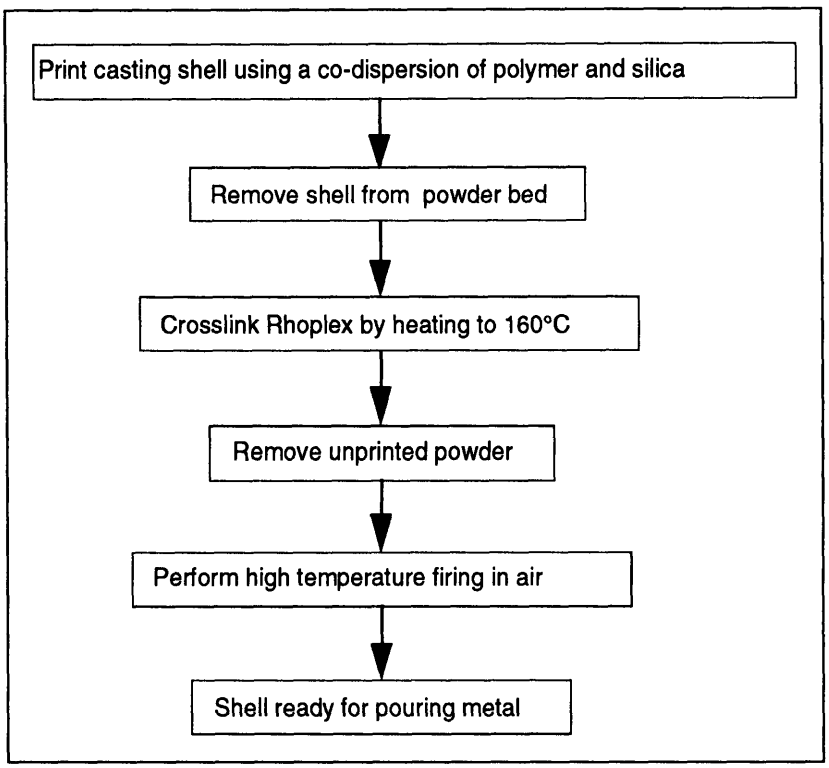

Figure 3.1: Flowchart of printing ceramic casting shells with co-dispersions

electrostatically deflects the droplets into a catching mechanism. By toggling the charging signal, the droplets can be made to either deflect into the catcher or pass through to the target surface.

The operation of the printhead dictates some basic requirements on the binder:

1. The binder must have an average particle size that is much smaller than the nozzle or orifice diameter.
2. The binder must be stable, even under the higher shear rates of passing through an orifice, so that no agglomerates large enough to clog the orifice will be formed.
3. The viscosity of the binder must be sufficiently low such that it will flow through the orifice under reasonable pressure.
4. The binder must have a minimum conductivity, so the droplets can be electrically charged.

The printhead currently used by 3D Printing is an out-of-production tuned resonator made by the Diconix Corporation (ex-division of Kodak, now Scitex) for ink-jet applications. The orifice has a 50 μm diameter electroformed opening, and the resonance frequency of the chamber is normally 78±1 kHz.

3.3 Preliminary Investigation

The stability of aqueous dispersions such as Nyacol 9950 can be achieved by two different techniques. The Nyacol product contains colloidal silica dispersed in an alkaline medium. Silanol groups on the silica particles produces a negative surface. Since the particles are all negatively charged, they tend to repel each another. This is called electrostatic stabilization [Hunter 1991]. The other technique is known as steric or polymeric stabilization. In this scheme, polymers groups are added to the dispersion. They adsorb onto the surface of the dispersed particles and form a layer of polymer "cushion". These cushioning layers prevent the particles from coming close enough to stick together.

Both steric and electrostatic stabilization can fail if certain conditions, such as a critical pH in electrostatic stabilization, are not satisfied. A breakdown in stability causes an electrostatically stabilized dispersion to coagulate or gel, and a sterically stabilized dispersion to flocculate. In both cases, the colloidal particles form large clusters. Since the printhead orifice is only 50 μm, in diameter, large flocculent can become lodged in the opening, resulting in a deflected or blocked binder stream. In addition, the viscosity of unstable binder can increase, reducing the flowrate at a given pressure.

To study the feasibility of a co-dispersed binder, a simple compatibility test was performed. At the time of the study, binders made with Nyacol 9950 and Rhoplex® HA-16 were regularly used to print alumina casting shells and metal tooling. These formulations, described in Section 2.2.1, were believed to have good stability. As the first attempt to create a co-dispersion, samples of these two "Standard" binders were simply poured together in a one-to-one volumetric ratio.

This approach, considering its simplicity, was remarkably successful. The mixture showed no immediate signs of flocculation or separation, and remained stable after three weeks. At this point, a large batch of this 1:1 co-dispersion was made for flowrate and jet stability tests.

3.3.1 The Nozzle Test Stand

The nozzle test stand consists of two 50X Direct Measuring microscopes (Edmond Scientific Co., Barrington, NJ) mounted so that their line of sight intersects at 90°. A Diconix resonator is clamped onto the frame of the microscope assembly. The binder stream is aligned to be in the frame of view of both microscopes. A flashlight bulb illuminates the jet, and its position is measured using the scales in the scopes. By aligning the scopes at right angles, any axial shifting or "walk" of the jet can be recorded. A schematic of the test stand is shown in Figure 3.2.

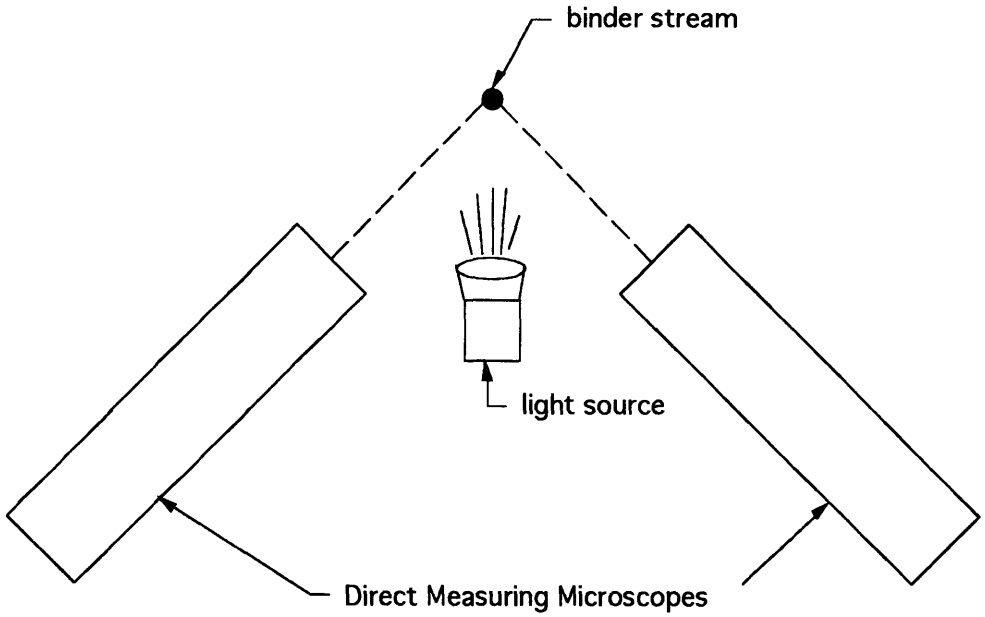

Figure 3.2: Schematic of the nozzle test stand

Binder is supplied to the resonator from a two liter reservoir, which is pressurized

with a helium tank. Using inert helium reduces the possibility of adverse reactions with the binder. The fluid passes through two Calyx capsule filters with polypropylene elements (Micro Separations Inc., Westborough, MA) plumbed in series. The first filter has statistically 5 μm openings, and the second filters down to 1.2 μm. As a final precaution, a sintered stainless steel pellet that filters down to 5 μm (Mott Metallurgical Corp., Farmington, CT) is placed immediately upstream of the entrance to the resonator. A water supply is similarly plumbed, with the exception of having only one 5 μm Calyx filter.

The flowrate of the binder jet is calculated by measuring the amount of time required to collect a certain volume of binder in a graduated cylinder, and dividing that volume by the elapsed time.

The purpose of the nozzle testing stand is to observe flowrate and axial shifts in the position of the jet over a period of time. An acceptable binder should have constant flowrate and minimal stream walk.

3.3.2 Jet Stability Results

Results of the first run with the 1:1 co-dispersion are shown in Figure 3.3 and Figure 3.4. The pressure for both runs was kept at 25 psi. Although the flowrate dropped by 0.38 mL/sec, or 36%, in 682 minutes, the position only varied by 0.001" to 0.002" in either direction. This indicates that the reduction in flowrate is not the result of a clogged orifice, but rather a problem with the binder delivery system. The sintered final filter, with much less filtration capacity then the large capsule filters, was probably becoming loaded with captured particles. In another test without the sintered filter, the flowrate and jet position are quite steady (Figure 3.3 and Figure 3.5). "S" and "T" are axes perpendicular to the line of view of the two microscopes.

This was a puzzling observation. After passing through the 1.2 μm polypropylene filter, why would the binder clog a 5 μm stainless filter? It is possible that the particles in

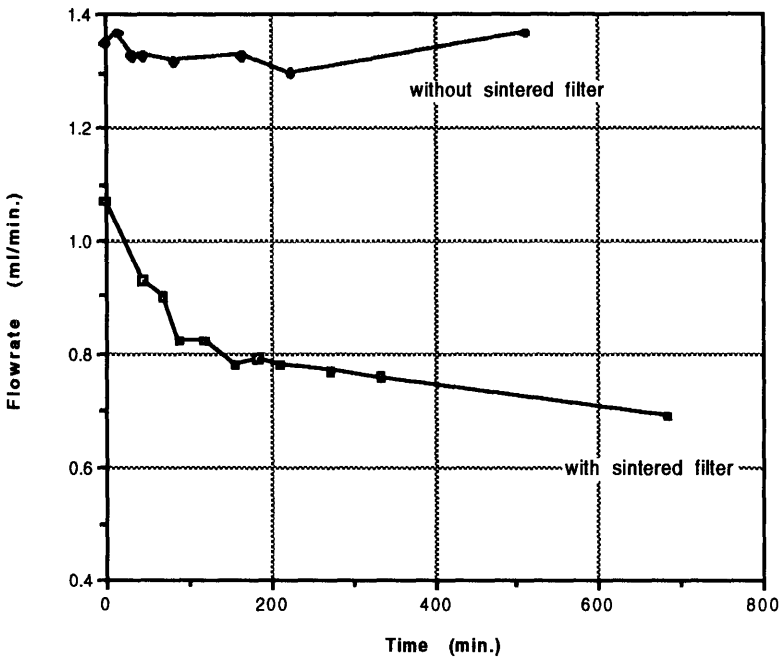

Figure 3.3: Flowrate versus time, 1:1 co-dispersion. Pressure was held constant at 25 psi.

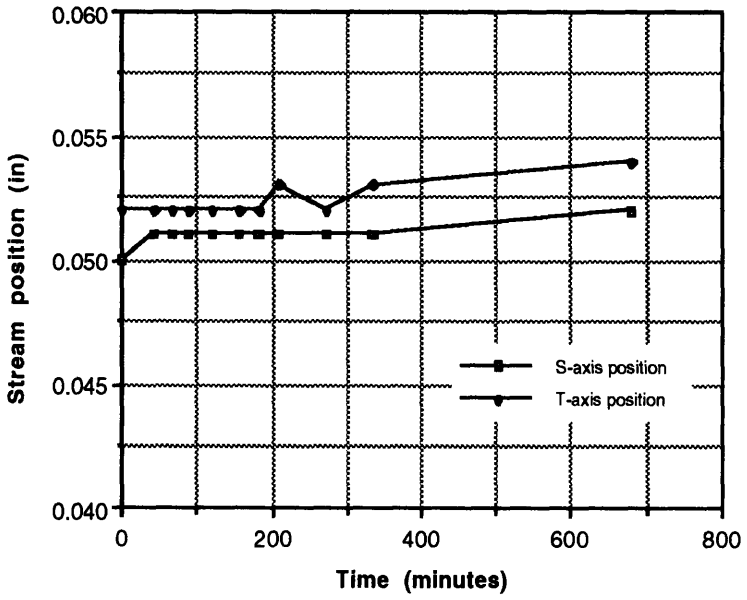

Figure 3.4: Stream position versus time, 1:1 co-dispersion, with final filter. Pressure was constant at 25psi. The S and T axes are perpendicular to the line-of-sight of the two microscopes.

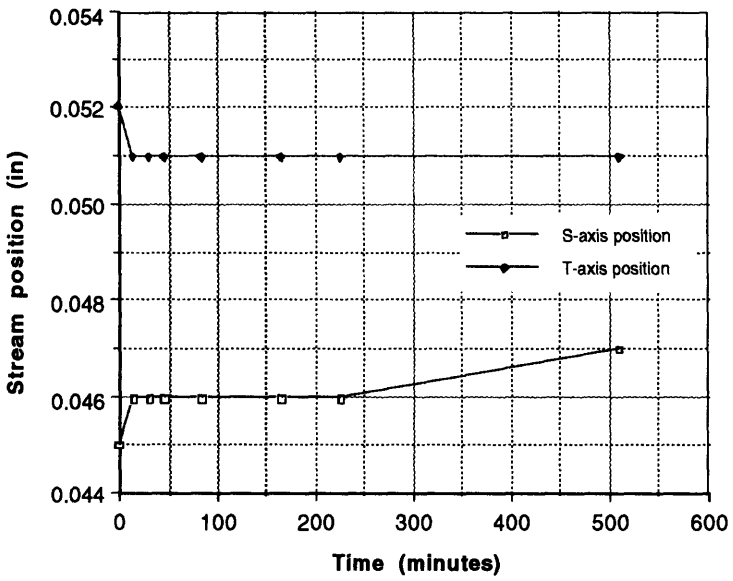

Figure 3.5: Stream position versus time, 1:1 co-dispersion, no final filter. Pressure was constant at 25psi. The S and T axes are perpendicular to the line-of-sight of the two microscopes.

the binder reacts differently to the two filter materials.

3.3.3 Printing Test Bars

After the initial success in achieving a stable jet, the next logical step was printing test bars with the 1:1 co-dispersion. Printing involves additional issues that are not examined on the test stand, such as stimulation of the stream to form discrete droplets, charging of droplets, and electrostatic deflection of the charged droplets. Nonetheless, the 1:1 co-dispersion was loaded into the proto 3D Printing machine.

To allow comparison of data, the same test bars from the infiltration study were made using the standard printing parameters. The powder was 30 μm spherical alumina, with 0.3 wt.% citric acid mixed in. Citric acid lowers the alkalinity of the binder below pH 9, causing rapid aggregation of the silica and thus defining a finite line width [Iler 1979]. The optimal percentage of citric acid is still being studied, but at the time 0.3 wt.%

was the accepted amount for printing with the Standard silica binder.

The test bars were removed from the powder bed and crosslinked at 160°C. After removing unbound powder, samples were fired at 750°C, 900°C and 1100°C. Four point bend tests were performed on crosslinked and fired bars, and the fracture surfaces were examined in a scanning electron microscope.

3.3.4 Results

On the whole, the printing was successful. Figure 3.6 and Figure 3.7 are micrographs of interparticle necks in co-dispersion bars fired at 750°C. In contrast to the samples made by infiltration, silica in these necks exhibits good wetting on alumina. The necks are narrow and solid, and appear to be intimately bonded to the alumina particles. There are no "blobs" of silica, as seen in the infiltrated samples. Examination of co-dispersion parts fired to 900°C and 1100°C resulted in the same conclusion.

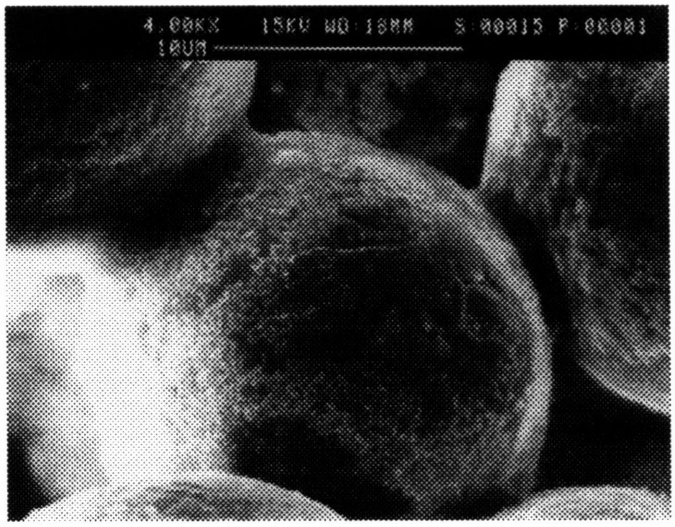

Figure 3.6: Necks of test bar printed with co-dispersion, fired at 750°C

A possible concern is the small surface pores that are visible in the close-up view in Figure 3.7. If these voids exist throughout the neck, a porous structure will result. This

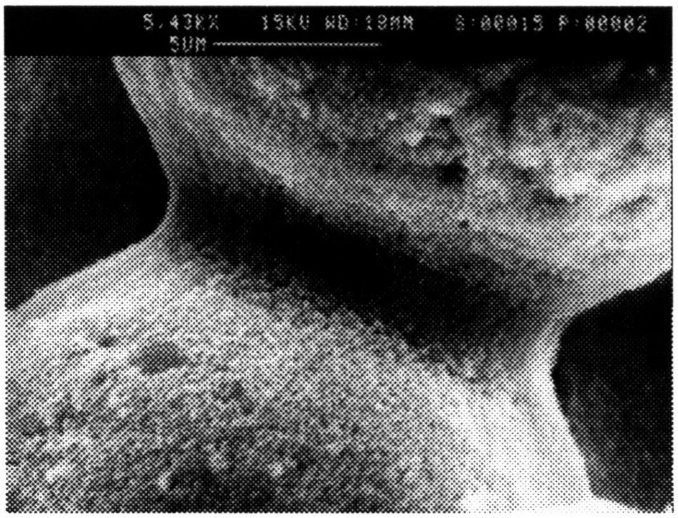

Figure 3.7: Close-up of a neck in a co-dispersion bar fired at 750°C. The neck exhibits a porous surface.

may weaken the integrity of the neck and reduce the fired strength of parts.

The modulus of rupture was surprisingly good. From the graph presented in Figure 3.8, it is obvious that co-dispersion out-performed infiltration in terms of fired strength for all temperatures. The green strength of co-dispersion bars was comparable to that of infiltrated bars. The fired strength increases with the firing temperature, a trend also observed during the infiltration study. This phenomenon will be discussed in more detail in Section 4.1.

In spite of the success in printing, the performance of the co-dispersion was not satisfactory. The MOR data indicates that the fired strength of co-dispersion bars is lower than that of bars printed with regular silica binder. Although there are no visible effects of residue from decomposed Rhoplex, fired strength may still suffer from unseen degradation. In addition, the reduced strength may be an artifact of reduced silica content in the co-dispersion bars. Standard silica binder contains 18 vol.% silica. Co-dispersion, made by combining the Standard silica and Rhoplex binders in a 1:1 volumetric ratio, has only 9 vol.% silica.

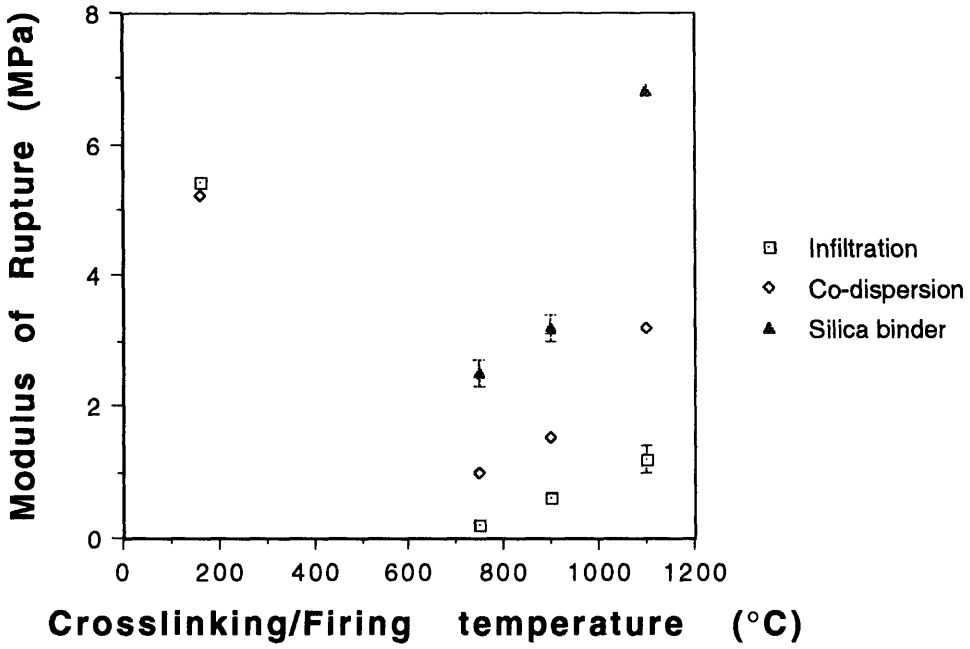

Figure 3.8: MOR data for infiltration with Nyacol 9950, 1:1 co-dispersion, and Standard 18 vol.% silica binder. When given, the error bars represent the standard deviation of the mean for the data set. The data points without error bars came from only one sample.

To test the last hypothesis, bars were printed using Standard silica binder that was diluted to 9 vol.% solids. As shown in Figure 3.9, the fired strength of these bars, although lower than bars printed with 18% silica, was still greater than co-dispersion parts. Therefore the effects of Rhoplex residue and the reduced silica content both contribute to lower fired strength in the co-dispersion bars.

To establish the effect of using spherical alumina instead of the platelet-shaped powder normally used to print shells, test bars were printed in Norton 7920 powder using 9 vol.% silica binder. Spherical powder was suspected to lower the fired strength, since individual particles only make point contact with the neighboring particles, where as the irregularly shaped platelets can form necks that cover a larger area. These samples were fired at the same three temperatures, and measured by the four-point bend test. The results, shown in Figure 3.9, indicate that platelet-shaped powder has a positive impact on strength

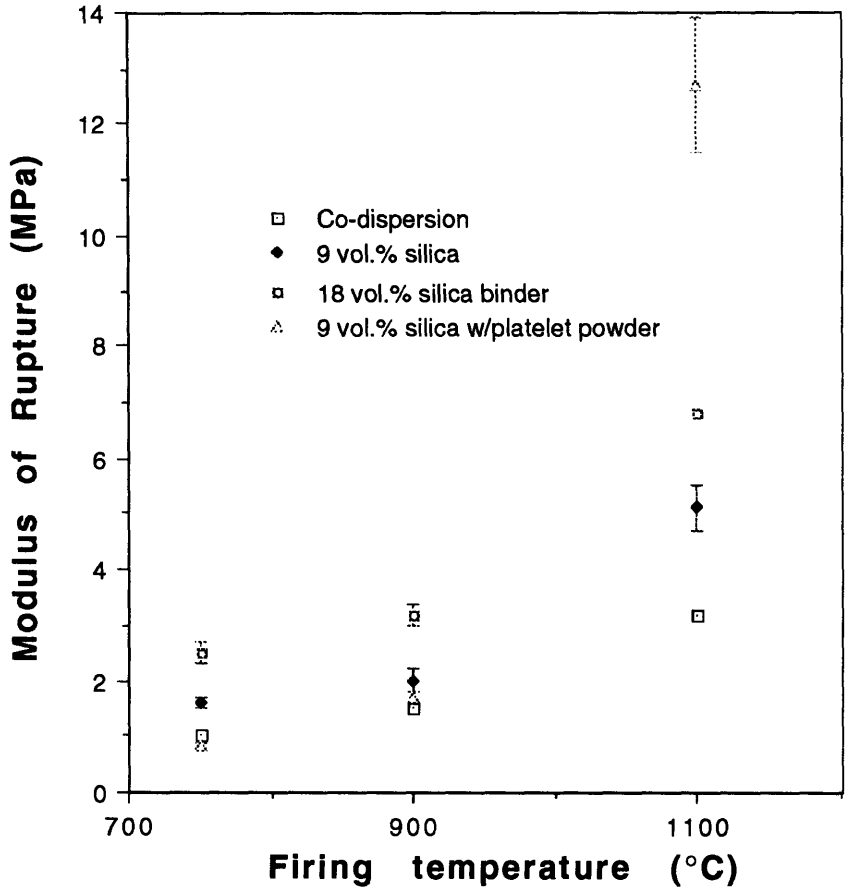

Figure 3.9: MOR for 1) 1:1 co-dispersion in spherical powder, 2) binder with 9 vol.% silica in spherical powder, 3) binder with 18 vol.% silica in spherical powder, and 4) binder with 9 vol.% silica in 7920 platelet-shaped powder. When given, the error bars represent the standard deviation of the mean for the data set. The data points without error bars came from only one sample.

only after firing at 1100°C.

Up to this point, we have only worked with the 1:1 co-dispersion. The next step of the investigation is to utilize another advantage of co-dispersions: the ability to control the ratio of silica to polymer in the parts.

3.4 Reformulation

Although the preliminary investigation of co-dispersions was successful, the fired strength still needs improvement. The results so far indicate that adjusting the relative amounts of silica and polymer in the binder should alleviate the reduction in strength. Therefore, new co-dispersions containing various ratios of Rhoplex® HA-16 and Nyacol 9950 were formulated.

Two new requirements were set for the co-dispersion. First, the binder must contain 18 vol.% silica, regardless of the amount of Rhoplex. This is to maintain silica content in the fired parts at the same level as parts printed with the Standard silica binder. Simplicity, the second rule, reduced the composition of the co-dispersion down to silica, Rhoplex, water, and an additive to stabilize the mixture.

As received from the manufacturer, Rhoplex® HA-16 is acidic and has a pH of 4. Since this is below the range where colloidal silica is stable, Rhoplex must be made basic before the two can be mixed. It was discovered that by adding enough ammonium hydroxide (NH_4OH) to stock Rhoplex to increase its alkalinity to pH 10, a stable co-dispersion can be created.

Calculation of the relative proportions of Rhoplex, silica, and distilled water to produce a given Rhoplex/silica ratio is straight-forward. For example, to make a co-dispersion containing 10 vol.% Rhoplex and 17.5 vol.% silica, start with the following expression:

$$1.0\text{L} = 0.1\text{ L Rhoplex solids} + 0.175\text{ L silica solids} + 0.75\text{ L water} \quad (3.1)$$

This is the desired final composition of the binder. Analysis of stock 9950 and HA-16 reveal that

$$\text{stock 9950 silica} = 30\text{ vol.\% silica solids} + 70\text{ vol.\% water} \quad (3.2)$$

$$\text{stock HA-16} = 43\text{ vol.\% Rhoplex soilds} + 57\text{ vol.\% water} \quad (3.3)$$

Using these volume percentages, the volume of stock solutions required to obtain the desired solid contents can be calculated. For example, 0.223 liters of Rhoplex containing

43 vol.% solids is needed for 0.1 liter of Rhoplex solids, i.e.

$$0.223L \times 0.43 = 0.1L \tag{3.4}$$

Similar calculations for silica reveals that 0.583 liters of stock silica is needed to produce 0.175 L of silica solids. Combining the above expressions and adding water to make 1.0 L of final product gives:

$$\begin{aligned} 1.0\,\text{L} &= 0.233\,\text{L}(0.43\,\text{Rhoplex}+0.57\,\text{water}) \\ &+ 0.583\text{L}\,(0.3\,\text{silica}+0.7\,\text{water})+0.184\,\text{water} \end{aligned} \tag{3.5}$$

This gives the relative proportions of the ingredients by volume: 1 part water, 1.27 parts stock Rhoplex (pH modified w/ammonia), and 3.17 parts stock 9950 colloidal silica. This produces a co-dispersion containing 10 vol.% Rhoplex and 17.5 vol.% silica.

To mix these ingredients, first add the water to beaker and start stirring with a magnetic stirrer. Gradually pour in the silica and allow to mix for 5 minutes. Slowly add the pH modified Rhoplex and stir for at least one-half hour.

Three different co-dispersions were made for testing. The silica content was maintained at 17.5 vol.%, while the amounts of Rhoplex were 2 vol.%, 5 vol.%, and 10 vol.%. To recap, this new formulation of co-dispersion contains:

1. Stock Rhoplex® HA-16 emulsion
2. Ammonium hydroxide to increase the pH of Rhoplex to 10
3. Nyacol 9950 colloidal silica dispersion
4. Distilled water

3.4.1 MOR Results

The 1.0" by 0.125" by 0.125" test bars were chosen for expedience of printing. The samples were made on the proto machine using the standard printing conditions. The goal was to observe the effects that varying the amount of Rhoplex has on the green and fired strength of ceramic parts.

To obtain results that are applicable towards printing actual casting shells, we chose

to use the Norton 7920 Electronic Grade powder that is normally used in printing shells. The platelet-like particles in this powder have an average diameter of 30 microns. 0.2 wt.% citric acid was added as a gelling agent.

After crosslinked at 160°C, samples were fired at 750°C, 900°C, and 1100°C. Test bars were also printed with the Standard silica binder (18 vol.% silica) to provide a control for the experiment. Flexural strength for green and fired samples were measured by the four point bend test. The results of these tests are shown in Table 3.1. As before, the results are presented as "mean(x)±SDOM(X)", where the mean values are taken of three samples.

Table 3.1: MOR of HA-16 co-dispersions with varying polymer content

Firing Temp	**2 vol.%**	**5 vol.%**	**10 vol.%**	**Standard silica binder 18 vol.%**
"green"	1.0±0.1 MPa	2.5±0.1 MPa	3.8±0.1 MPa	0.39±0.04 MPa
750°C	2.8±0.5 MPa	2.6±0.6 MPa	2.3±0.4 MPa	3.5±0.1 MPa
900°C	3.5±0.1 MPa	4.2±0.3 MPa	3.6±0.3 MPa	4.0±0.3 MPa
1100°C	23±2 MPa	30±3 MPa	29±5 MPa	32±5 MPa

With 10 vol.% Rhoplex, the green strength was 3.8 MPa; a 900% increase from 0.4 MPa for the green silica parts. By plotting green strength against volume percentage of Rhoplex, we see that the green MOR increases monotonically with increasing polymer content (Figure 3.10). This suggests that adding more Rhoplex to the co-dispersion will further improve the green strength. But fired strength may decrease with increasing polymer content, as suggested by Figure 3.11. In addition, we discovered that the viscosity of the co-dispersion increases rapidly with polymer content. Therefore the amount of Rhoplex in the co-dispersion was capped at 10 percent by volume.

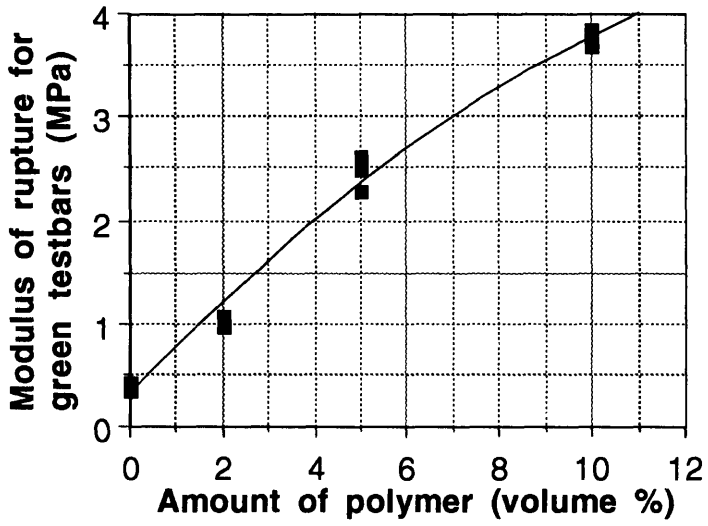

Figure 3.10: Green MOR versus percent polymer for HA-16

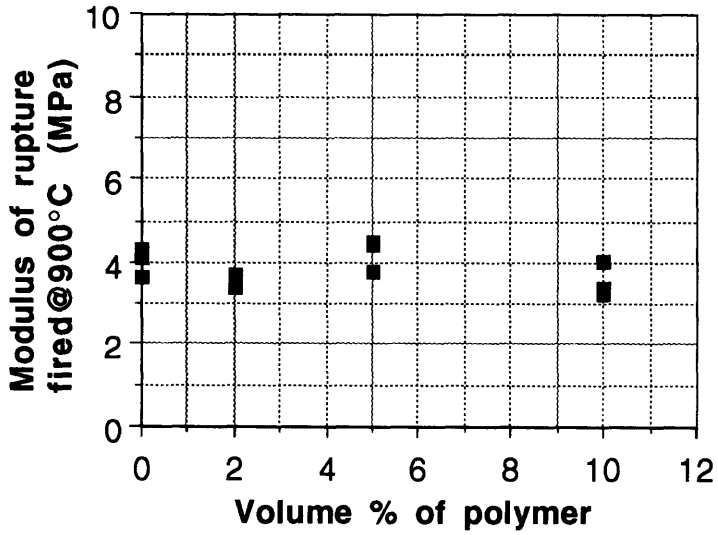

Figure 3.11: MOR versus percent HA-16 polymer, fired at 900°C

The key result of this experiment is that a co-dispersion containing 10 vol.% Rhoplex produces parts that:

1. have higher green strength than parts printed with silica (3.8±0.1 MPa versus 0.4±0.1 MPa)
2. have strength comparable to parts printed with silica after firing at 900°C (3.6±0.3 MPa versus 4.0±0.3 MPa).

3.5 Commercial Green Strength Additives

In light of the success with co-dispersion made with Rhoplex® HA-16 we decided to explore some commercial green strength enhancers from the investment casting industry. A survey showed that there are two categories of products. The first type of additives are emulsions of various polymers, similar to the HA-16. The other product is a colloidal silica that contains a polymer in solution. The following table lists the samples that were obtained. A special case is the Customcoat binder from Ransome & Randolph, which is an emulsion already co-dispersed with colloidal silica.

Table 3.2: Commercial Green Strength Products

Name	**Manufacturer**	**Polymer**	**Contains silica?**
Tylac 68138	Reichhold Chemicals, Inc.	styrene-butadiene copolymer dispersion	No
Adbond BV	Remet Corp.	proprietary dispersion	No
Rhoplex AC-604	Rhom & Hass Co.	acrylic emulsion	No
Customcoat	Ransom & Randolph	proprietary dispersion	Yes
Ludox SK-215	DuPont	PVA in solution	Yes

3.5.1 Compatibility Issues

With the exception of Ludox SK 215 and Customcoat, the green strength enhancer are intended to be added to a slurry of colloidal silica and alumina powder for investment casting purposes. Two criteria were used to select candidates for further testing. The addition of these products to Nyacol 9950 must not cause instability in the resulting mixture. These additives must also be compatible with the more complex problem of passing through a 50 μm orifice.

A simple test was conducted by mixing these additives with the 9950 dispersion in various ratios. The pH of the additives were first increased to 10 by adding ammonia. Mixing was done in a test tube by dropwise addition of the polymer to silica. The test tubes were capped and inverted several times to insure thorough mixing.

Incompatible samples were readily observed due to immediate flocculation or coagulation. Flocculation of the binder leads to separation and settling of the dispersed particles from the aqueous medium. Coagulation is indicated by a large increase in viscosity of the fluid to a level comparable to that of heavy-cream or cottage cheese.

To our disappointment, all but one of the additives failed these compatibility criteria. The only successful candidate was Rhoplex® AC-604, another emulsion from Rohm and Hass. Co-dispersion containing 18 vol.% silica and 2 vol.%, 5 vol.%, and 10 vol.% AC-604 particles were formulated for additional experiments

3.5.2 Ludox SK

Since Ludox SK already contains 7 vol.% colloidal silica, it bypasses the first compatibility criterion. Initial attempts to print this binder failed because the binder stream could not be properly deflected. This lead to a more detailed look into the nature of the stream.

Using a technique developed by members of the group, the droplets were captured by stop-motion video. The binder stream is backlit by a strobing light-emitting diode syn-

chronized to the frequency of the droplets. This allows close-up video recordings of the binder stream and a detailed look into droplet breakoff and formation.

Examination of a stream of Ludox SK 215 revealed the existence of tiny threads connecting the droplets. Without clean breakoff, the droplets cannot be properly charged, thus leading to poor deflection. Figure 3.12 shows a still frame of the Ludox droplet train and an example of good droplet formation.

Discussion of this phenomenon with Dr. Arthur Soucemarianadin of Imaje, an ink-jet manufacturer in France, provided an explanation. Solutions containing polymer that are greater than 25,000 in molecular weight (MW) tend to exhibit non-Newtonian rheology. These solutions have shear/strain behavior that is different from Newtonian fluids. Since Ludox SK 215 contains 2 vol.% of 56,000MW polyvinyl alcohol (PVA), it acts as a non-Newtonian fluid. Dr. Soucemarianadin recommended reducing the molecular weight and the concentration of polymer to alleviate this problem.

A different formulation of Ludox was obtained from DuPont. Designated Ludox SK-B, this solution contains 13 vol.% silica and 1% of the 56,000MW PVA. While video examination revealed what appeared to be good droplet formation, deflection problems again prevented printing. We suspect that there are still tiny strands of polymer filaments, which are masked by the limited resolution of the video system, connecting the droplets.

3.5.3 Printing Procedure

To rapidly generate bars for strength measurement with many different binders, a new printing scheme was developed. Since tuning the printhead to obtain optimal deflection of the jet is a time-consuming and at times frustrating task, it was eliminated from the printing process. The binder jet remains undeflected at all times, and a mask over the powder bed defines the outline of the bars. This is similar to the method used to create the first 3D Printed parts, when binary deflection of the droplet stream still under development [Esterman 1990]. Since deflection was no longer an issue, an attempt was also made to make

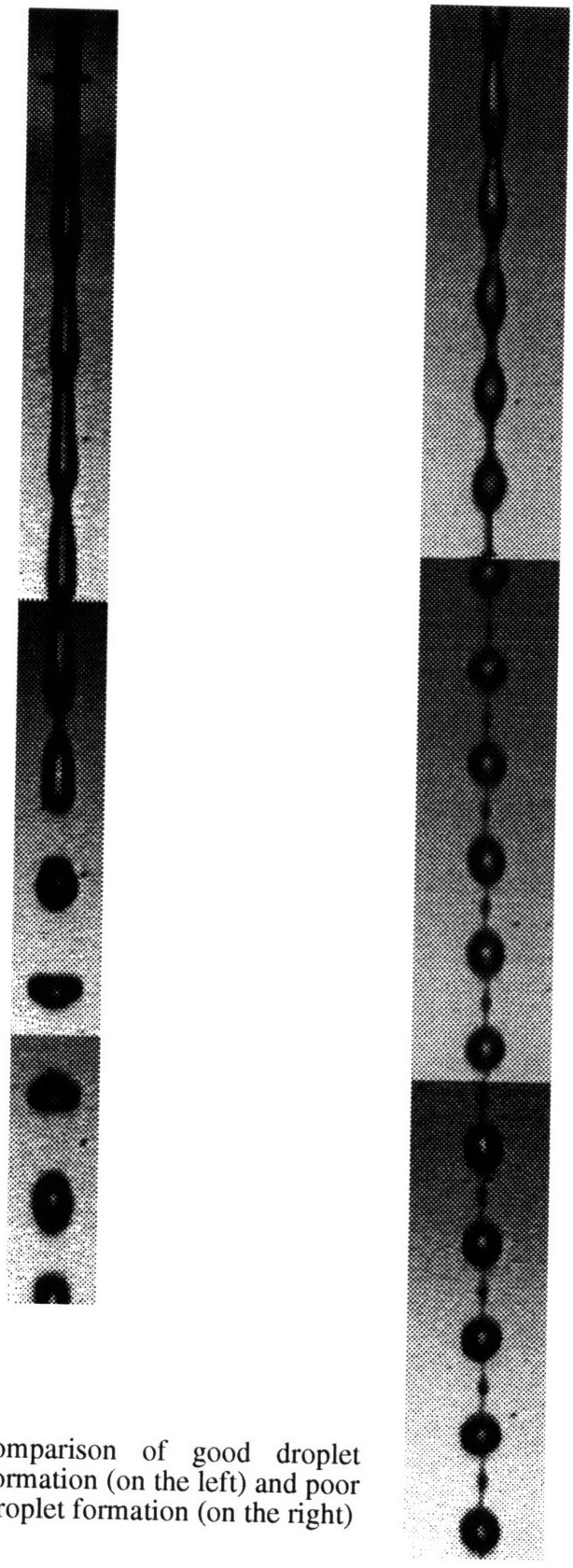

Figure 3.12: Comparison of good droplet formation (on the left) and poor droplet formation (on the right)

test bars with the two formulations of Ludox SK.

Another problem, however, developed in filtering these binders. To simplify the switching of binders without risking cross-contamination, a simplified fluid delivery system was used and replaced after printing each binder. A sintered stainless steel filter was used in place of the larger Calyx capsule filters. Unfortunately, all of the binders, with the exception of Ludox SK-B, clogged the stainless steel filter. The reason for this is unclear, but it probably involves incompatibilities between the surface chemistry of polymeric emulsions and stainless steel. Attempts to use a nylon screen mesh filters and to print without filtering were also unsuccessful. As a result, acceptable test bars were only printed with Ludox SK-B and three co-dispersions containing 2%, 5%, and 10% Rhoplex AC-604.

3.5.4 Flexural Strength Results

The samples produced with Rhoplex AC-604 co-dispersions were crosslinked at 175°C and subsequently fired at 750°C, 900°C, and 1100°C. The parts made with Ludox SK-B did not require crosslinking and were simply fired. The results from four-point bend tests, shown in the following graphs, are disappointing. The green strength obtained with AC-604 co-dispersions, although higher than that of the Standard silica binder, are still less than those of HA-16 co-dispersions (see Figure 3.13). In addition, Figure 3.14 shows that the fired strength of AC-604 bars decreases more rapidly (as the polymer content increased) than that of HA-16. Lastly, the green strength of bars printed with Ludox SK-B is only 2.0 MPa, which is much lower than that obtained with co-dispersion containing 10 vol.% Rhoplex HA-16. Figure 3.15 is a comparison of the green MOR from the various binder tested.

An interesting fact is that as the volume percentage of HA-16 increases from 2 vol.% to 5 vol.%, the MOR of bars fired at 900°C increases. This is reversed from our prior observations and the hypothesis that the fired strength decreases as polymer content increases. The reason for this reversal is unclear.

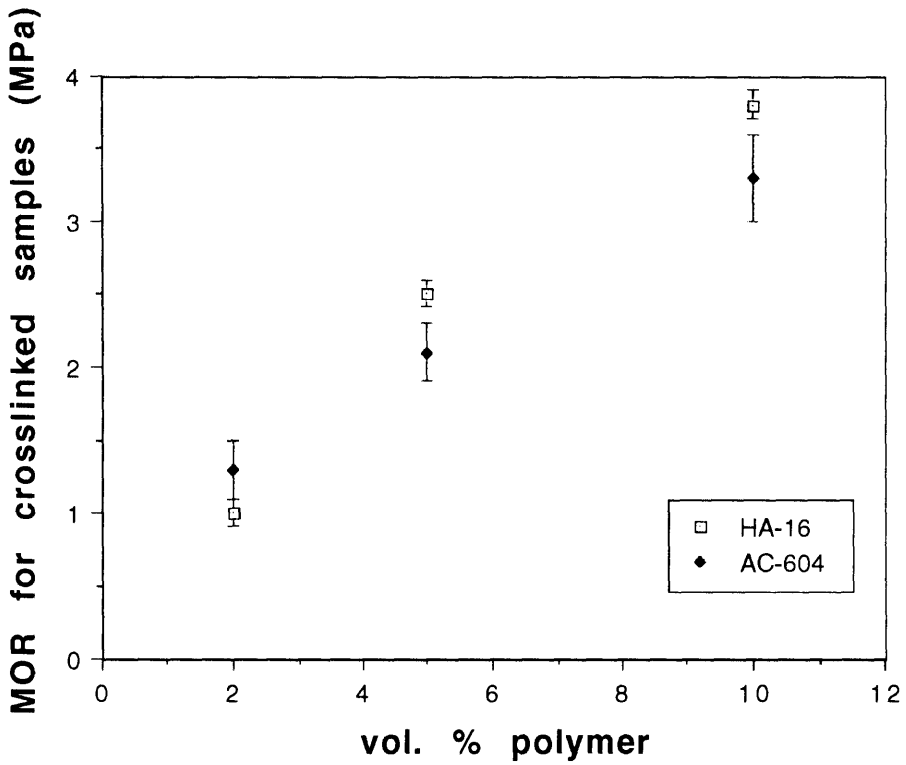

Figure 3.13: Green MOR for HA-16 and AC-604 co-dispersions. Error bars represent the standard deviation of the mean (where there is more than one sample)

3.6 Conclusions on Co-Dispersions

From the various experiments described above, we discovered that Rhoplex® HA-16 acrylic emulsion and Nyacol 9950 colloidal silica produces an usable co-dispersion. A formulation of 18 vol.% silica and 10 vol.% polymer provides the optimal balance of green and fired strength for 3D Printed ceramic parts. Additional experiments involving post processing and dimensional control of ceramic parts were performed using this co-dispersion.

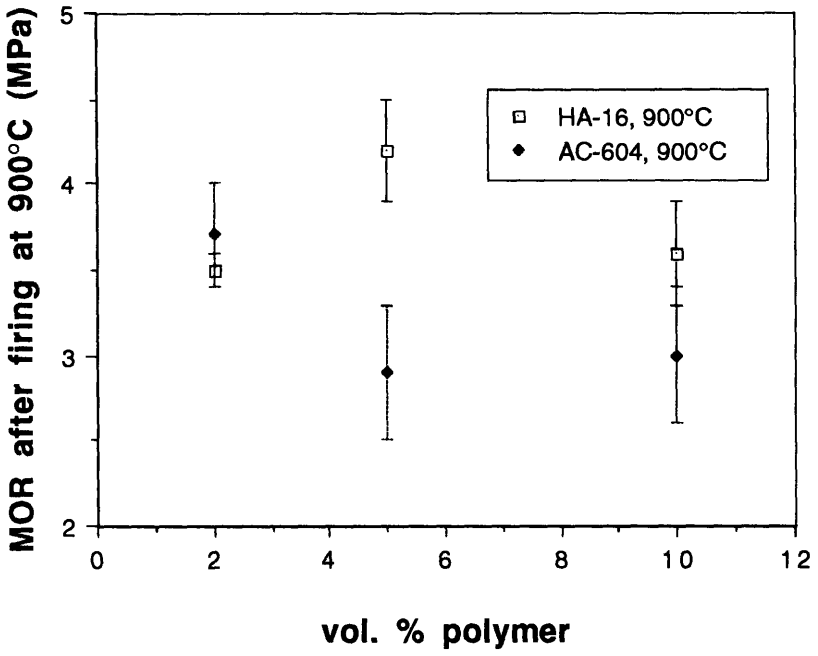

Figure 3.14: MOR (fired @ 900°C) for co-dispersion containing 10 vol.% HA-16 and co-dispersion containing 10 vol.% AC-604.

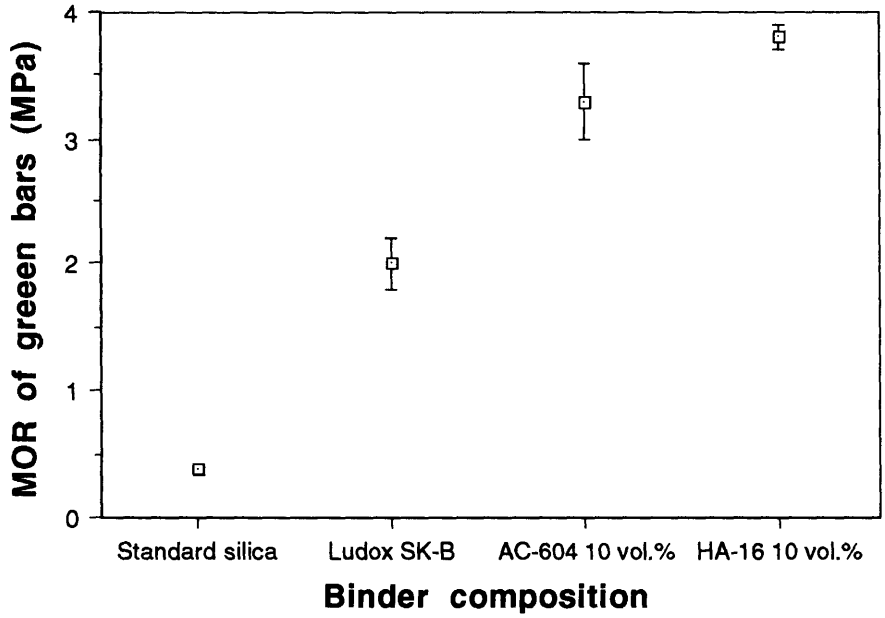

Figure 3.15: Comparison of green MOR for various binders

Chapter 4

Post Processing

With the composition of the co-dispersion finalized, we now proceed to the post processing of parts printed with this new binder. Post processing is defined as the treatment the part receives after being printed. The two specific issues addressed are the firing schedule and powder removal.

4.1 Firing Schedule

The initial investigation into the infiltration technique discovered that thermal decomposition of Rhoplex generates residue, which affects the wetting characteristics of silica on alumina. It was suggested that the method in which the polymer is heated may have an effect on the amount of residue. If the polymer is heated up too quickly, pure carbon may be evolved.

The atmosphere in which burnout occurs may also affect the amount of residue generated. The idealized chemical equation for the decomposition of Rhoplex is

$$\text{Hydrocarbon} + \text{oxygen} + \text{heat} \Rightarrow CO_x \text{ gases} + H_2O \text{ vapors:} \quad (4.1)$$

If oxygen is not readily available, this reaction may become:

$$\text{Hydrocarbon} + \text{limited oxygen} + \text{heat} \Rightarrow CO_x \text{ gases} + H_2O \text{ vapors} + \text{carbon} \quad (4.2)$$

The presence of carbon may reduce fired strength by inhibiting silica from wetting the alumina. Finally, we wished to find the minimum temperature threshold for the onset of burn-

out.

4.1.1 Thermo-Gravimetric Analysis

To gain more insight into the decomposition of Rhoplex® HA-16, thermo gravimetric analysis (TGA) was used. The Perkin-Elmer 7 Series Thermal Analysis System is essentially a high-precision electronic balance with a sample pan inside a computer-controlled furnace chamber. The computers heat the chamber according to any user-programmed schedule, i.e. heating rate, holding time, cooling rate, etc. During a run, the chamber can be filled with helium, nitrogen, argon, or atmospheric air.

A sample of Rhoplex® HA-16, as shipped from the manufacturer, was examined in the TGA. The liquid was dried and 25.932 mg. of the polymer were placed in the sample pan. Since this was pure Rhoplex, we expected it to completely decompose. The sample was heated to 1000°C at a rate of 1.0°C/minute in atmospheric air. A plot of mass, as a percentage of the initial mass of the sample, versus temperature is shown in Figure 4.1.

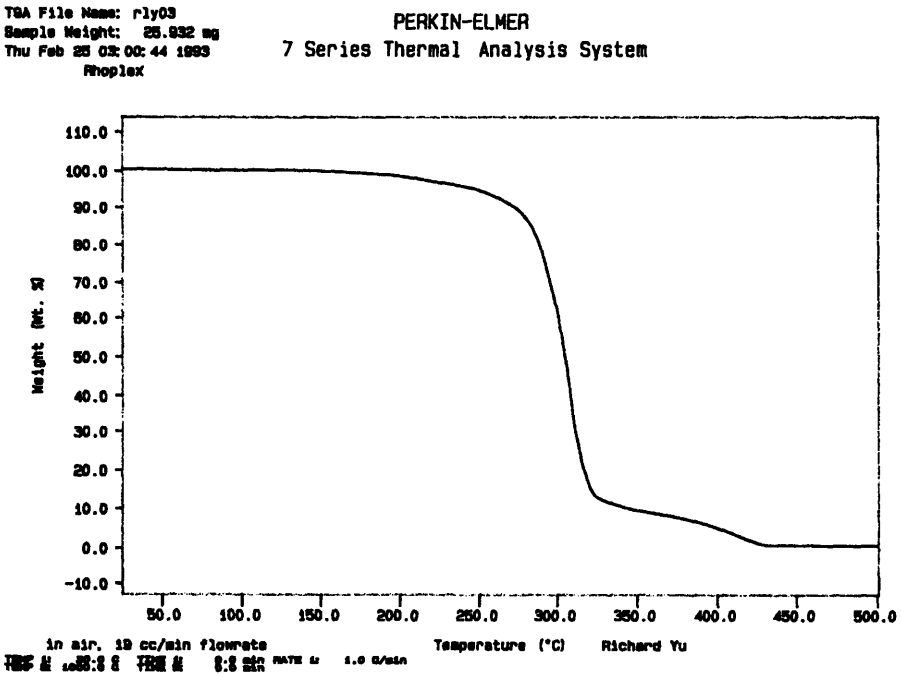

Figure 4.1: TGA for stock Rhoplex HA-16 in air

Data from the Perkin-Elmer system is only available in the plotted printout form shown in Figure 4.1. As a result, the graphs can not be read with high accuracy. The onset temperature of decomposition, indicated by the sudden change in the slope of this graph, is about 300°C. A more significant observation is that the mass does not go to zero. Above 430°C, the mass remained constant at roughly 1 ± 0.5% through the end of the run. This implies that there is residue remaining, even at high temperatures.

The next TGA was performed with Rhoplex binder, which contains tetramethylammonium hydroxide ([CH3]4NOH) and is diluted with water. These additions were not expected to affect the burnout characteristics. The binder was dried and the mass of the sample was 31.339 gm. The same heating schedule was used but a nitrogen environment examined the effect of removing oxygen from the decomposition process.

The onset temperature of this run raised to 340°C, as seen in Figure 4.2. The burnout progressed rapidly until the sample was at 5 ± 0.5% of initial mass. This sample still had 3 ± 0.5% mass retention at 430°C, compared to the 1 ± 0.5% of the previous run. Only toward the end, at more than 900°C, did the mass drop to 1 ± 0.5%. The lack of oxygen and the presence of TMAH, therefore, increases the onset temperature and the rate of decomposition. In addition, higher temperature is required to reach the completion (1 ± 0.5% mass retention) of burnout.

Lastly, a sample of co-dispersion containing 18 vol.% silica and 19 vol.% Rhoplex was analyzed. These volume percentages translates to 63 wt.% silica and 34 wt.% Rhoplex after driving off the water in the co-dispersion. Since burnout is not greatly affected by the availability of oxygen, this run was performed in an air atmosphere. The heating schedule was still 1.0°C/min up to 1000°C. The onset temperature, as expected with an oxygen environment, dropped back to about 280°C. The final mass was 63 ± 1%, which corresponds with the theoretical silica content plus Rhoplex residue. Figure 4.3 contains the plot for this run.

By performing TGA on Rhoplex®HA-16 and its co-dispersion, we have deter-

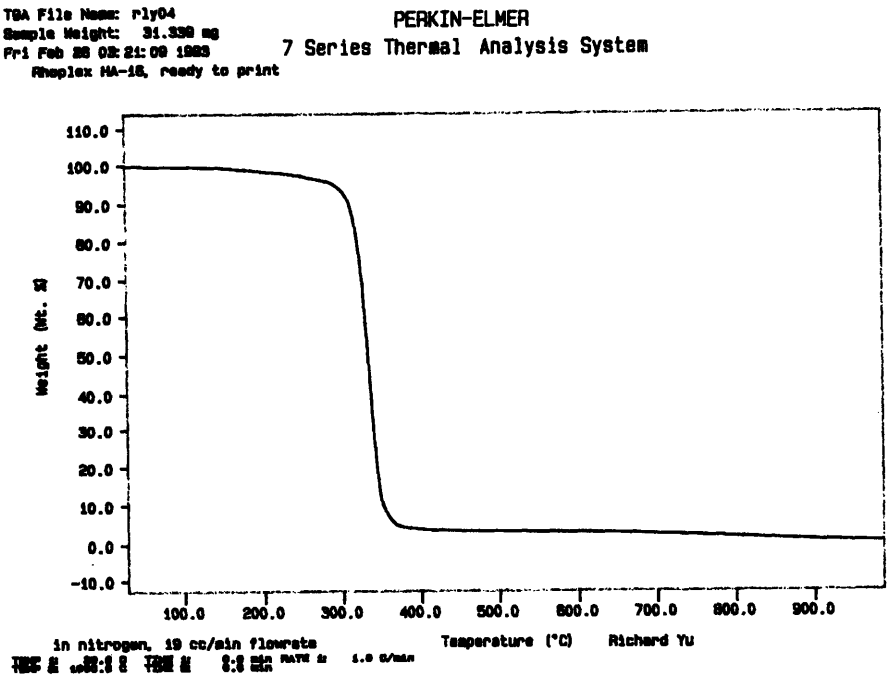

Figure 4.2: Standard Rhoplex binder for printing metal parts, TGA performed in nitrogen.

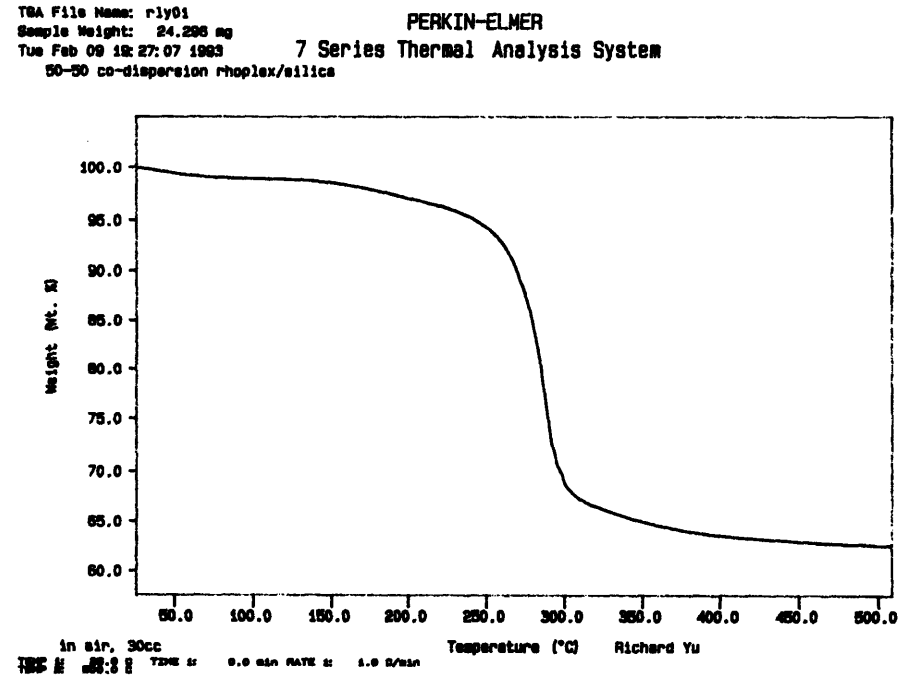

Figure 4.3: TGA of 1:1 mixture of Standard silica binder and Standard Rhoplex binder. TGA performed in air.

mined the minimum temperature for the onset of decomposition. We also learned that up to 1% of the mass of the polymer is converted into refractory residue. The availability of oxygen, although not crucial, does aid in the burnout process.

4.1.2 Firing Temperature

All of the MOR data have shown a common trend, that the fired strength of ceramic parts increases with firing temperature. This was true of the Standard silica binder, the co-dispersions of silica and acrylic, and the Ludox SK. The plot of MOR versus firing temperature for the Standard silica binder in Figure 4.4 demonstrates the rapid increase in the fired strength at higher temperatures.

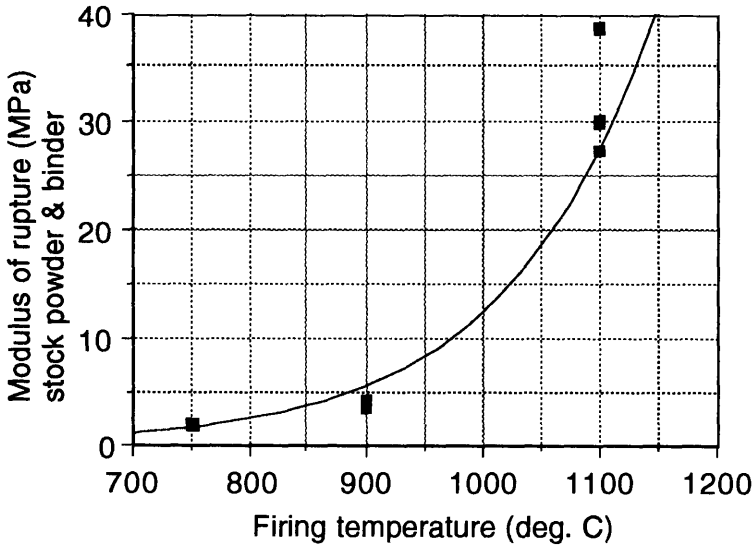

Figure 4.4: MOR vs. firing temperature for Standard binder/powder

During 1992, the accepted practice was to fire ceramic parts at 750°C. Previous powder removal considerations suggested that higher firing temperatures complicate powder removal. This was also one of the original motivations for higher green strength, which allows powder removal before firing. More recent data has refuted this conclusion, but the

practice of firing at 750°C continued due to tradition. Fired shells often cracked and broke, indicating that their fired strength was insufficient. The data presented here indicates that the fired strength can be increased from 3.5MPa to 4.0 MPa simply by increasing the firing temperature from 750°C to 900°C.

4.1.3 Conclusions on Firing

Thermo-gravimetric analysis has shown that Rhoplex will decompose at elevated temperatures. In an oxygen-rich atmosphere, the onset temperature of decomposition is around 300°C, and roughly 1% by mass residue is left after burnout. This determines the first holding temperature. We also found that the fired strength of parts can be improved by increasing the firing temperature, which sets the second holding temperature. With these results, a schedule for firing parts printed with co-dispersion of Rhoplex and silica is established. To allow proper burnout and obtain good strength, parts printed with the co-dispersion should be fired according to this schedule:

1. Heat at 1°C/minute to 300°C
2. Hold at 300°C for 2 hours for burnout
3. Resume heating, at 5°C/minute, to 900°C
4. Hold at 900°C for 2 hours for vitrification of silica

Note that prior to firing, the part should have been crosslinked at 160°C and undergone powder removal.

4.2 Powder Removal

An essential step in creating casting shells with 3D Printing is removing unprinted powder from the internal cavities. Any powder left in the shell will result in casting defects. As the complexity of the casting increases, so does the intricacy of the casting cavity and the difficulty of powder removal.

Normally, shells are fired with unbound powder still inside the casting cavities. The

bulk of the loose powder is then extracted using a vacuum. The last remaining powder in the unreachable areas of the cavity is removed by a microwave boiling technique.

4.2.1 Microwave Boiling

In microwave boiling, the casting shell is placed in a beaker of distilled water. A drop of dishwashing detergent is added to the water and then heated in a microwave oven until the water boils. As the water inside the cavities begins to boil, water vapor bubbles loosen the unbound powder and forces it out of the cavity. The soap is believed to act as a lubricant to help the passage of loose powder out of the cavity.

Microwave heating is used because conventional heating of the water bath will not boil the water inside the shell, since walls of the ceramic shell are good thermal insulators. Microwave energy can pass through ceramic to reach the water inside of the cavity.

After boiling for ten minutes, the shell is cooled and washed to remove residual soap. The shell is dried by heating in a conventional oven at 90°C for a few hours. Depending on the complexity of the shell, two to three repetitions of boiling will satisfactorily remove all unbound powder.

4.2.2 Temperature Considerations

Although microwave boiling works well for casting shells printed with the standard silica binder, it is not suitable for co-dispersions. Powder removal for a shell printed with co-dispersion is performed between crosslinking and firing. Although strong and water-resistant, crosslinked Rhoplex polymers have a glass transition temperature (T_g) of only 35°C. This means that the polymer will soften when subjected to boiling water, resulting in dimensional distortions.

4.2.3 Soda Water Technique

Since boiling is merely a means of generating bubbles inside the shell, we tried to

devise a low-temperature alternative. A can of soda-pop inspired the idea of using carbonated water to remove unbound powder in shells printed with co-dispersion. A special part was used to test this idea. Shown in Figure 4.5, this test part has four channels that are 2.64" long, 0.188" tall, and have varying widths of 0.080", 0.060", 0.040", and 0.020". The idea of the decreasing widths is to create increasingly difficult passages for powder removal. Samples of this part were printed with a co-dispersion containing 10 vol.% Rhoplex and 18 vol.% silica.

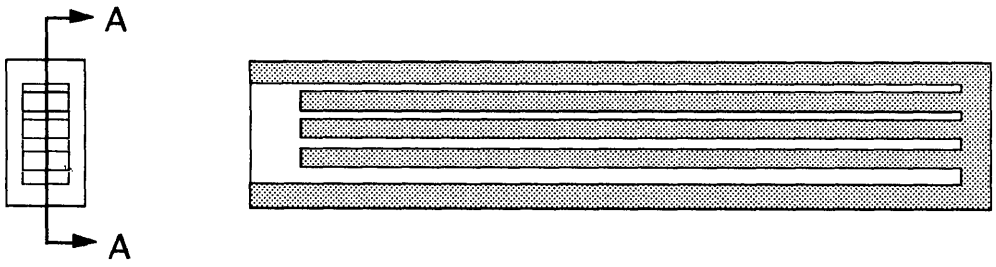

Figure 4.5: First part for testing powder removal

After crosslinking at 160°C, powder removal was performed by the "soda water" technique. A part was placed in a beaker, and 500mL of a sodium-free seltzer water was poured over the part. The opening of the part faced up so that the evolving bubbles of CO_2 are visible. To increase bubble formation, the beaker is vibrated in a Sonicor ultrasonicator. When this depleted the carbonation in the seltzer, the part was removed and the process repeated with fresh seltzer.

The technique was not very effective, especially on the 0.020" channel. A tin casting made from the part revealed that the majority of unbound powder remained in the smallest slot.

4.2.4 Refinements

Jain Charnnarong and Mark Grodzinsky have developed the concept of powder re-

moval with carbonated water into a useable technology. To increase the evolution of CO_2 bubbles, a vacuum was employed. A schematic of the setup is shown in Figure 4.6. The part is placed into the vacuum chamber and 1000 mL of fresh seltzer water is added. With the valve to the vacuum chamber closed, the pump evacuates the reservoir down to 29 inches of mercury (in.Hg). The valve between the pump and the reservoir is shut, and the valve to the chamber is opened. The sudden drop in pressure causes rapid formation of large quantities of CO_2 bubbles in the soda water. Unbound powder in the parts is blown out of the internal cavities by these bubbles.

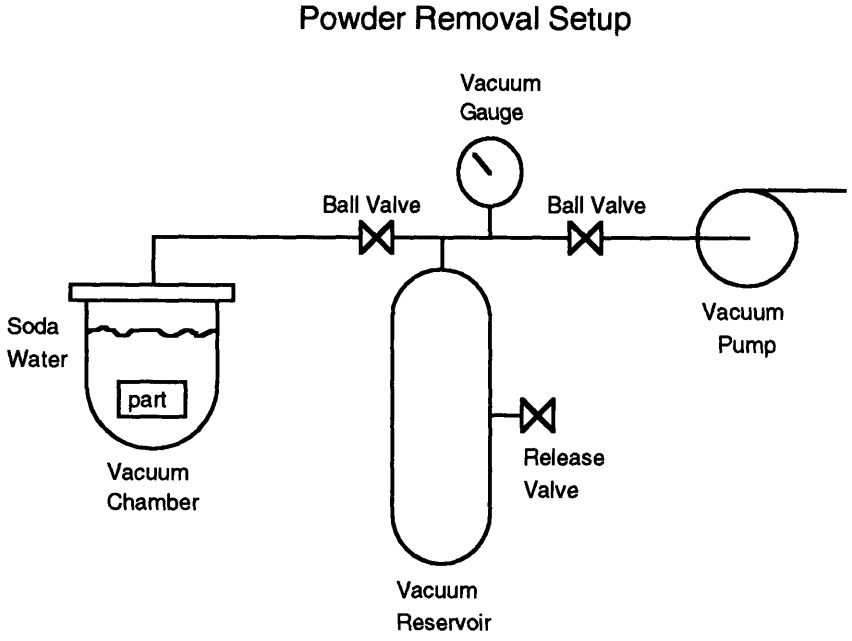

Figure 4.6: Schematic of powder removal setup using soda water

In the development of this process, a custom test shell was designed. This part incorporates long, skinny slots with a zig-zagging channel. A horizontal section of this part is shown in Figure 4.7. The slots are 0.170" long and have varying widths of 0.014", 0.028", and 0.035". The zig-zagging channel is 0.035" width throughout. The ingenious feature of this part was a top that was only attached by a thin strip of printed powder. This made the top easily removable to allow inspection of the slots. The extent of powder removal is

judged by the amount of powder remaining.

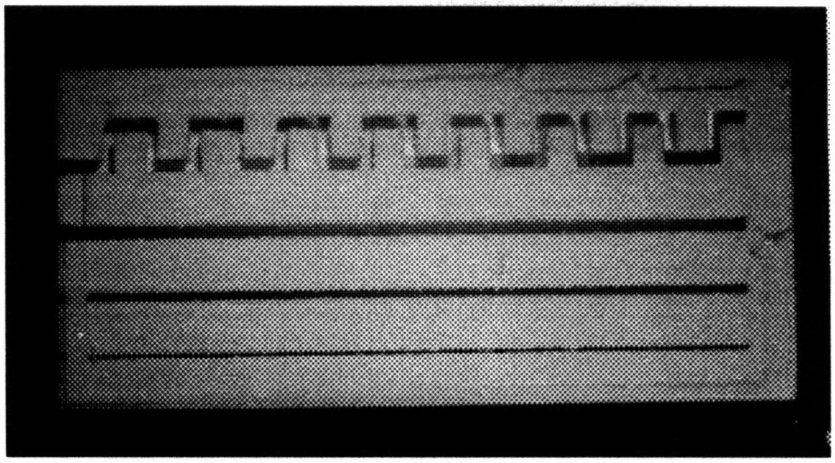

Figure 4.7: Picture of the new powder removal part showing the internal channels. This part was printed with the Standard silica binder in 7920 powder containing 0.5% citric acid.

Samples of the powder removal part were printed with a co-dispersion containing 10 vol.% Rhoplex and 18 vol.% silica. The soda water technique worked well for these parts. Powder removal was thorough, and there were no visible distortions from glass transition. Compare the photographs of parts after the soda water treatment, shown in Figure 4.8 and Figure 4.9, to the part in Figure 4.7. The part in Figure 4.7 was printed using the Standard silica binder and exhibits complete powder removal. The parts in Figure 4.8 and Figure 4.9 were printed with the same 10% Rhoplex-18% silica co-dispersion but the citric acid content of the powder was varied. The part with less citric acid was expected to suffer more bleeding, therefore making it more difficult for powder removal. The photographs, however, reveal that the soda water technique is able to effectively remove unbound powder from both of the co-dispersion parts.

In conclusion, the addition of vacuum to the soda water technique creates a viable method of removing unprinted powder from shells printed with co-dispersion.

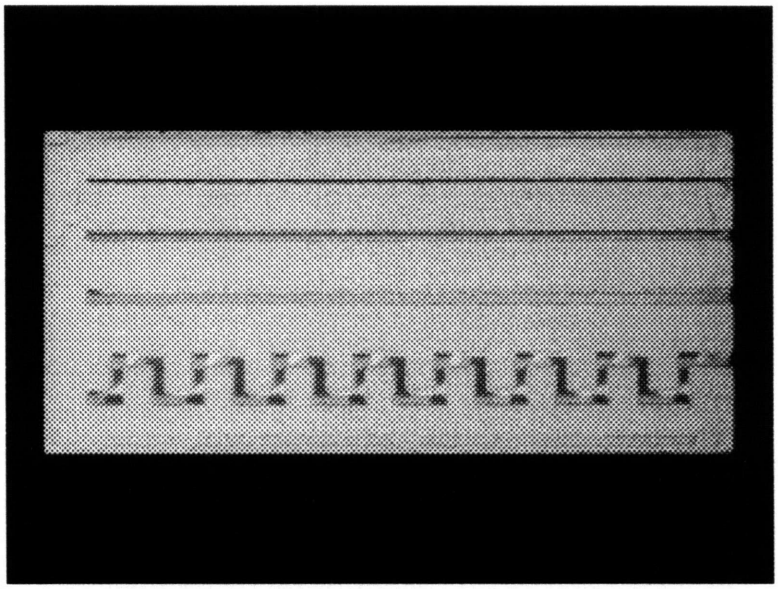

Figure 4.8: Powder removal part printed using co-dispersion in powder with 0.3% citric acid

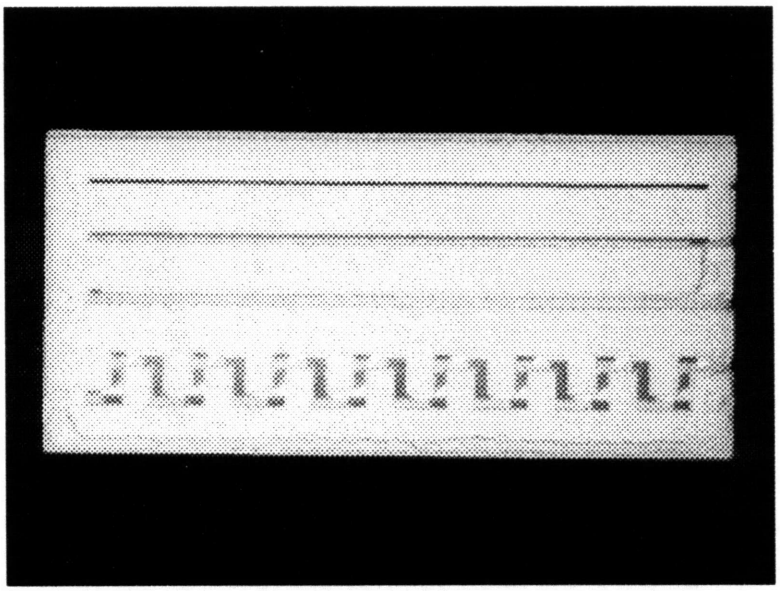

Figure 4.9: Powder removal part printed using co-dispersion in powder with 0.5% citric acid

Chapter 5

Dimensional Control

A common requirement of the various applications of Three Dimensional Printing is the ability to accurately produce the geometry and dimensions of a specified part. This is crucial for ceramic casting shells since it is not possible to modify the casting cavity after printing. Factors contributing to loss of accuracy in parts made by 3D Printing can be broken into two categories: errors occurring during printing and errors developed during post processing. On-going effort is reducing the first type of inaccuracies, which stem from the limitations of the 3DP machine and the physics of the printing process. This chapter presents a preliminary look into the errors that occur during post processing, with an emphasis on benchmarking co-dispersion binders.

Post processing of casting shells includes drying, crosslinking (for co-dispersion binders), powder removal, firing, and second firing after post dipping. While these steps are necessary to strengthen and prepare the shell for metal pouring, they also cause errors in dimension and geometry. The three types of errors investigated here are shrinkage, warping, and drooping.

5.1 Shrinkage

Shrinkage is reduction in the linear dimensions of parts. It is undesirable since it leads to lost of dimensional accuracy and distortion. Severe shrinking can also cause parts to warp, crack, and delaminate.

Past and continuing research on shrinkage in 3DP parts provided a foundation for the work presented here. In 1990, Marcos Esterman Jr. reported measuring more shrinkage in plates fired to 1500°C than in those fired to 1000°C [Esterman 1990]. Using a Pratt & Whitney Supermicrometer, Chris Harris measure 1.42% shrinkage in three parts fired to 1500°C [Harris 1991].

A more in depth look by Khalil Sardouk with a larger sample size discovered 0.2-0.3% linear shrinkage in fired bars. Made by a contact method using calipers, these measurements suffer from noise [Sardouk 1993]. Nonetheless, this provided a start for continuing research on shrinkage in silica/alumina parts.

A step in the development of co-dispersed binders for 3D Printing is an investigation in to the shrinkage of these parts and a comparison to the benchmark set by the Standard silica binder.

5.1.1 Contributing Factors

Shrinking of ceramic 3DP components occur during several stages of post processing. Immediately after printing, the part is saturated with binder. This allows particle rearrangement since the liquid acts as a lubricant between particles. Therefore the initial packing density of the powder bed can be a factor in shrinking. At this point, dissolution of citric acid (added to induce gelling of the binder) in the powder can also contribute to shrinkage. The combined effect may be comparable to the shrinkage from the following steps in post processing.

DRYING

A large amount of shrinkage occurs during drying. As water evaporates from the parts, the partially saturated pores can exhibit either a funicular or pendular structure. The first state of drying is indicated by a funicular structure in which there is a connected network of fluid with interlacing vapor capillaries. The pendular bond, where a ring of binder exists at the necks between particles, is predominant at binder saturations of less than 24 percent [German 1990]. The Laplace equation for the pressure change across a curved surface is

$$\Delta P = \gamma_{LV} \cdot \left(\frac{1}{R_1} + \frac{1}{R_2} \right) \tag{5.1}$$

where ΔP is the pressure change across the surface, γ_{LV} is the surface energy, and R_1 and R_2 are the principal radii of curvature at a point on the surface. It is the formation of small radius pendular bonds in the later stages of drying that causes large pressure differences and capillary forces.

The binder/powder system in 3DP is designed with low contact angles to promote wetting. At low contact angles, capillary forces develop in the pendular bonds. To minimize the liquid-vapor interface and maximize the liquid-solid surface area, the particles are attracted towards one another until they contact. Surface energy is minimized in this configuration. Capillary forces induce particles to rearrange into a more densely packed structure. Therefore higher initial packing density in the dry powder bed can reduce shrinkage.

Higher solids loading in the binder will increase the density of the green body, thus reducing shrinkage during drying. Another possible contributor to shrinkage is densification of colloidal silica and polymer particles in the necks upon drying.

CROSSLINKING

A step necessitated by co-dispersion binders is crosslinking. Although heating to 160°C causes thermal expansion, molecular rearrangement during crosslinking may actu-

ally densify the polymer. This may shrink the interparticle necks and the part as a whole.

FIRING

Additional shrinkage develops during higher temperature firing from decomposition of organic materials and sintering of silica particles. The organics in the part, such as Rhoplex polymers and citric acid, thermally decompose at high temperatures. The loss of these materials may cause porosities, and subsequent shrinkage. More significantly, densification of the necks during sintering of silica can produce shrinkage comparable to that caused by drying.

POST DIPPING & SECOND FIRING

After firing, casting shells are reinforced by adding silica. Dipping in colloidal silica infiltrates the shell, and a second high temperature firing bonds the silica. More shrinkage can result from densification of the additional silica.

5.1.2 Experimental Procedure

Research to understand and reduce shrinkage in 3D Printing is currently being conducted by Jain Charnnarong. To allow comparison of data, the same experimental procedure was used to study co-dispersions.

A set of 50 bars were designed to allow non-contact measurement of length. These bar are 0.375" wide, 0.210" thick, and have five different lengths. The are printed so that the longitudinal axes of the bars are parallel to the slow axis. On the top four layers, a line is skipped at each end of the bars so that slots are formed (see Figure 5.1). These slots act as length markers and have separations of 0.1309", 0.3720", 0.7441", 1.9980" and 3.9961".

Sets of bars were printed using a co-dispersion containing 17 volume percent (vol.%) silica and 10 vol.% Rhoplex HA-16 polymer. The powder was Norton 7920 Electronic Grade alumina, which has 28 μm platelet shaped particles. Two different citric acid percentages, 0.3 and 0.5 (wt.%), were added to the powder to examine the effect of citric acid dissolution. A set of bars was also printed with a 10 vol.% Rhoplex binder in powder

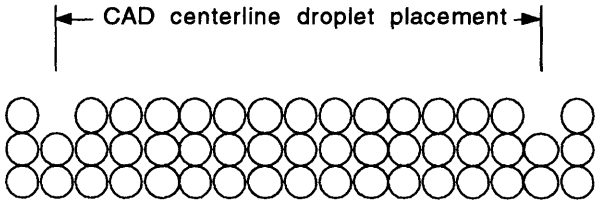

Figure 5.1: Schematic view of a side section of shrinkage bars with markers. The circles represent cross-sections of the individual lines. Notice the missing lines that act as markers.

containing 0.5 wt.% acid.

Printing was done on the Alpha 3DP machine, which has a larger printing area to accommodates the size of the bars. The Alpha machine is also faster and more accurate than the proto 3DP machine. The binder flowrate was kept between 1.2 ml/min. to 1.3 ml/min. Standard printing parameters were used, including misting the powder bed with the humidifier set at "30%" of maximum output (this number is subject to the opinion of the machine operator). The line width and layer thickness were both set at 0.170 mm, and the scan speed of the printhead was 1.5 m/sec.

An optical measuring system was used to measure the distance between the centering of the markers. This is preferable to contacting measurements due to higher accuracy and repeatability, as well as being non-destructive. A CCD video camera was mounted to a Brown & Sharp MicroVal PFx coordinate measuring machine. Crosshairs on the video monitor were used to find the center of the markers and the coordinates were recorded. Some estimating was necessary because the markers are sometimes irregular or hard to see, but the results are far superior to that of contacting methods.

Within 5 minutes after printing, the length of the marked bars was measured. This provides the shrinkage in the green, or "wet" condition. The bars were measured again after drying at 75°C for at least three hours. More measurements were made after crosslinking at 160°C for 30 minutes and firing at 900°C for 2 hours. Lastly, the bars were post

dipped in a 1:3 Nyacol 830 to water mixture, re-fired to 900°C, and measured. The bars printed with Rhoplex binder were only taken through crosslinking, since firing would leave them binderless.

5.1.3 Results

The results of the length measurements are shown in the graphs below. Lines were fitted to the data to bring out the trends. Due to the amount of scatter in the data, higher order curve fitting was inappropriate. The plots differentiate the amount of shrinkage developed in each step of post processing. For clarity, we will only refer to the longest sample (3.996") in the following discussion and quoted percentages.

Figure 5.2 shows that about 0.4% linear shrinkage develops after crosslinking in the 3.996" bars printed with co-dispersion in powder with 0.3 wt.% citric acid. The bars lose an additional 0.1% length during firing for a total shrinkage of 0.5%. Post dipping and second firing shrinks the bars another 0.1%.

Data for bars printed with standard silica binder and otherwise identical conditions is shown in Figure 5.3 [Charnnarong 1994]. In contrast to co-dispersion, the 3.996" bars in this case only shrank 0.2% after drying. They incurred an additional 0.12% shrinkage during the first firing and 0.06% during the second firing. Total shrinkage was 0.38% compared with 0.6% of the co-dispersion.

Figure 5.4 and Figure 5.5 are bars printed in powder with 0.5% citric acid using co-dispersion and standard silica binder, respectively. The 3.996" samples of the co-dispersion bars shrank 0.42% after crosslinking. By comparison, the silica bars only had 0.28% shrinkage after drying. Both the first and second firings added 0.1% shrinkage to the co-dispersion bars for a total of 0.62% linear shrinkage. The bars printed with silica shrank 0.14% during firing and 0.08% during second firing for a total of 0.5%. The shrinkage data is summarized in Table 5.1.

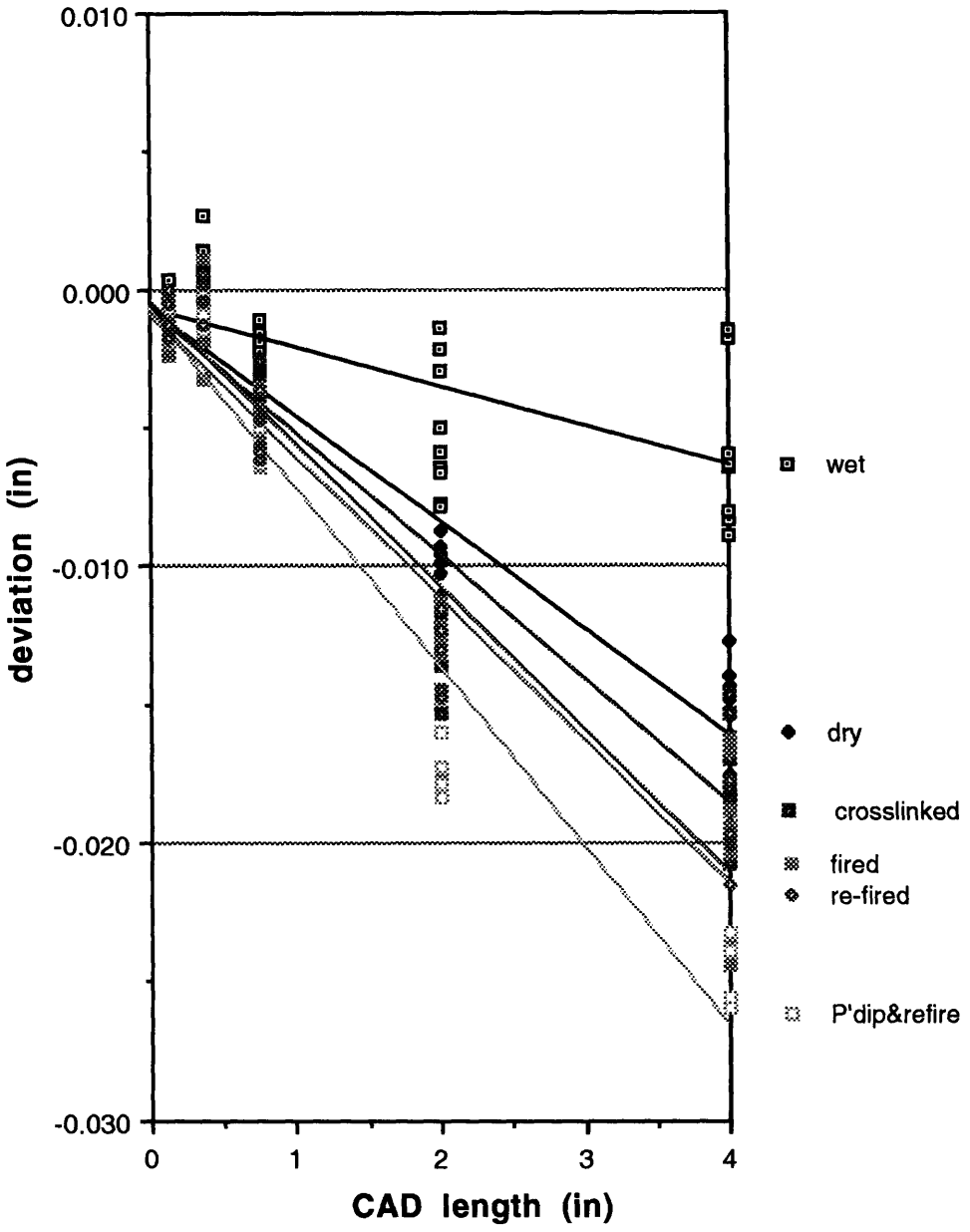

Figure 5.2: Shrinkage of bars printed with 10-17 vol.% Rhoplex-silica co-dispersion in powder with 0.3 wt.% citric acid. Shrinkage occurs in each step of post processing: drying, crosslinking, firing, and second firing. Crosslinking is at 160°C for 30 minutes, and both firings are at 900°C for two hours.

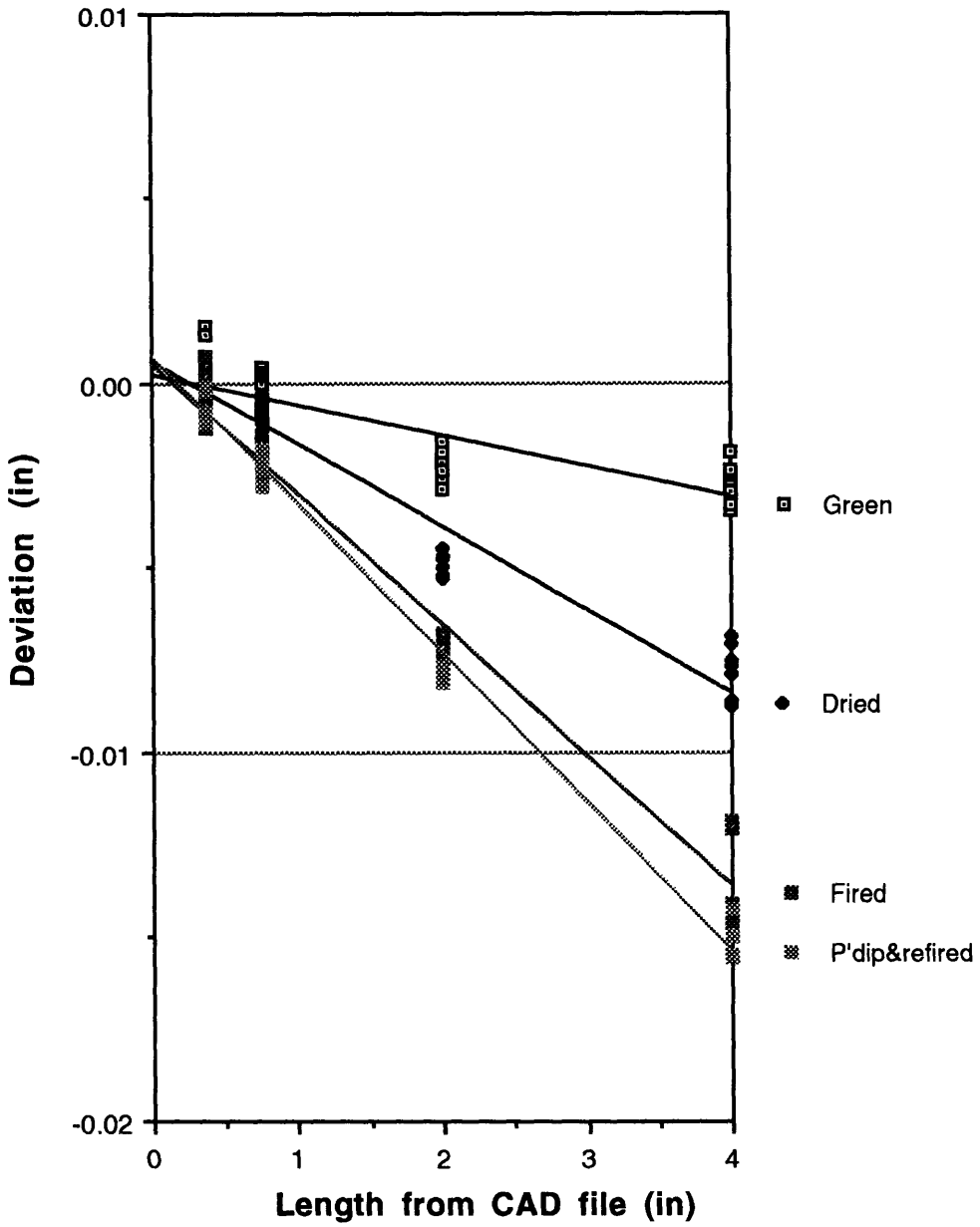

Figure 5.3: Shrinkage of bars printed with Standard silica binder in powder with 0.3 wt.% citric acid. Shrinkage is shown for bars in the green, dried, fired, and second fired conditions. Drying is at 75°C for at least 3 hours, and both firings are at 900°C for two hours.

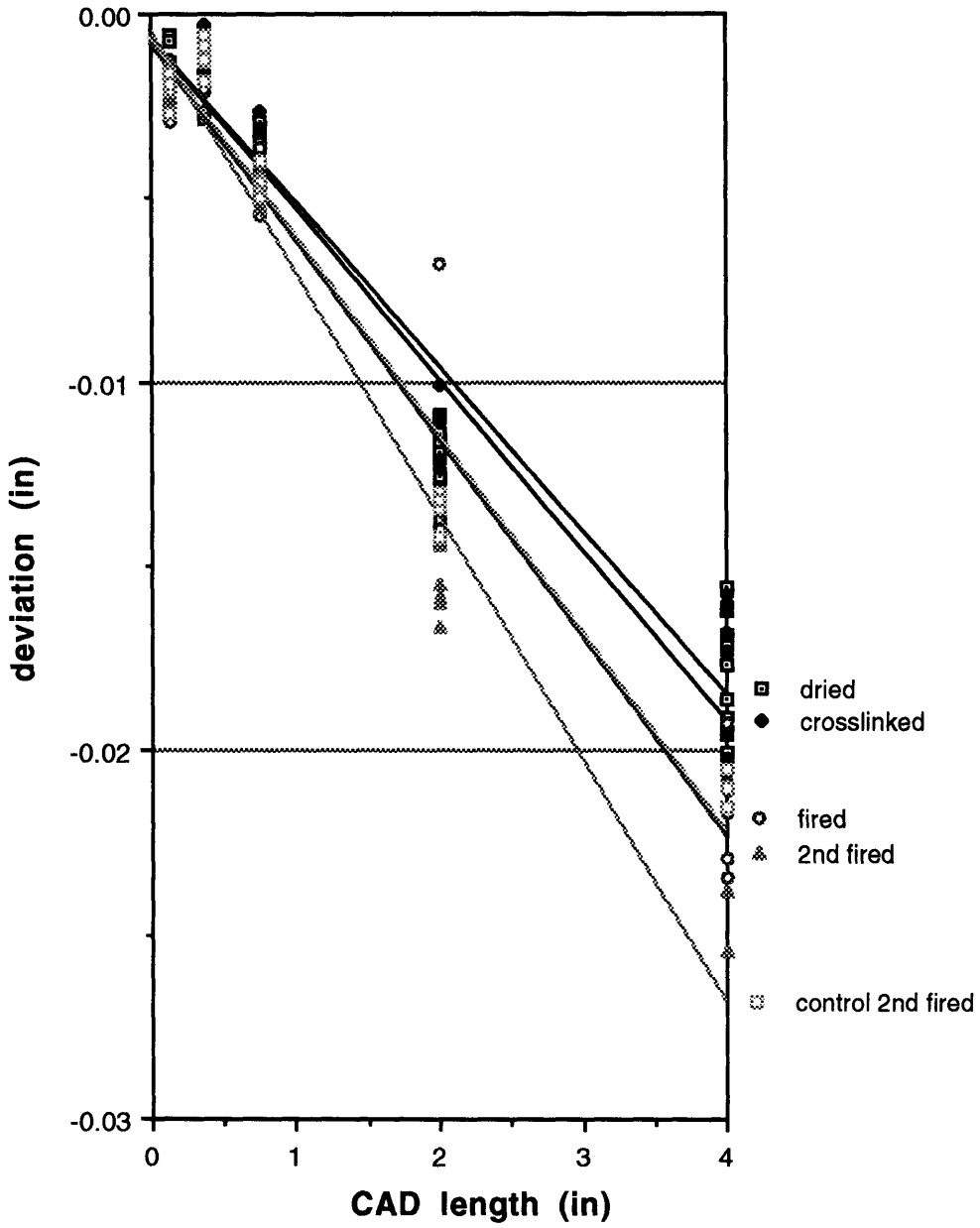

Figure 5.4: Shrinkage of bars printed with 10-17 vol.% Rhoplex-silica co-dispersion in powder with 0.5 wt.% citric acid. Shrinkage from each of the processing steps, drying, crosslinking, firing, and second firing are shown.

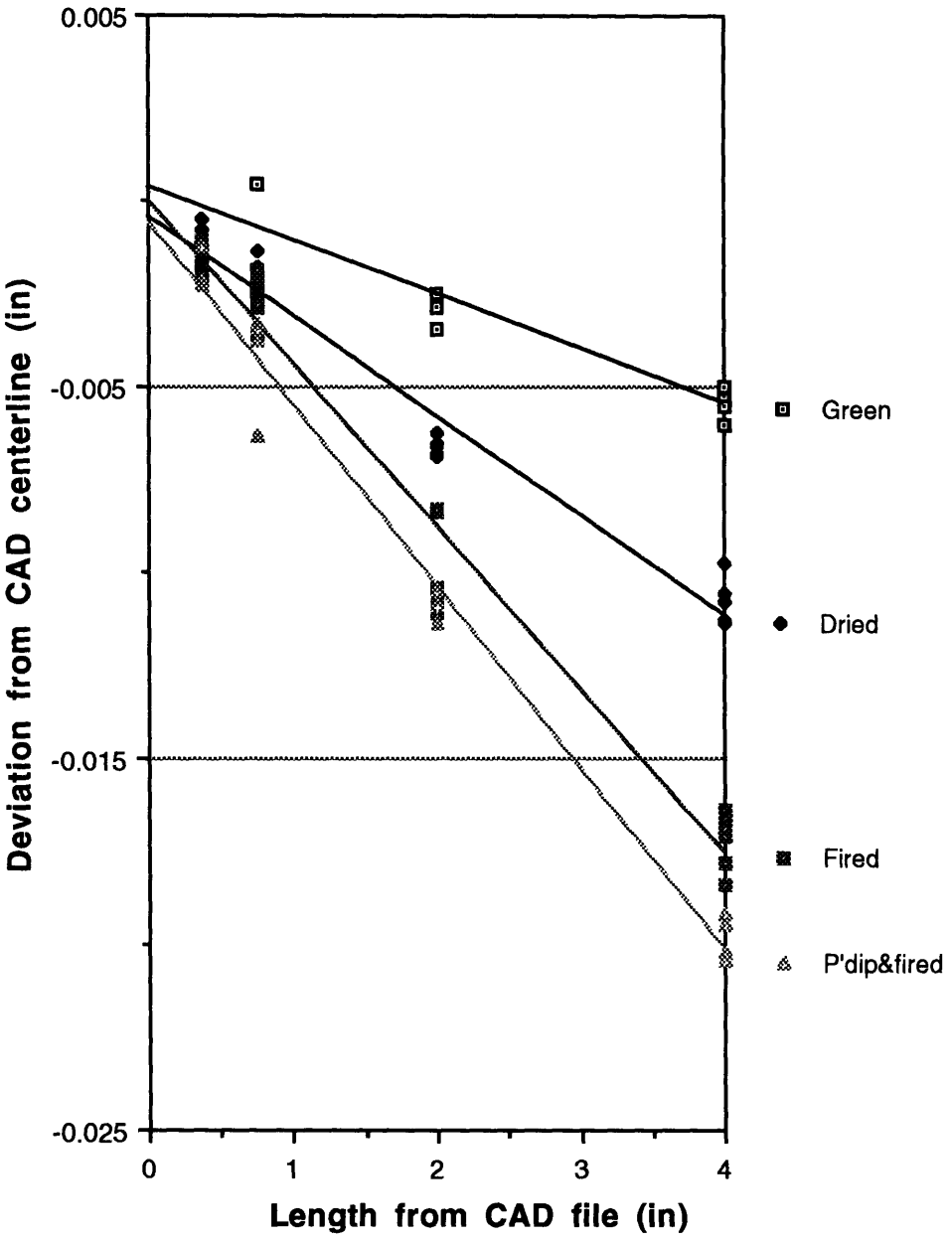

Figure 5.5: Shrinkage of bars printed with Standard silica binder in powder with 0.5 wt.% citric acid. Shrinkage is shown for bars in the green, dried, fired, and second fired conditions. Drying is at 75°C for at least 3 hours, and both firings are at 900°C for two hours.

Table 5.1: Percent shrinkage broken down by process step

Binder	% acid	drying	x-link	fired	2nd fired	total
co-disp	0.3	0.35	0.05	0.1	0.1	0.6
silica	0.3	0.2	N/A	0.12	0.06	0.38
co-disp	0.5	0.38	0.05	0.1	0.1	0.62
silica	0.5	0.28	N/A	0.14	0.08	0.5
Rhoplex	0.5	0.0	0.05	N/A	N/A	0.05

Increasing citric acid content caused shrinkage in the bars printed with silica binder to increase from 0.38% to 0.50%. The co-dispersion bars, however, was not affected by the increase in citric acid. Figure 5.6 is compares shrinkage after firing between the two citric acid levels for bars printed with co-dispersion.

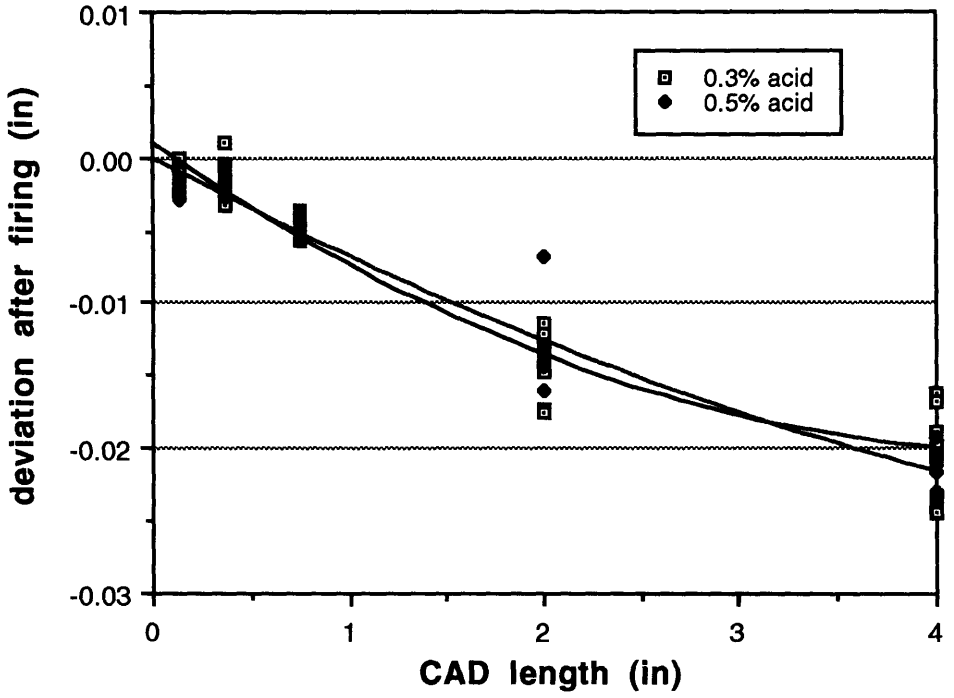

Figure 5.6: Shrinkage after firing in bars printed with co-dispersion (10% Rhoplex-18% silica) in powder with 0.3 wt.% compared to bars printed in 0.5 wt.% citric acid. The shrinkage of bars printed with co-dispersion is not affected by citric content.

Figure 5.7 shows the shrinkage, or lack of, for bars printed with Rhoplex HA-16 binder containing 10 vol.% solids. No shrinking occurred in drying. After crosslinking a 160°C, the bars only shrank 0.05%. Since co-dispersion bars shrank much more in drying than silica bars, the absence of shrinkage in Rhoplex bars was quite surprising.

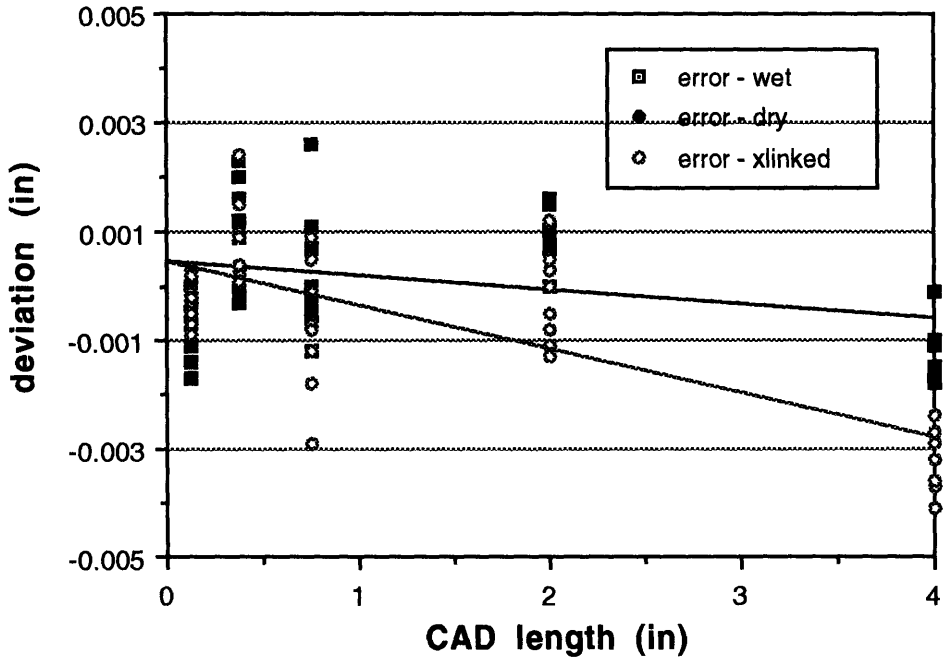

Figure 5.7: Shrinkage of bars printed with the Standard Rhoplex binder. The lines for the wet and the dried data are overlapping. There is very little shrinkage in crosslinked Rhoplex bars.

5.1.4 Conclusions on Shrinking

The co-dispersed binder resulted in an increase in overall shrinkage. The majority of the increase occurs during drying and crosslinking (0.4%), leading us to suspect Rhoplex as the cause. Printing bars with Rhoplex binder showed that they only shrank 0.05% after crosslinking. The combination of silica and polymer seems to have a synergistic effect in terms of shrinkage.

Increasing citric acid content of the powder, while dramatically increasing shrinkage in bars printed with silica binder, does not affect bars printed with co-dispersions.

Additional work is required to understand the fundamental causes of shrinkage and to reduce its magnitude.

5.2 Warping

An issue related to and possibly caused by shrinkage, warping is the distortion of 3DP parts so that planar elements are no longer planar. Warping can occur within a layer or perpendicular to them. It is undesirable due to the resulting loss of dimensional accuracy. Excessive warping can reduce the strength of shells and even lead to cracking or delamination.

Factors that contribute to shrinking, such as evaporation of binder liquid, capillary forces, and dissolution of citric acid, are suspected to also promote warping. In fact, shrinkage itself can lead to warping. Scherer has shown that the a plate of gel drying by evaporation from one side becomes concave towards the direction of evaporation [Scherer 1986]. The top surface experience the highest evaporation rate and therefore contracts the fastest, resulting in an upward curvature. A similar mechanism is at work in the warping of 3DP components.

Up to now, warping was an issue that has received little attention in 3D Printing. This section presents a preliminary look into the warping of alumina parts printed with the standard silica binder and with the co-dispersion binder.

5.2.1 Working Model

Warping of parts made by 3DP is an extremely complex phenomenon involving time dependent variables. The green body, consisting of alumina particles in a gel of silica, responds non-elasticly to stress. In addition, the capillary forces within the part change with time. Both of these variables depend on evaporation of water in the binder, which is

itself a complicated problem.

As first approximation, we can model warping in a plate printed by 3DP as elastic response to a uniform temperature distribution across its thickness. Thermal expansion/ contraction produces free strain, which is the same approach taken by Scherer in his first order analysis for warping in drying gels [Scherer 1986]. Assuming that the plate has a constant and uniform modulus of elasticity, the solution to a circular plate subjected to thermal free strain is

$$z = \frac{\alpha \Delta T}{2t} r^2 \tag{5.2}$$

where

z is the vertical deflection measured from the center of the plate

α is the coefficient of thermal expansion

ΔT is the temperature difference between the top and bottom surfaces

t is the thickness of the plate

and r is the radial distance from the center of the plate.

This solution has the form $z = c_1 r^2$. Substituting $r^2 = x^2+y^2$ into this expression reveal the equation for a ellipsoidal paraboloid.

Another model based on laminated plates is similar to the theory of bimetallic strips [Timoshenko 1925]. Once again, certain assumptions and simplifications are made. Looking at a two-dimensional "beam" made with 3D Printing, assume that the first layer dries and shrinks completely before the next layer is printed. The second assumption is that there is perfect adhesion between the layers. As the second layer shrinks, shear stresses are induced on the top surface of the previous layer. Summing the distributed shear into one compressive stress and translating to the neutral axis of the beam produces an axial compression along with a upward bending moment. The solution for the deflection due this loading condition, found in any basic statics reference, has the form of

$$y = c_1 x^2 \ , \tag{5.3}$$

which is the equation for a parabola. Extending this line of thinking to three-dimensions, we again arrive at the paraboloid.

Both models, although simple and full of assumptions, provided the paraboloid as the first order solution to the plate warping problem.

5.2.2 Experimental Procedure

. Due to bleeding, the first or bottom layer of a part can be rough and uneven. Measurement of this surface is noisy and inaccurate. Past experience indicates that the bottom of parts tend to warp more than the top surface. To accurately gauge the extent of warping, we needed to measure the top surface of a layer near the bottom of the part. A special part was designed for this requirement. It is a 3.25" by 3.25" by 0.134" plate. Being large and thin promotes warping for easier observation. An array of 25 blind holes are centered on the plate at 0.5" intervals. The 3 mm diameter holes reach the third layer of the part. By measuring the top surface of the floors of the holes, an accurate representation of warping on the bottom of the part can be obtained. A sketch of this part can be seen in Figure 5.8.

The plates were printed in sets of three on the Alpha 3D Printing machine using both co-dispersions and standard silica binder. To see the effect of citric acid, powders containing 0.3 wt.% and 0.6 wt.% were used. Since the evaporation rate of the binder is also a contributing factor, a slightly different co-dispersion was also formulated. Instead of using the volatile ammonium hydroxide (NH_4OH) to modify pH, TRIS(hydroxymethyl) aminomethane ($C_4H_{11}NO_3$) was instead chosen for it zero vapor pressure. The combination of high acid content (0.6 wt.%) and high evaporation rate (NH_4OH) was suspected to cause the most warping. The Standard binder (18 vol.% silica) was printed into Norton 7920 powder containing 0.5 wt.% citric acid, which constitutes the standard material system for 3DP casting shells.

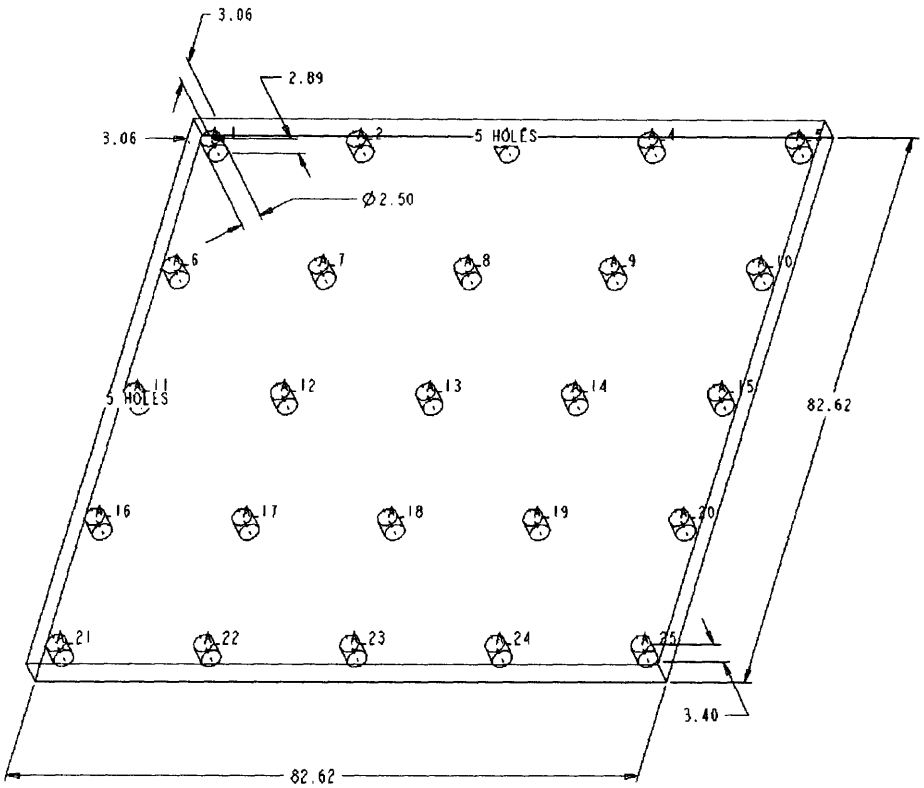

Figure 5.8: The plate used for warping measurements. All dimensions are given in millimeters

The co-dispersion plates were removed form the powder bed and crosslinked at 160°C while sitting in powder. After powder removal, the plates were measured using a Brown & Sharp MicroVal PFx coordinate measuring machine running the Micromeasure IV software. A Renishaw PH1 TP2 Touch Trigger Probe was used with a 1 mm diameter spherical ruby tip. A program was written to instruct the CMM to probe into all 25 holes and measure the vertical (z-axis) location of the tops of the floors. The co-dispersion plates were fired at 900°C while sitting on a loose bed of large zirconia grogs. They were measured after firing for additional warping.

The silica plates were fired to 900°C while fully supported in unprinted powder. After powder removal, they were similarly measured on the CMM.

5.2.3 Results

The measured coordinates were analyzed using an exploratory data analysis program call Data Desk® Professional. To simplify the analysis, the x-axis and y axis coordinates were first coded into a non-dimensional form. This gives the coefficients of regression the unit of inches without affect the results of the regression. Coding the coordinates involves subtracting the mean value of the parameter from each element, then dividing by one-half of the range of that parameter. This produced a set of non-dimensional numbers ranging from -1 to 1. For example, the coded x-axis coordinates are:

$$x_{ni} = \frac{2 \cdot (x_i - mean(x))}{range(x))} \tag{5.4}$$

The coded values can be easily converted back to actual coordinates.

The data was examined in two ways. A 3-D plot of the x, y, and z-coordinates was made to facilitate visualization of the warped surface and a linear regression was performed using Data Desk.

Based on the models presented earlier, the z-coordinates were regressed against x^2, y^2, xy, x, and y. A constant term was also calculated. This general equation

$$z = c_1 x^2 + c_2 y^2 + c_3 xy + c_4 x + c_5 y + c_6 \tag{5.5}$$

allows the paraboloid to shift in the x and y directions, rotate about the z-axis, and have elliptical horizontal sections. In the ideal case, c_1 is equal to c_2, and c_3, c_4, and c_5 are identically zero.

The regression results for the plates printed with Standard silica binder after firing at 900°C were surprisingly good. Figure 5.9 contains the regression data. The high values of R^2, adjusted R^2, and F-ratio indicate a very good fit to the paraboloid model. Since the t-ratios are small for all of the coefficients except for the x^2 and y^2 terms, the data correlates strongly with the prediction of the model.

Another confirmation of correlation can be seen in the contour plot of the parabo-

loid obtained by regression. The measured z-coordinates are superimposed on the same plot (the black dots). By comparing the measured points to the value of the contours, we can see that there is good correlation. The same observations are true for the other two samples of fired plates printed with Standard silica binder. Their contour plots and regression data are shown in Figure 5.10 and Figure 5.11.

The downside of this data for silica plates is that there is on average 0.01" of warping at 2.1" radially out from the center of the plate. This is an unexpected amount of warping.

Due to unfortunate errors in printing, data could not be collected from two sets of samples: TRIS co-dispersion binder with 0.3 wt.% citric acid and NH_4OH co-dispersion binder with 0.6 wt.% citric acid. Lacking data to complete the experimental matrix, the intended study into the effects of citric acid dissolution and evaporation rate could not be completed.

The contour plots and regression data for plates printed with TRIS co-dispersion in powder containing 0.6 wt.% citric acid after crosslinking are shown in Figure 5.12 through Figure 5.14. Unlike the silica plates, the measured z-coordinates are less indicative of a paraboloid. This is reflected by the regression results. The maximum warpage at 2.1" from the center is about 0.007".

The same lack of fit in regression was true for plates printed with co-dispersion containing ammonium hydroxide in powder containing 0.3 wt.% citric acid after crosslinking. The maximum warping was reduced to 0.006", but the parabolic shape is not as readily apparent. Figure 5.15 and Figure 5.16 contain the contour plots and regression results for these samples.

The plates printed with TRIS co-dispersion were fired at 900°C. The maximum warping increased to 0.014", 0.017", and 0.0097" for the three plates. The fit of the linear regression improved, as indicated by higher confidence factors. The data is shown in Figure 5.17 through Figure 5.19. The fact that the linear regression provides better fit after

Dependent variable is: **zn**
R□ = 94.1% R□(adjusted) = 92.6%
s = 0.0008 with 25 - 6 = 19 degrees of freedom

Source	Sum of Squares	df	Mean Square	F-ratio
Regression	0.000196	5	0.000039	60.9
Residual	0.000012	19	0.000001	

Variable	Coefficient	s.e. of Coeff	t-ratio
Constant	-0.000018	0.0003	-0.058
xn	0.000076	0.0002	0.335
yn	-0.000516	0.0002	-2.27
xn^2	0.005183	0.0004	13.5
yn^2	0.004086	0.0004	10.6
xy	0.000596	0.0003	1.86

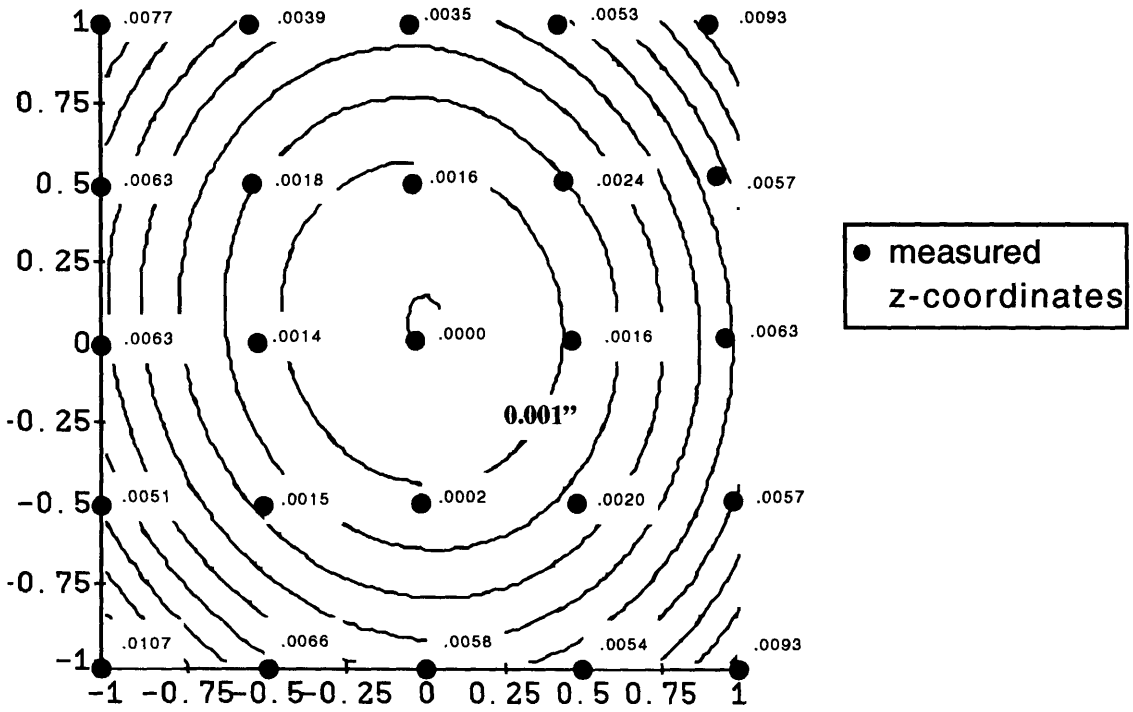

Figure 5.9: Contour plot and regression data for silica plate, fired at 900°C, sample #1 (right side of powder bed). The contour levels start at 0.000" and have 0.001" increments. The 0.001" contour level is so indicated on the contour plot.

Dependent variable is: z
R□ = 92.4% R□(adjusted) = 90.4%
s = 0.0010 with 25 - 6 = 19 degrees of freedom

Source	Sum of Squares	df	Mean Square	F-ratio
Regression	0.000219	5	0.000044	46.3
Residual	0.000018	19	0.000001	

Variable	Coefficient	s.e. of Coeff	t-ratio
Constant	-0.000434	0.0004	-1.13
xn	-0.000412	0.0003	-1.50
yn	-0.000740	0.0003	-2.69
xn^2	0.004966	0.0005	10.7
yn^2	0.004806	0.0005	10.3
xn*yn	-0.000472	0.0004	-1.21

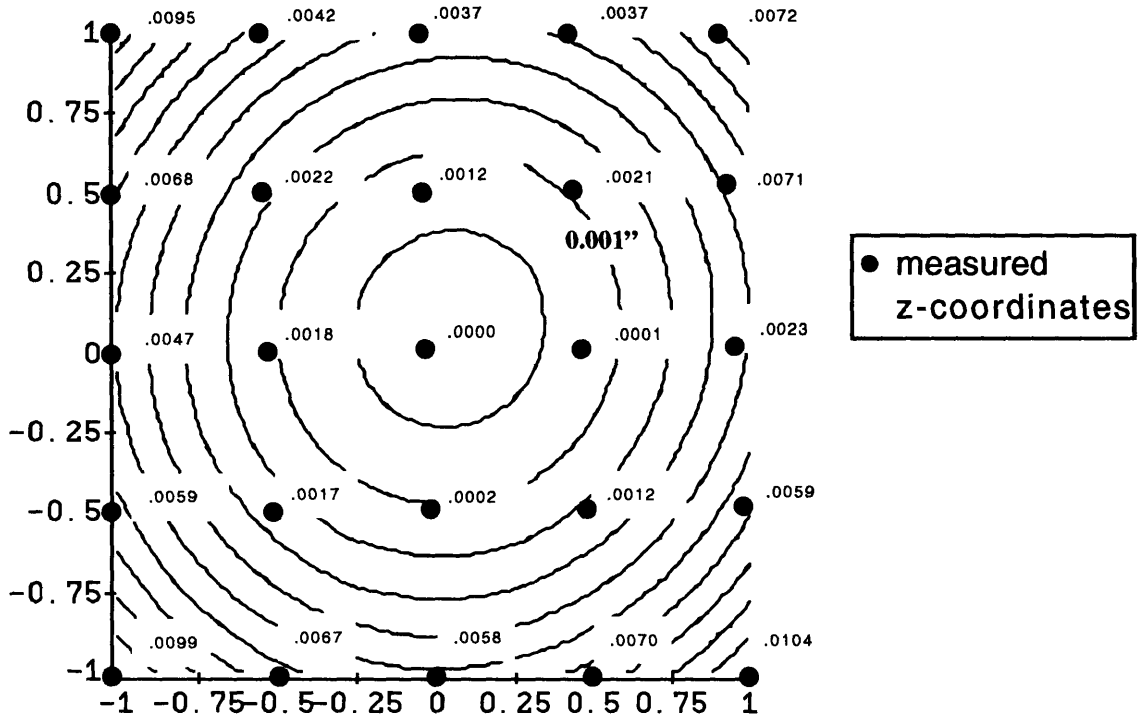

Figure 5.10: Contour plot and regression data for silica plate, fired at 900°C, sample #2 (middle of powder bed). The contour levels start at 0.000" and have 0.001" increments. The 0.001" contour level is so indicated on the contour plot.

Dependent variable is: z
R¤ = 95.9% R¤(adjusted) = 94.8%
s = 0.0008 with 25 - 6 = 19 degrees of freedom

Source	Sum of Squares	df	Mean Square	F-ratio
Regression	0.000260	5	0.000052	89.0
Residual	0.000011	19	0.000001	

Variable	Coefficient	s.e. of Coeff	t-ratio
Constant	-0.000940	0.0003	-3.13
xn	-0.000208	0.0002	-0.962
yn	0.000636	0.0002	2.94
xn^2	0.005154	0.0004	14.1
yn^2	0.005606	0.0004	15.3
xn*yn	0.000352	0.0003	1.15

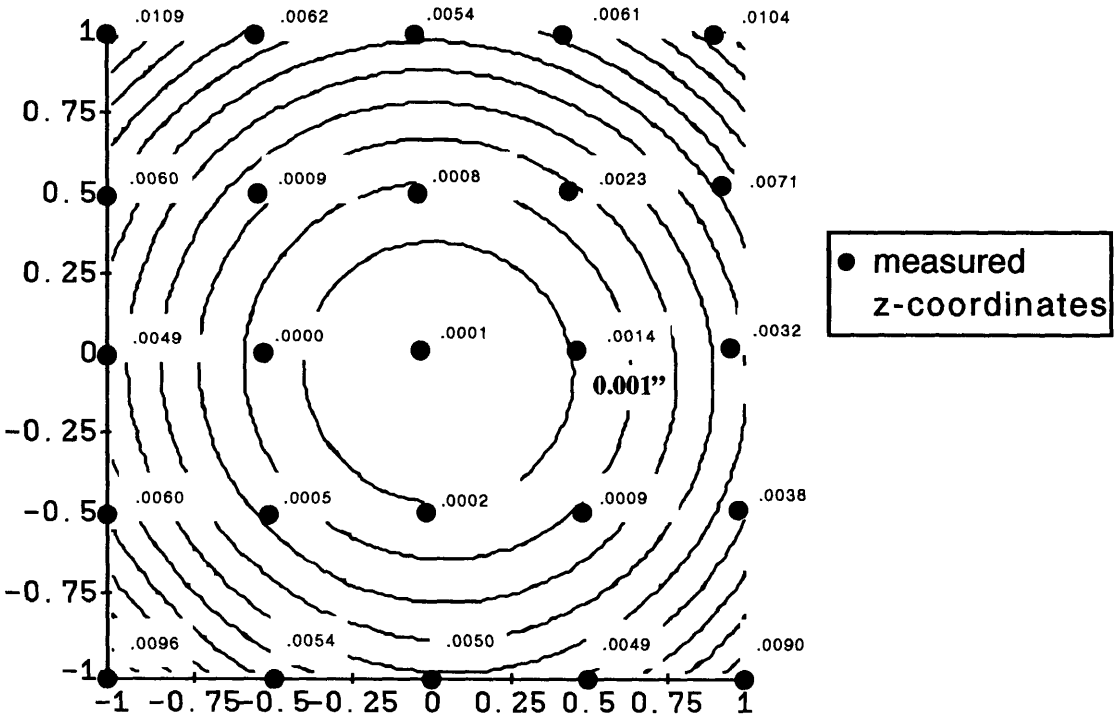

Figure 5.11: Contour plot and regression data for silica plate, fired at 900°C, sample #3 (left side of the powder bed). The contour levels start at 0.000" and have 0.001" increments. The 0.001" contour level is so indicated on the contour plot.

Dependent variable is: z
R² = 61.5% R²(adjusted) = 51.3%
s = 0.0013 with 25 - 6 = 19 degrees of freedom

Source	Sum of Squares	df	Mean Square	F-ratio
Regression	0.000047	5	0.000009	6.07
Residual	0.000030	19	0.000002	

Variable	Coefficient	s.e. of Coeff	t-ratio
Constant	0.001877	0.0005	3.82
xn	0.000292	0.0004	0.825
yn	0.000340	0.0004	0.961
xn^2	0.002863	0.0006	4.79
yn^2	0.001400	0.0006	2.34
xn*yn	-0.000292	0.0005	-0.583

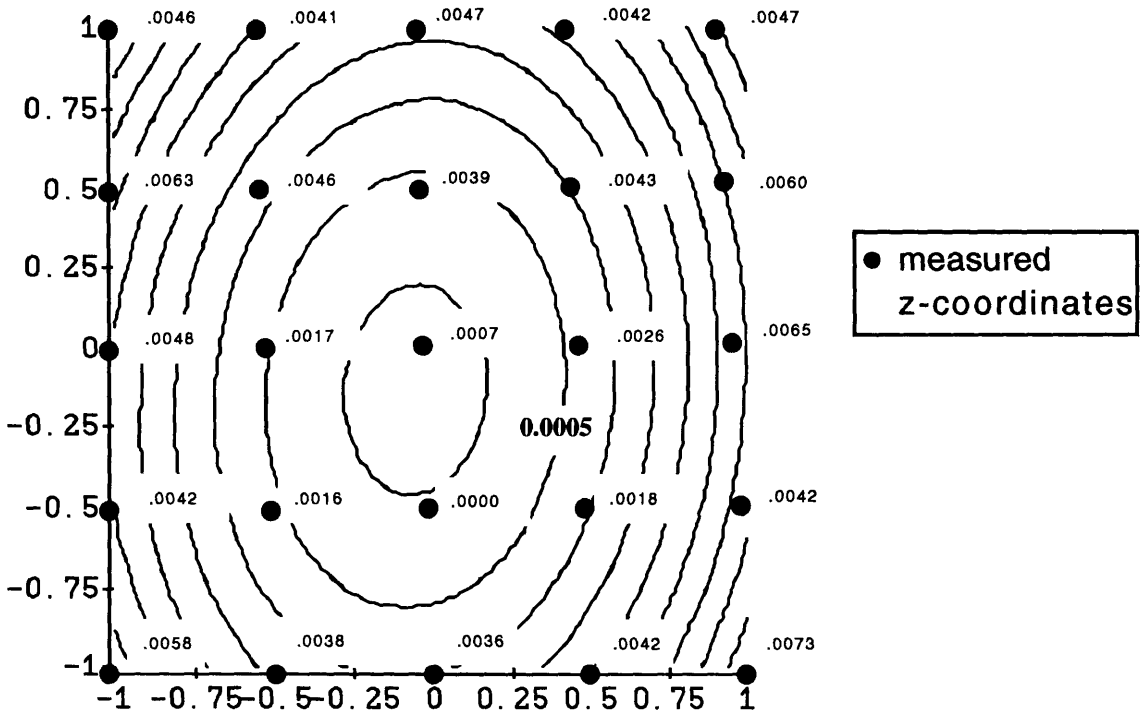

Figure 5.12: Contour plot and regression data for TRIS co-dispersion plate, crosslinked at 160°C, sample #1 (right side of powder bed). The contour levels start at 0.0000" and increase by 0.0005" increments. The 0.0005" contour level is so indicated on the contour plot.

Dependent variable is: z
R¤ = 75.4% R¤(adjusted) = 68.9%
s = 0.0011 with 25 - 6 = 19 degrees of freedom

Source	Sum of Squares	df	Mean Square	F-ratio
Regression	0.000069	5	0.000014	11.6
Residual	0.000023	19	0.000001	

Variable	Coefficient	s.e. of Coeff	t-ratio
Constant	0.001655	0.0004	3.87
xn	0.000428	0.0003	1.39
yn	0.001020	0.0003	3.31
xn^2	0.003160	0.0005	6.07
yn^2	0.001457	0.0005	2.80
xn*yn	-0.000380	0.0004	-0.872

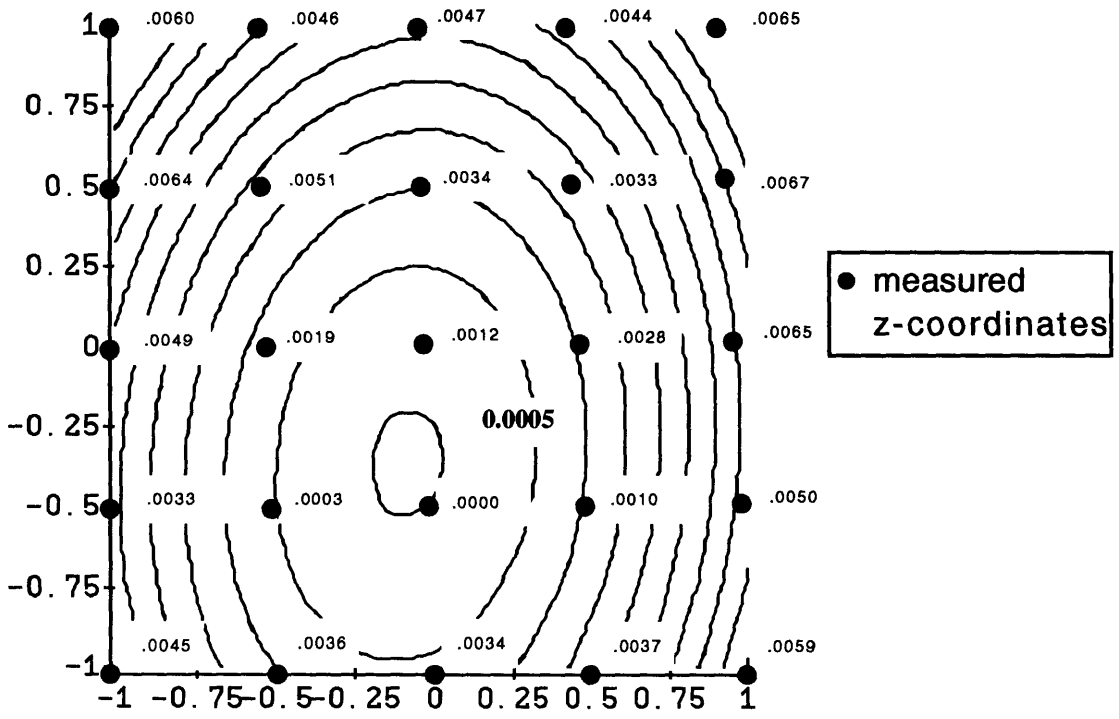

Figure 5.13: Contour plot and regression data for TRIS co-dispersion plate, crosslinked at 160°C, sample #2 (middle of powder bed). The contour levels start at 0.0000" and increase by 0.0005" increments. The 0.0005" contour level is so indicated on the contour plot.

Dependent variable is: z
R□ = 68.4% R□(adjusted) = 60.1%
s = 0.0012 with 25 - 6 = 19 degrees of freedom

Source	Sum of Squares	df	Mean Square	F-ratio
Regression	0.000062	5	0.000012	8.23
Residual	0.000029	19	0.000002	

Variable	Coefficient	s.e. of Coeff	t-ratio
Constant	0.001660	0.0005	3.44
xn	-0.000284	0.0003	-0.818
yn	0.001168	0.0003	3.36
xn^2	0.002398	0.0006	4.09
yn^2	0.002053	0.0006	3.50
xn*yn	-0.000247	0.0005	-0.502

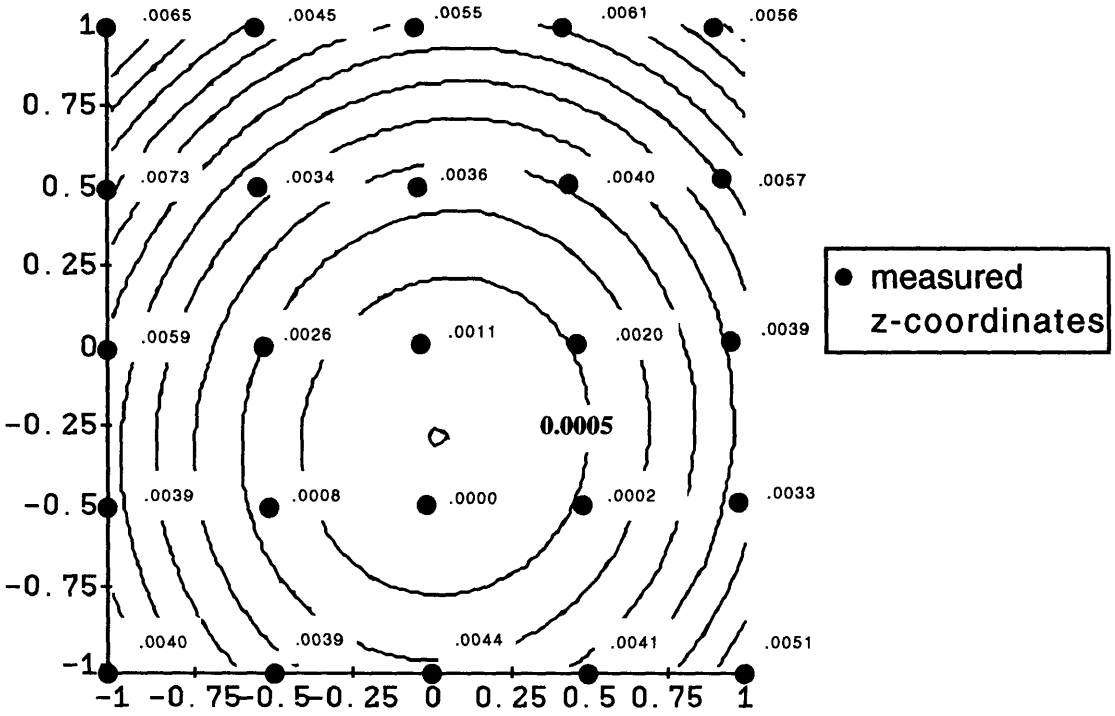

Figure 5.14: Contour plot and regression data for TRIS co-dispersion plate, crosslinked at 160°C, sample #3 (left side of the powder bed). The contour levels start at 0.0000" and increase by 0.0005" increments. The 0.0005" contour level is so indicated on the contour plot.

Dependent variable is: z
25 total cases of which 1 are missing
R□ = 51.0% R□(adjusted) = 37.5%
s = 0.0011 with 24 - 6 = 18 degrees of freedom

Source	Sum of Squares	df	Mean Square	F-ratio
Regression	0.000021	5	0.000004	3.75
Residual	0.000021	18	0.000001	

Variable	Coefficient	s.e. of Coeff	t-ratio
Constant	0.001472	0.0004	3.39
xn	-0.000117	0.0003	-0.383
yn	0.001262	0.0003	4.12
xn^2	0.000431	0.0005	0.836
yn^2	0.000126	0.0005	0.244
xn*yn	-0.000446	0.0004	-1.04

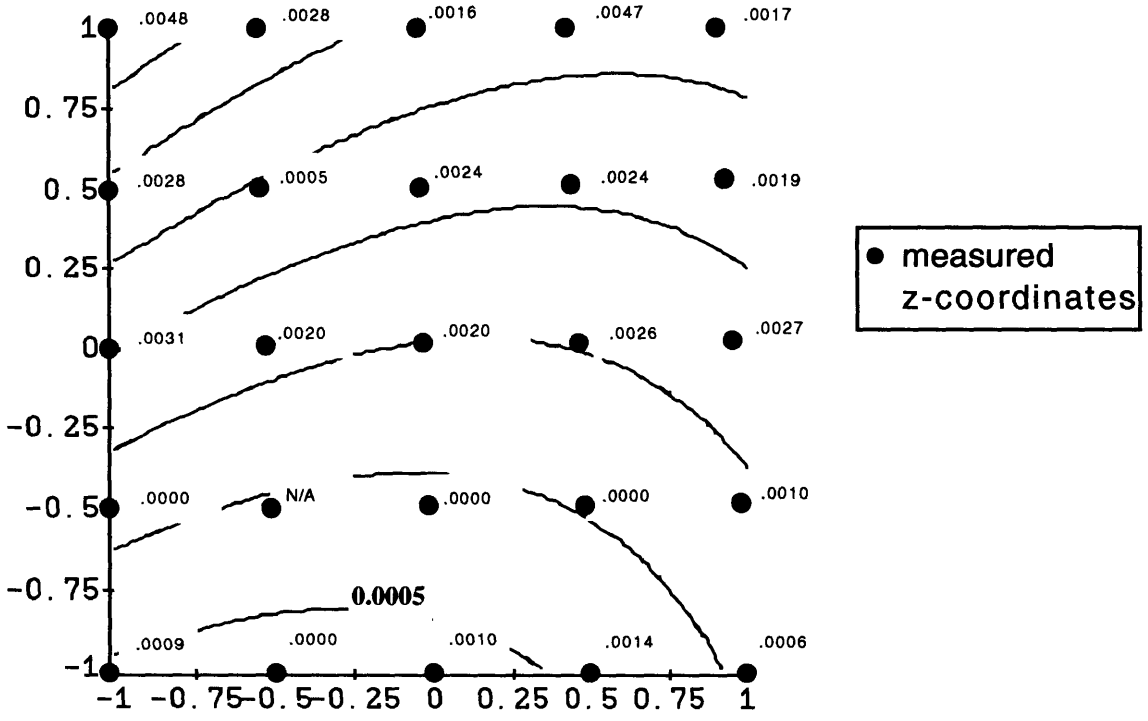

Figure 5.15: Contour plot and regression data for ammonia co-dispersion plate, crosslinked at 160°C, sample #1 (right side of powder bed). The contour levels start at 0.0005" and increase by 0.0005" increments. The 0.0005" contour level is so indicated on the contour plot.

Dependent variable is: z
R¤ = 76.3% R¤(adjusted) = 70.1%
s = 0.0008 with 25 - 6 = 19 degrees of freedom

Source	Sum of Squares	df	Mean Square	F-ratio
Regression	0.000044	5	0.000009	12.2
Residual	0.000014	19	0.000001	

Variable	Coefficient	s.e. of Coeff	t-ratio
Constant	0.001792	0.0003	5.40
xn	-0.000617	0.0002	-2.58
yn	0.001392	0.0002	5.82
xn^2	0.001667	0.0004	4.12
yn^2	-0.000107	0.0004	-0.264
xn*yn	-0.000643	0.0003	-1.90

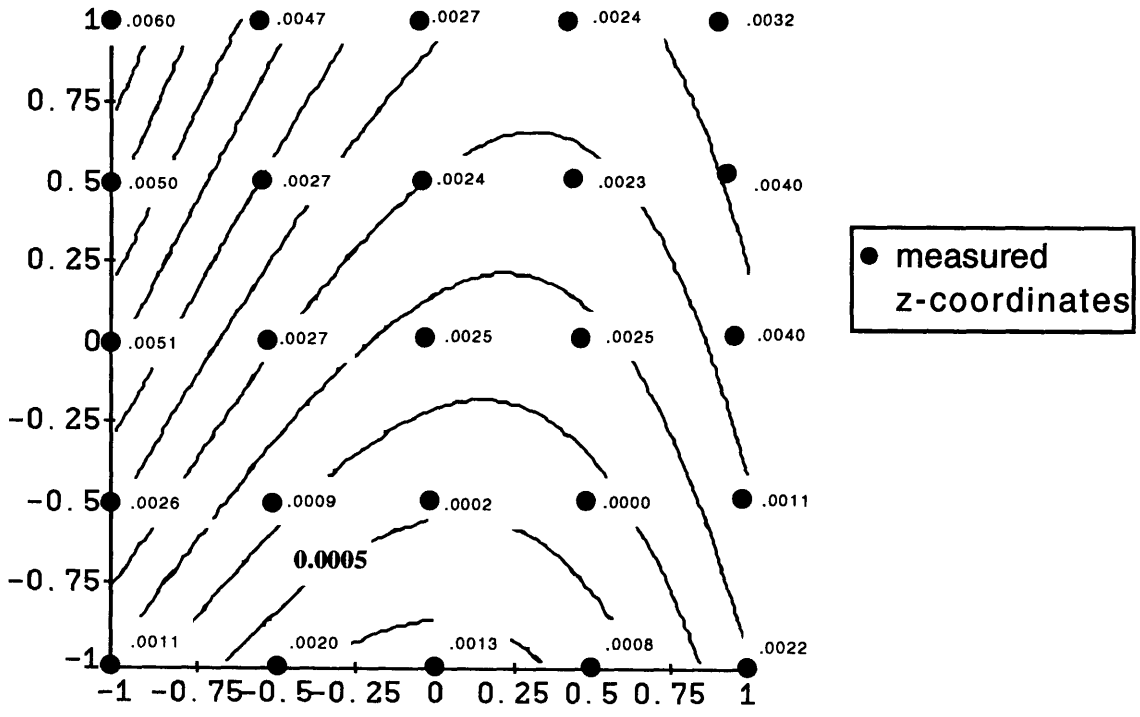

Figure 5.16: Contour plot and regression data for ammonia co-dispersion plate, crosslinked at 160°C, sample #3 (right side of powder bed). The contour levels start at 0.0005" and increase by 0.0005" increments. The 0.0005" contour level is so indicated on the contour plot.

firing indicates that the drying and crosslinking behavior of Rhoplex are too complex for the assumptions of the model.

To confirm our belief that the bottom layers tend to warp more than the top layers, the z-coordinate of the silica plates were measured on the top surface adjacent to the holes. Results of regression show that the maximum warping on top layer was, on average, only 0.001" less than the bottom. The same paraboloidal shape was obtained on the top and bottom surfaces. Figure 5.20 through Figure 5.22 contain the contour plot and regression output for one sample.

5.2.4 Conclusions on Warping

The above experiment provides an introductory look into the phenomenon of warping in 3DP ceramic parts. Starting with a simple model, good regression results were obtained with silica parts. The model does not work as well for co-dispersion plates, which were warped more randomly after crosslinking. During firing, the co-dispersion plates continued to distort, resulting in up to 70% more final warpage than the fired silica plates.

It should be notes that the experimental procedure used to post process the co-dispersion plates does not exactly correspond to the process used for the silica plates. The co-dispersion plates were fired after powder removal, while the silica plates were surrounded by unprinted powder during firing.

The large amount of warping observed in these experiments may also not be reflective of the average 3DP part. During normal post processing, parts are commonly covered with loose powder. The weight of this extra powder can limit warping in actual casting shells. The plates in this study were allowed to warp freely. In essence, we observed warping in an experiment designed to produce warping.

Unfortunately, the effects of citric acid dissolution and binder volatility could not be addressed due to a lack of valid samples. More work is necessary to understand warping with co-dispersion binders.

Dependent variable is: **z**
R¤ = 80.8% R¤(adjusted) = 75.8%
s = 0.0018 with 25 - 6 = 19 degrees of freedom

Source	Sum of Squares	df	Mean Square	F-ratio
Regression	0.000259	5	0.000052	16.0
Residual	0.000061	19	0.000003	

Variable	Coefficient	s.e. of Coeff	t-ratio
Constant	0.004311	0.0007	6.11
xn	0.000512	0.0005	1.01
yn	0.001563	0.0005	3.07
xn^2	0.005928	0.0009	6.90
yn^2	0.004008	0.0009	4.66
xn*yn	-0.000339	0.0007	-0.471

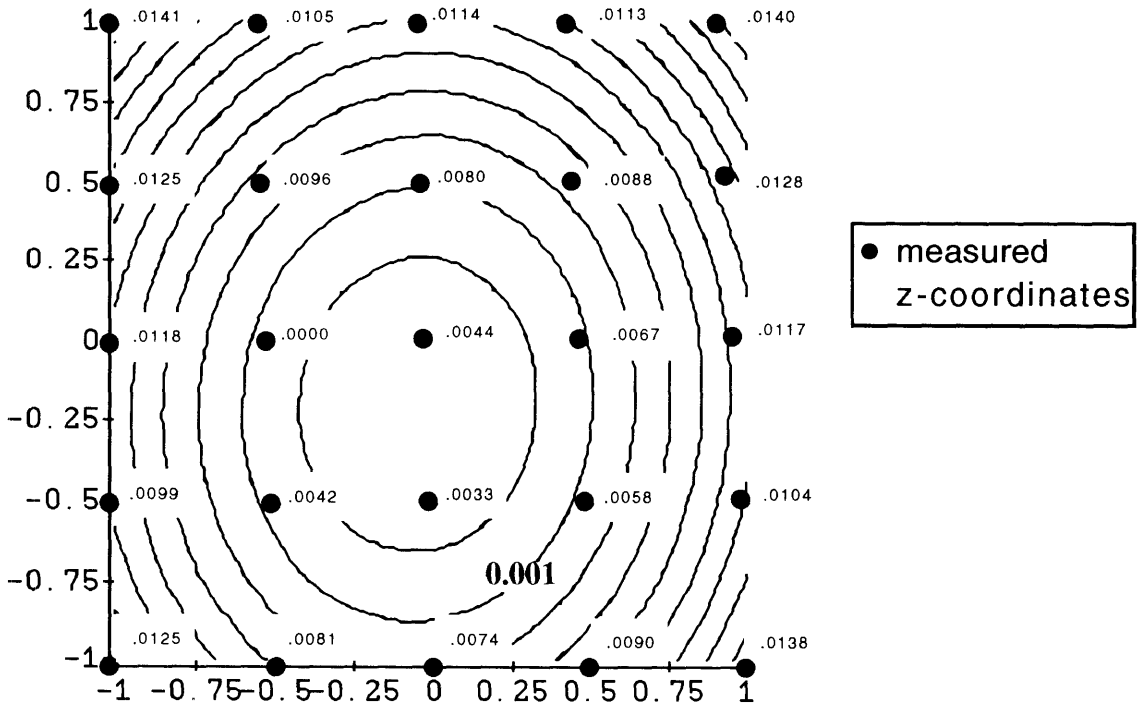

Figure 5.17: Contour plot and regression data for TRIS co-dispersion plate, fired at 900°C, sample #1 (right side of powder bed). The contour levels start at 0.000" and increase by 0.001" increments. The 0.001" contour level is so indicated on the contour plot.

Dependent variable is: z
R¤ = 73.6% R¤(adjusted) = 66.6%
s = 0.0023 with 25 - 6 = 19 degrees of freedom

Source	Sum of Squares	df	Mean Square	F-ratio
Regression	0.000283	5	0.000057	10.6
Residual	0.000101	19	0.000005	

Variable	Coefficient	s.e. of Coeff	t-ratio
Constant	0.006944	0.0009	7.65
xn	-0.000059	0.0007	-0.090
yn	0.001336	0.0007	2.04
xn^2	0.007417	0.0011	6.71
yn^2	0.002084	0.0011	1.89
xn*yn	0.000324	0.0009	0.351

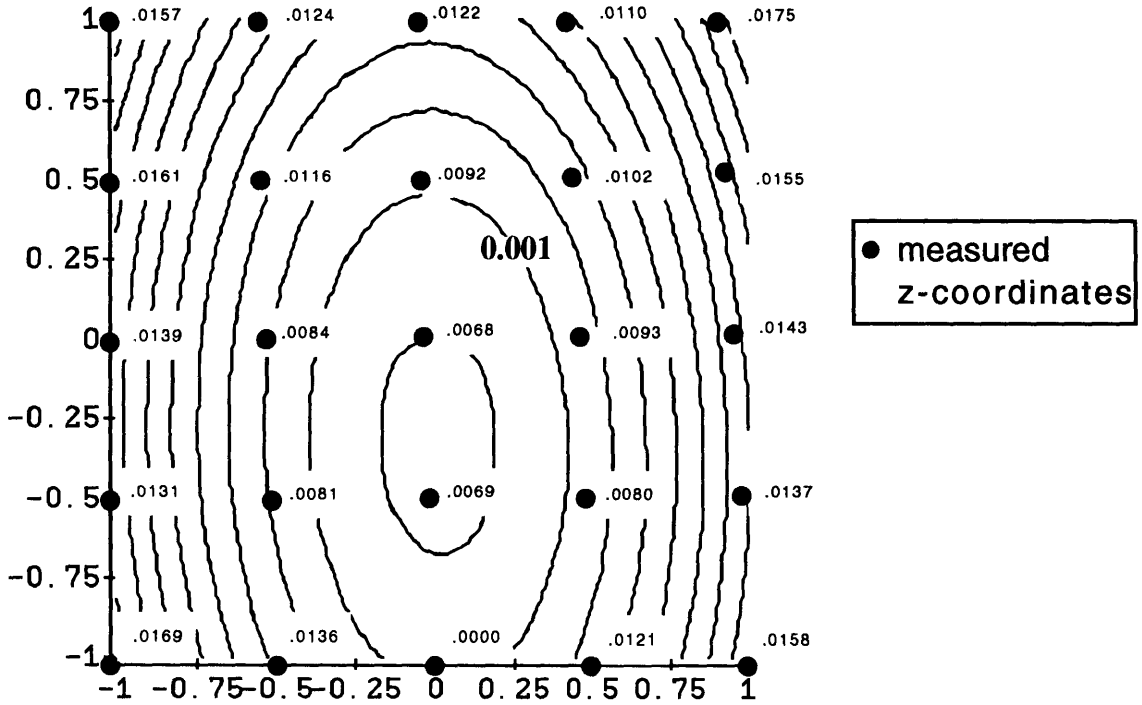

Figure 5.18: Contour plot and regression data for TRIS co-dispersion plate, fired at 900°C, sample #2 (middle of powder bed). The contour levels start at 0.000" and increase by 0.001" increments. The 0.001" contour level is so indicated on the contour plot.

Dependent variable is: z
R¤ = 87.2% R¤(adjusted) = 83.9%
s = 0.0012 with 25 - 6 = 19 degrees of freedom

Source	Sum of Squares	df	Mean Square	F-ratio
Regression	0.000174	5	0.000035	26.0
Residual	0.000025	19	0.000001	

Variable	Coefficient	s.e. of Coeff	t-ratio
Constant	0.000830	0.0005	1.82
xn	-0.000729	0.0003	-2.23
yn	-0.000749	0.0003	-2.29
xn^2	0.005377	0.0006	9.71
yn^2	0.002720	0.0006	4.91
xn*yn	-0.000491	0.0005	-1.06

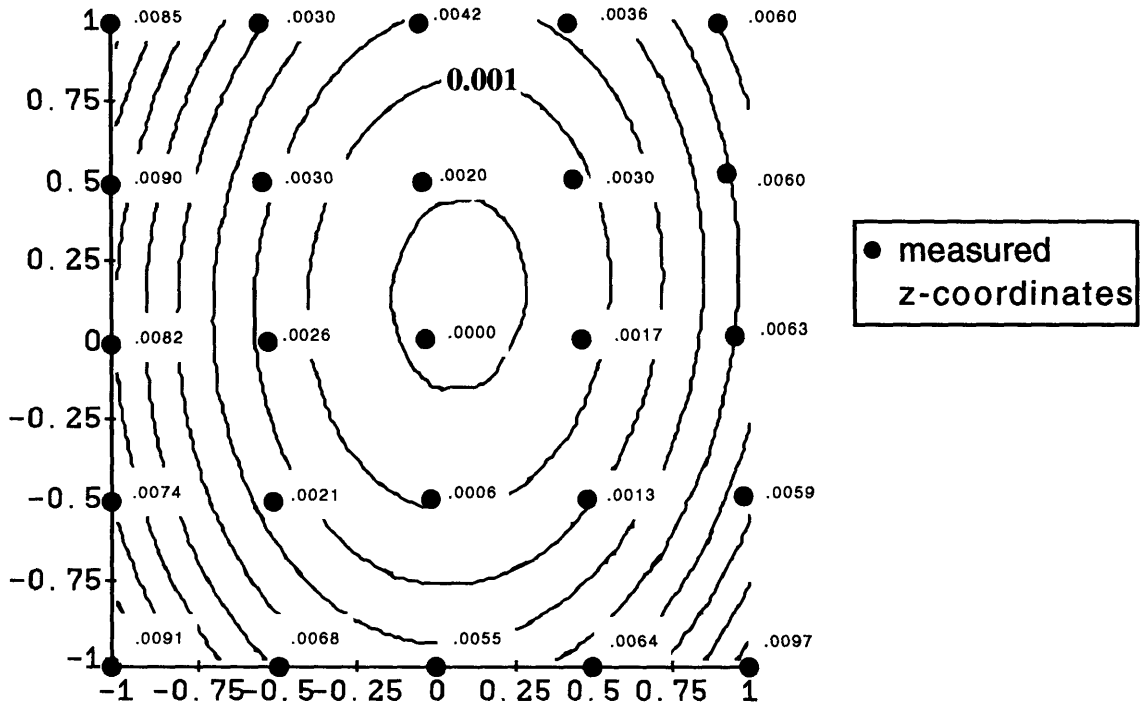

Figure 5.19: Contour plot and regression data for TRIS co-dispersion plate, fired at 900°C, sample #3 (left side of powder bed). The contour levels start at 0.000" and increase by 0.001" increments. The 0.001" contour level is so indicated on the contour plot.

Dependent variable is: z
R² = 93.7% R²(adjusted) = 92.1%
s = 0.0007 with 25 - 6 = 19 degrees of freedom

Source	Sum of Squares	df	Mean Square	F-ratio
Regression	0.000126	5	0.000025	56.7
Residual	0.000008	19	0.000000	

Variable	Coefficient	s.e. of Coeff	t-ratio
Constant	-0.000244	0.0003	-0.930
xn	-0.000396	0.0002	-2.10
yn	0.000400	0.0002	2.12
xn^2	0.003709	0.0003	11.6
yn^2	0.003771	0.0003	11.8
xn*yn	0.000120	0.0003	0.449

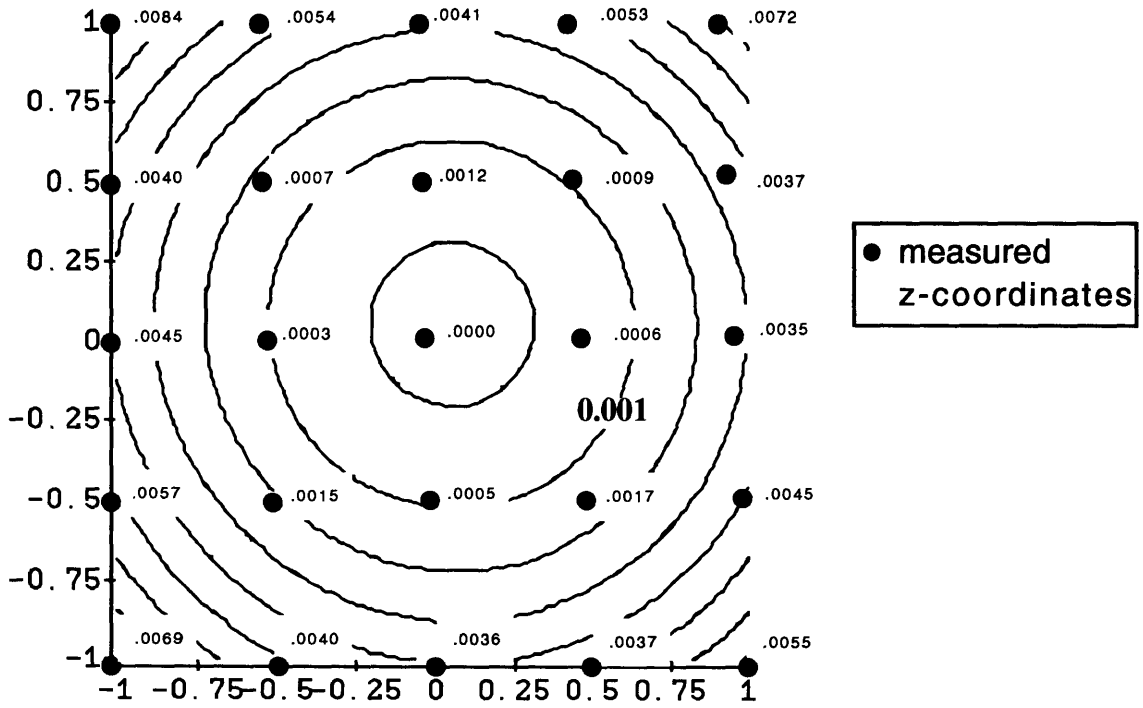

Figure 5.20: Contour plot and regression data for the top surface of silica plate, fired at 900°C, sample #1 (right side of powder bed). The contour levels start at 0.000" and increase by 0.001" increments. The 0.001" contour level is so indicated on the contour plot.

Dependent variable is: z
R¤ = 95.9% R¤(adjusted) = 94.8%
s = 0.0007 with 25 - 6 = 19 degrees of freedom

Source	Sum of Squares	df	Mean Square	F-ratio
Regression	0.000190	5	0.000038	88.7
Residual	0.000008	19	0.000000	

Variable	Coefficient	s.e. of Coeff	t-ratio
Constant	-0.000930	0.0003	-3.62
xn	-0.000572	0.0002	-3.09
yn	0.000769	0.0002	4.15
xn^2	0.004798	0.0003	15.3
yn^2	0.004196	0.0003	13.4
xn*yn	-0.000381	0.0003	-1.46

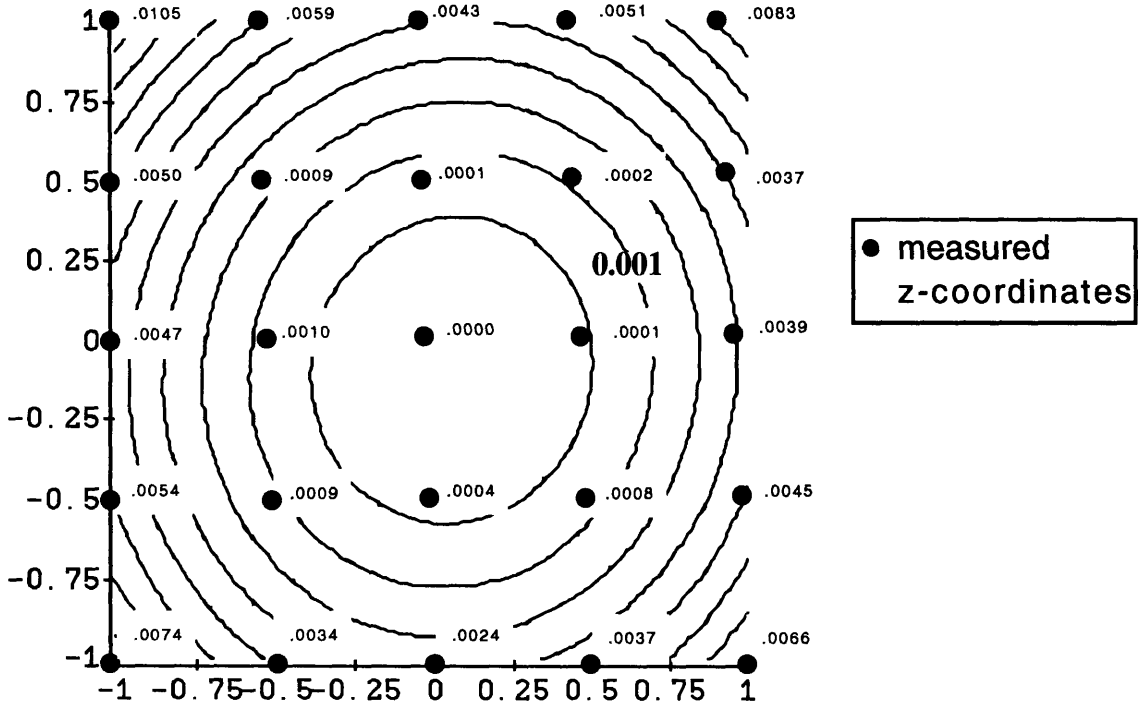

Figure 5.21: Contour plot and regression data for the top surface of silica plate, fired at 900°C, sample #2 (middle of powder bed). The contour levels start at 0.000" and increases by 0.001" increment. The 0.001" contour level is so indicated on the contour plot.

Dependent variable is: z
R¤ = 95.8% R¤(adjusted) = 94.6%
s = 0.0006 with 25 - 6 = 19 degrees of freedom

Source	Sum of Squares	df	Mean Square	F-ratio
Regression	0.000166	5	0.000033	85.9
Residual	0.000007	19	0.000000	

Variable	Coefficient	s.e. of Coeff	t-ratio
Constant	0.000073	0.0002	0.301
xn	0.000316	0.0002	1.80
yn	0.000404	0.0002	2.30
xn^2	0.003990	0.0003	13.4
yn^2	0.004596	0.0003	15.5
xn*yn	0.000161	0.0002	0.650

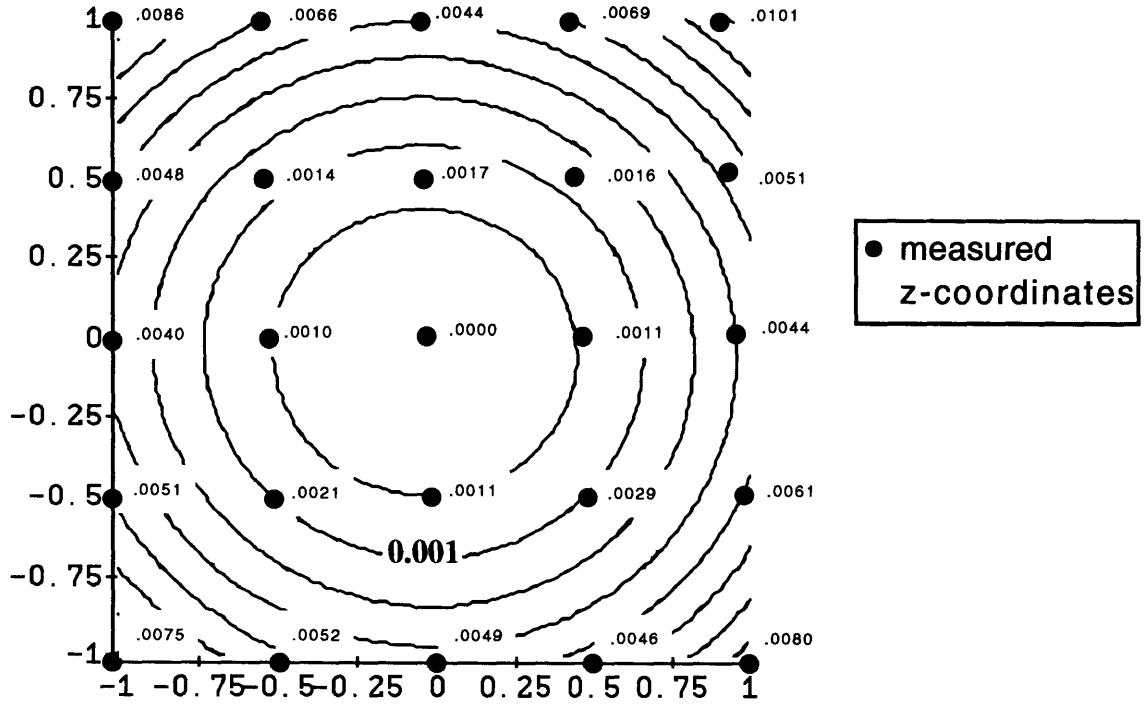

Figure 5.22: Contour plot and regression data for the top surface of silica plate, fired at 900°C, sample #3 (left side of powder bed). The contour levels start at 0.000" and increase by 0.001" increments. The 0.001" contour level is so indicated on the contour plot.

A final conclusion is that contrary to past belief, the data showed that the top surface of silica plates warped in a similar manner as the bottom surface.

5.3 Drooping

Drooping is an issue brought about by the success with co-dispersed binders, With co-dispersions, unbound powder can be removed from the parts prior to firing. During firing the unsupported overhangs and cantilevered section may slump from gravitational forces. This was not a concern with the standard binder, since parts were always fired along with unbound powder, which provides support and prevents drooping.

Drooping is a complex problem involving visco-elasticity and creep, which is time and temperature dependent. As a first look, we will see if drooping is actually occurring with test bars printed with the Standard silica binder.

5.3.1 Experimental Procure

Test bars measuring 2.5" by 0.25" by 0.125" were printed on the proto machine using standard machine parameters and Norton 7920 powder containing 0.2% citric acid. After drying overnight at 80°C, the bars were carefully removed from the surrounding powder and fired to 900°C for two hours. To produce drooping, the bars was simply supported at both ends. Control samples were fired simultaneously but fully supported in powder.

The bar was flipped so that the surface that was facing down during firing is facing up during measuring. Using the x-y stage of a Nikon Toolmaker's microscope, drooping was measured along the length of the bar by focusing on the surface of the bar and measuring the focal length. The data was unusable because the measurements were inaccurate and noisy. An improved method employed a modified dial indicator, which made contact measurements on the surface of the bars. The return spring was removed from the indicator to reduce the contact force on the bars and the chance of deformation.

It is possible that distortion of these bars could have developed during the printing

process. To test this hypothesis, samples were fired both in the as-printed configuration and flipped so that the top surface of the bar faced down during firing. Encasing these bars in powder during firing prevented drooping, therefore any measured distortion would have occurred before firing and is therefore not the result of drooping.

5.3.2 Results

Figure 5.23 shows the z-profile of a drooped bar overlaid with a "flat" sample. No-

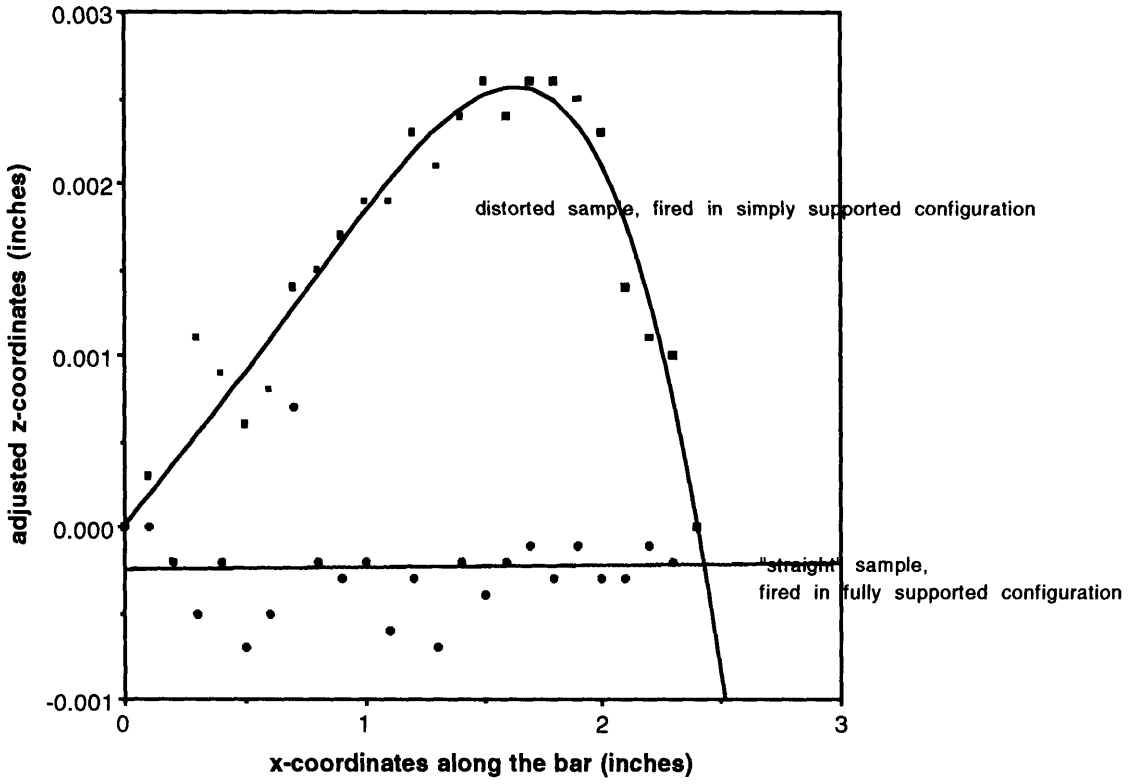

Figure 5.23: Drooped bar fired at 900°C for 2 hours in a two-point simply supported configuration versus straight bar fired fully supported in unprinted powder. Bars are printed with the Standard silica binder (18 vol.% silica) and Norton 7920 powder with 0.5% citric acid.

tice that the data for the "drooped" bar is reversed in orientation, i.e. the plot is flipped horizontally. This is an artifact of the measurement technique, and the part is actually lower

in the middle. The simply supported bar drooped approximately 0.0025" at the midspan, or 1.25" from the supports.

Due to time constraints, the top-side-up and up-side-down samples were not measured. Qualitative examination indicates that the two firing configurations produced identical and straight bars. This shows that the bars were not distorted before firing, and that drooping is definitely occurring. Additional experiments were not possible due to time limitation, but more work is necessary to understand the very complex phenomenon of drooping.

Chapter 6

Conclusions

The primary objective of the research presented here is to increase the green strength of ceramic casting shells made by Three Dimensional Printing. We have accomplished this by creating a new binder consisting of a co-dispersion of Nyacol 9950 colloidal silica and Rhoplex HA-16 acrylic emulsion. Although ceramic parts have been successfully printed with this new binder, dimensional distortions that occur during post processing are amplified by co-dispersions. Additional studies to better understand the issues of shrinkage, warpage, and drooping are required before co-dispersions can be fully implemented in the production of ceramic casting shells by 3D Printing.

The first attempt to increase green strength was to print bars with Rhoplex HA-16 binder and subsequently infiltrate with silica. This was unsuccessful due to the formation of residue upon thermal decomposition of Rhoplex, which prevented silica from wetting alumina. Poor wetting and subsequent lack of proper bonding between silica and alumina greatly reduced the fired strength of test samples.

Since the green strength of these sample did improve dramatically over the green strength of sample printed with the standard silica binder, the infiltration studies showed that incorporating a polymer binder such as Rhoplex into the printing process was an appropriate approach. The results suggest that adjusting the amount of Rhoplex and silica in an infiltrated sample may compensate for the loss of fired strength, but the residue from de-

composition of polymer is a fundamental problem that may never disappear completely. With additional effort, infiltration may become an acceptable method of producing shells. The reduction in fired strength, for example, can be compensated for by post dipping the parts in colloidal silica and refiring. However, time may be better spent on additional development of co-dispersions.

Co-dispersions can deliver exact proportions of polymer and silica to the powder bed. Another advantage is the homogeneous mixture of the two material in the interparticle necks. This facilitates densification of the necks by reducing the size of the pores that must be filled by the silica. The results of four-point bend testing showed that a co-dispersion containing 10 vol.% Rhoplex solids and 18 vol.% silica produces test bars that are nine times stronger in the green state than bars printed with the standard 18 vol.% silica binder. The fired strength (fired @900°C) only decreased by 10%.

Although the strength data is impressive, co-dispersions are far from perfect. The stability of the Rhoplex/silica mixture appears to be good, but we had experienced some problems in terms of binder stream stability and nozzle clogging. Initial nozzle startup is also more difficult than with the standard silica binder. Once the nozzle is running smoothly, however, the printing session is usually trouble-free. The colloidal science behind the stabilization of the binder is not fully understood, and more stability studies are necessary to increase confidence in co-dispersions.

The issue of dimensional control, more than any of the other concerns regarding co-dispersions, prevents actual full time implementation on the Alpha machine. Shrinking of alumina/silica bars made by 3DP increased from 0.4% to 0.5% due to co-dispersions. Bars printed with Rhoplex alone, however, does not shrink more than 0.005%. The combined effect of silica and Rhoplex, when used in a co-dispersion, is greater than the sum of each alone. There is either a synergistic effect at work, or there are fundamental issues regarding shrinkage that we do not understand.

For the first time ever, warping of 3DP parts during firing was studied in detail. Al-

though the results allow us to compare warping caused by the Standard silica binder to that of Rhoplex/silica co-dispersions, they are not indicative of the normal 3DP part. Casting shells are usually fired while encased in unprinted powder. The weight of this powder, combined with the cohesive strength developed with water and citric acid, probably prevents warping of the magnitude observed with the test plates. The study provided valid data for the warping of these plates, but not for the 3DP processin general.

The data suggests that co-dispersion plates warped more than the silica plates. This may actually be just another effect of the additional shrinkage observed in co-dispersion bars. Therefore a better understanding of shrinkage and subsequent reduction may also benefit the warping problem. Possible migration of the Rhoplex particles during drying of parts printed with co-dispersions can create a Rhoplex concentration gradient across the thickness of the part. Such a gradient can result in warping.

The rate of drying is likely an important factor in the amount of warping in a 3DP part. Past experience seems to indicate that slow drying rates reduce warping, but a detailed study of drying rates is called for.

The issue of drooping or slumping during firing is a new problem brought on by the use of co-dispersions. Powder removal in the green state leaves the shell unsupported during firing. Cantilevered parts such as in-situ cores may slump out of position during firing. Due to time constraints, we were only able to demonstrate the existence of drooping. More work to characterize this phenomenon is needed. A way to bypass this issue is to simply leave the powder in the shell during firing, i.e. only remove the unprinted powder from the outside of shells before firing.

On a more positive note, the problem of powder removal is solved. The idea of using carbonated water to produce the bubbles to loosen unprinted powder was refined by the addition of a vacuum system. This technique not only works for parts printed with co-dispersion, but for the standard 3DP shells as well.

Looking back at the original motivation of facilitating the handling of parts in the

green state, the Rhoplex co-dispersion is not the perfect solution. This binder does have good strength after drying, but the crosslinking step is mandatory before powder removal involving water can be done. We have actually added a step to the shell printing process. The ideal green strength additive would achieve high green strength without drying or crosslinking. This may be a bit unrealistic.

Finally, the recommended course of action is to continue studying co-dispersions. This thesis has shown the advantages and the drawbacks of printing with co-dispersion. Although the Rhoplex/Nyacol 9950 co-dispersion developed here is "printable", its ability to produce a good casting shell is still questionable. The unresolved problems are periodic instabilities in the binder stream, excessive shrinking/warping, and possible distortions during firing. We must learn to control all of these issues before ceramic shells can actually be printed with co-dispersion.

References

Charnnarong, Jain, Doctorate Candidate in Mechanical Engineering and 3D Printing Researcher, Private conversation during 1993-1994.

Esterman, Marcos, Jr., "Characterization of The Powder/Binder Interaction in the Three Dimensional Printing Process", MIT M.S. Thesis, 1990

German, Randall M., *Powder Injection Molding*, Metal Powder Industries Federation, Princeton, NJ, 1990.

Harris, Chris L., "Characterization of Dimensional Variability and Part Bleeding Using the Three Dimensional Printing Process", MIT B.S. Thesis, 1991

Hunter, Robert J., *Foundations of Colloidal Science Volume I*, Clarendon Press, Oxford, 1991

Iler, R. K., *The Chemistry of Silicas*, J. Wiley & Sons, New York, 1979.

Lauder, Alan J., "Microstructure and Particle Arrangement in Three Dimensional Printing", MIT M.S. Thesis, 1992

Richerson, David W., *Modern Ceramic Engineering: Properties, Process, and Use in Design*, Marcel Dekker, Inc., New York, 1982.

Rusher, R.L., "Strength Factors of Ceramic Casting Shells", *AFS Cast Metals Research Journal*, vol. 11, no. 1 (March 1975), pp 21-26.

Sardouk, Khalil, "Analysis of Dimensional Control in 3D Printing", MIT B.S. Thesis, 1993

Scherer, George W., "Drying Gels III. Warping plate", *Journal of Non-Crystalline Solids*, vol. 91, 1987, pp 83-100.

Timoshenko, S., *Applied Elasticity*, Westinghouse Technical Night School Press, East Pittsburgh, PA, 1925

Young, Warren C., *Roark's Formula for Stress and Strain*, McGraw-Hill Book Company, New York, 1989

Appendix A

Metal Matrix Composites

To date, two types of silicon carbide (SiC) pre-forms have been made for pressure infiltrated metal matrix composites (MMC's) using Three Dimensional Printing Techniques. The first type are "microscopically toughened" pre-forms consisting of discrete fibers of silicon carbide. The second type of pre-forms are uniformly packed SiC bars. These parts were printed using colloidal silica binder in SiC powder.

Tests have shown that the toughness of the "macro-toughened" MMC's is superior to that of composites made from conventionally prepared pre-forms. The MMC's made from the uniformly packed 3DP pre-forms were, however, less tough than the conventionally prepared composites. These results indicate that the colloidal silica binder used to print the pre-forms interferes with the metal-SiC bond and weakens the MMC. An alternative binder is needed for printing pre-forms.

There are three requirements for this new binder. First of all, the pre-form must have high green strength to survive the handling involved in the preparation for infiltration. Secondly, the pre-form must be strong enough to withstand the flow of molten metal. Finally, the binder materials must not affect the bond between the SiC and the matrix material.

The green strength can be improved by printing a Rhoplex/silica co-dispersion binder. Silica is necessary to give the pre-form strength at infiltration temperatures, even though it seems to interfere with the final toughness of the composite. The composition of

the co-dispersion should be mostly Rhoplex with the minimum amount of silica to give the pre-form sufficient high-temperature strength to survive pressure infiltration.

An experiment was designed to find this critical binder composition. Bars were printed on the proto machine using various compositions of co-dispersions. 320 mesh green silicon carbide powder was used. The machine parameters were: 1.2 ml/min flowrate, 7 mil line width, 7 mil layer thickness, and 65 in/sec printhead scanning speed. The powder bed was humidified to reduce ballistic ejection of the powder. The bars were 2.0" long and 0.125" by 0.125" in cross section.

Five different compositions were used to print the pre-forms. The volume percentages of Rhoplex and silica in the co-dispersions were:

19 vol.% Rhoplex, 0 vol.% silica
18 vol.% Rhoplex, 1 vol.% silica
17 vol.% Rhoplex, 2 vol.% silica
13 vol.% Rhoplex, 6 vol.% silica
10 vol.% Rhoplex, 9 vol.% silica

These bars were placed in an infiltration jig which exposed a 1 inch section in the middle of the bars. During infiltration, this unsupported section would be subjected to the force of crossflowing molten metal. The resulting composite could be sectioned to reveal which bars survived the infiltration process.

The printing was fairly straightforward, but the bars came out rhomboidal in cross section due to mushing caused by excessive moisture. They were still usable for the infiltration study.

Unfortunately, the experiment did not proceed any further due to circumstances beyond the author's control. Nonetheless, the study has shown that printing pre-forms for metal matrix composites is another application of co-dispersions.

Appendix B

List of Binder Material

The following appendix given pertinent information about the various binders and green strength additives mentioned in the main body of this thesis:

Nyacol 9950 - a colloidal silica dispersed in water. Nominal particle size is 100 nm. Contains 50% solids by weight. Manufactured by Nyacol Products Inc. in Ashland MA.

Nyacol 830 - a colloidal silica dispersed in water. Nominal particle size is 8 nm. Contains 30% solids by weight. Manufactured by Nyacol Products Inc. in Ashland MA.

Rhoplex HA-16 - a nonionic acrylic emulsion. Contains 45.5% solids by weight. Glass Transition temperature is 35°C. Self crosslinks at 160°C. Manufactured by the Rohm and Hass Co. in Philadelphia, PA

Rhoplex AC-604 - an acrylic emulsion. Contains 46% solids by weight. Self Crosslinks at 175°C. Manufactured by the Rohm and Hass Co. in Philadelphia, PA

Tylac 68138 Synthetic rubber latex - a carboxylated styrene-butadiene copolymer latex. Contains 49% by weight solids. Glass transition temperature is 2°C. Manufactured by Reichhold Chemicals, Inc. in Research Triangle Park, NC.

Tylac 68139 Synthetic rubber latex - a carboxylated styrene-butadiene copolymer latex. Contains 47.5% by weight solids. Glass transition temperature is -34°C. Manufactured by Reichhold Chemicals, Inc. in Research Triangle Park, NC.

Adbond BV Concentrate - water based polymeric emulsion, composition is proprietary. Contains 50% solids by weight. Manufactured by Remet Corp. in Chadwicks NY.

Customcote Binder - colloidal silica binder with proprietary additive. Contains 50% by weight silica and 10% by weight of the additive. Manufactured by Ransom & Randolph in Mauee, OH.

Ludox SK 215B - colloidal silica containing polyvinyl alcohol (PVA) in solution. Contains 2 wt.% PVA and 16 wt.% silica. Manufactured by Du Pont Chemicals in Wilmington, DE.

Ludox SK-B - colloidal silica containing polyvinyl alcohol (PVA) in solution. Contains 1 wt.% PVA and 26 wt.% silica. Manufactured by Du Pont Chemicals in Wilmington, DE.

Appendix C

Experimental Data

Presented in the following pages are the raw data from the strength, shrinkage, and warping experiments. Section C.1 contains the MOR from all of the four point bend tests. Section C.2 contains data obtained from the shrinkage study. Section C.3 contains data measured in the warping study.

C.1 Strength Data

Sample	Mass (gm)	Load (N)	MOR (MPa)	Comments	Description of Sample
9	n/a	#VALUE!	#VALUE!	bar broken intransit	infiltrated w/9950, new fired to 750C
10	115	1.13	0.67		infiltrated w/830, new fired to 750C
11*	105	1.03	0.61	actual mass <105	infiltrated w/9950, new fired to 900C
12	214	2.10	1.25		infiltrated w/830, new fired to 900C
13*	828	8.12	4.83	overfired	infiltrated w/9950, new fired to 1100C
14*	1540	15.11	8.99	overfired	infiltrated w/830, new fired to 1100C

*Note: Samples 15-17 were co-dispersion bars that delaminated.

18	175	1.72	1.02		50-50 co-dispersion, fired to 750C
19	260	2.55	1.52		50-50 co-dispersion, fired to 900C
20	540	5.30	3.15		50-50 co-dispersion, fired to 1100C
21	895	8.78	5.23		50-50 co-dispersion, green
1	926	9.08	5.41		green Rhoplex
3*	35.1	0.34	0.20	actual mass <35.1	infiltrated w/9950, fired to 750C
4a	391	3.84	2.28		printed w/9950, fired to 750C
4b	474	4.65	2.77		printed w/9950, fired to 750C
5a	96	0.94	0.56		infiltrated w/9950, fired to 900C
5b	96	0.94	0.56		infiltrated w/9950, fired to 900C
6a	591	5.80	3.45		printed w/9950, fired to 900C
6b	529	5.19	3.09		printed w/9950, fired to 900C
7a	171	1.68	1.00		infiltrated w/9950, fired to 1100C
7b	255	2.50	1.49		infiltrated w/9950, fired to 1100C

8a	1166	11.44	6.81	printed w/9950, fired to 1100C
8b	1173	11.51	6.85	printed w/9950, fired to 1100C

*Note: Samples 1 through 21 were 30 micron spherical powder bars.

Data in ascending strength

Sample	Mass (gm)	Load (N)	MOR (MPa)	Description of Sample
3*	35.1	0.34	0.20	infiltrated w/9950, fired to 750C
5a	96	0.94	0.56	infiltrated w/9950, fired to 900C
5b	96	0.94	0.56	infiltrated w/9950, fired to 900C
11*	105	1.03	0.61	infiltrated w/9950, new fired to 900C
10	115	1.13	0.67	infiltrated w/830, new fired to 750C
7a	171	1.68	1.00	infiltrated w/9950, fired to 1100C
18	175	1.72	1.02	50-50 co-dispersion, fired to 750C
12	214	2.10	1.25	infiltrated w/830, new fired to 900C
7b	255	2.50	1.49	infiltrated w/9950, fired to 1100C
19	260	2.55	1.52	50-50 co-dispersion, fired to 900C
4a	391	3.84	2.28	printed w/9950, fired to 750C
4b	474	4.65	2.77	printed w/9950, fired to 750C
6b	529	5.19	3.09	printed w/9950, fired to 900C
20	540	5.30	3.15	50-50 co-dispersion, fired to 1100C
6a	591	5.80	3.45	printed w/9950, fired to 900C
13*	828	8.12	4.83	infiltrated w/9950, new fired to 1100C
21	895	8.78	5.23	50-50 co-dispersion, green
1	926	9.08	5.41	green Rhoplex
8a	1166	11.44	6.81	printed w/9950, fired to 1100C
8b	1173	11.51	6.85	printed w/9950, fired to 1100C
14*	1540	15.11	8.99	infiltrated w/830, new fired to 1100C
9	n/a	#VALUE!	#VALUE!	infiltrated w/9950, new fired to 750C

Data from 4 point bending test 5-17-93

Sample	Mass (gm)	Load (N)	MOR (MPa)	Comments	Description of Sample
22	254	2.49	1.48		spherical, 9 vol.% silica, fired to 750C
23	279	2.74	1.63		" "
24	206	2.02	1.20	jarred	" "
25	297	2.91	1.73		spherical, 9 vol.% silica, fired to 900C
26	344	3.37	2.01		" "
27	370	3.63	2.16		" "
28	917	9.00	5.35		spherical, 9 vol.% silica, fired to 1100C
29	781	7.66	4.56		" "
30	946	9.28	5.52		" "
31	139	1.36	0.81		stock powder, 9 vol.% silica, fired to 750C
32	134	1.31	0.78		" "
33	150	1.47	0.88		" "
34	295	2.89	1.72		stock powder, 9 vol.% silica, fired to 900C
35	277	2.72	1.62		" "
36	312	3.06	1.82		" "
38	2350	23.05	13.72		stock powder, 9 vol.% silica, fired to 1100C
39	2290	22.46	13.37		" "
40	1890	18.54	11.04		" "

Data from 4 point bending test 6-16-93

Sample	Mass (gm)	Load (N)	MOR (MPa)	Comments	Description of Sample
41	42.8	0.42	0.42	0.097" thick bar	stock powder, stock binder, green
42	34.3	0.34	0.33	"	" "
43	43.9	0.43	0.43	"	" "
			average= 0.39		
44	346.9	3.40	3.37	calculated as	stock powder, stock binder, 750C
45	361	3.54	3.51	0.097" thick bar	" "
46	359.3	3.52	3.49		" "
			average= 3.46		
47	373.8	3.67	3.64	0.097" thick bar	stock powder, stock binder, 900C
48	423.7	4.16	4.12	"	" "
49	441.5	4.33	4.29	"	" "
			average= 4.02		
50	2805	27.52	27.28	0.097" thick bar	stock powder, stock binder, 1100C
51	3073	30.15	29.89	"	" "
52	3983	39.07	38.74	"	" "
			average= 31.97		

*Note: stock powder is Norton 7920 electronic grade alμmina, 30μm, 0.2% citric acid
stock binder is ~18 volμme % silica, Jim Bredt's formulation

Data from 4 point bending test 6-16-93

Sample	Mass (gm)	Load (N)	MOR (MPa)	Comments	Description of Sample
53	182.7	1.79	1.07		stock powder, 2 vol. % rhoplex, green
54	167	1.64	0.98		" "
55	182	1.79	1.06		" "
			average= 1.03		
56	300	2.94	1.75	got dropped on	stock powder, 2 vol. % rhoplex, 750C
57	501.5	4.92	2.93		" "
58	447.3	4.39	2.61		" "
			average= 2.77		
59	636.9	6.25	3.72		stock powder, 2 vol. % rhoplex, 900C
60	600.5	5.89	3.51		" "
61	578.7	5.68	3.38		" "
			average= 3.53		
62	4870	47.77	28.44		stock powder, 2 vol. % rhoplex, 1100C
63	3920	38.46	22.89		" "
64	4080	40.02	23.82		" "
			average= 23.36		

*Note: stock powder is Norton 7920 electronic grade alμmina, 30μm, 0.2% citric acid
binder is 2 vol. % rhoplex,18 volμme % silica, water, and ammoniμm hydroxide to increase pH to 10

Data from 4 point bending test 6-16-93

Sample	Mass (gm)	Load (N)	MOR (MPa)	Comments	Description of Sample
65	447.3	4.39	2.61		stock powder, 5 vol. % rhoplex, green
66	390.5	3.83	2.28		" "
67	426.1	4.18	2.49		" "
			average= 2.46		
68	396.8	3.89	2.32	as printed orientation	stock powder, 5 vol. % rhoplex, 750C
69	608.7	5.97	3.55	90 deg. orientation	" "
70	353.4	3.47	2.06	as printed orientation"	"
			average= 2.19		
71	756.8	7.42	4.42		stock powder, 5 vol. % rhoplex, 900C
72	766.8	7.52	4.48		" "
73	644	6.32	3.76		" "
			average= 4.22		
74	4795	47.04	28.00		stock powder, 5 vol. % rhoplex, 1100C
75	4793	47.02	27.99		" "
76	6000	58.86	35.03	actually >6000 gm	" "
			average= 30.34		

*Note: stock powder is Norton 7920 electronic grade alμmina, 30μm, 0.2% citric acid
binder is 5 vol. % rhoplex, 18 volμme % silica, water, and ammoniμm hydroxide to increase pH to 10

Data from 4 point bending test 6-16-93

Sample	Mass (gm)	Load (N)	MOR (MPa)	Comments	Description of Sample
77	629.6	6.18	3.68		stock powder, 10 vol. % rhoplex, green
78	656.9	6.44	3.84		" "
79	642.9	6.31	3.75		" "
			average= 3.76		
80	466.2	4.57	2.72		stock powder, 10 vol. % rhoplex, 750C
81	388.5	3.81	2.27		" "
82	310	3.04	1.81	broke during loading"	"
			average= 2.27		
83	585	5.74	3.42		stock powder, 10 vol. % rhoplex, 900C
84	689	6.76	4.02		" "
85	565	5.54	3.30		" "
			average= 3.58		
86	3930	38.55	22.95		stock powder, 10 vol. % rhoplex, 1100C
87	5760	56.51	33.63		" "
88	5330	52.29	31.12		" "
			average= 29.23		

*Note: stock powder is Norton 7920 electronic grade alμmina, 30μm, 0.2% citric acid
binder is 10 vol. % rhoplex, 18 volμme % silica, water, and ammoniμm hydroxide to increase pH to 10

Data from 4 point bending test 7-6-93

Sample	Mass (gm)	Load (N)	MOR (MPa)	Comments	Description of Sample
89	296	2.90	2.88	0.097" thick bar	stock powder, stock binder, 750C
90	375	3.68	3.65	"	" "
91	346	3.39	3.37	"	" "
92	333	3.27	3.24	"	" "
93	340	3.34	3.31	"	" "
			average= 3.29		
94	483	4.74	2.82		stock powder, 2 vol. % rhoplex, 750C
95	617	6.05	3.60		" "
96	329	3.23	1.92		" "
97	510	5.00	2.98		" "
98	451	4.42	2.63		" "
99	416	4.08	2.43		" "
100	433	4.25	2.53		" "
101	417	4.09	2.43		" "
102	434	4.26	2.53		" "
			average= 2.65		
103	604	5.93	3.53		stock powder, 5 vol. % rhoplex, 750C
104	614	6.02	3.59		" "
105	543	5.33	3.17		" "
106	393	3.86	2.29		" "
107	419	4.11	2.45		" "
108	554	5.43	3.23		" "
109	471	4.62	2.75		" "
110	411	4.03	2.40		" "
			average= 2.93		

*Note: stock powder is Norton 7920 electronic grade alμmina, 30μm, 0.2% citric acid

Data from 4 point bending test 7-6-93

Sample	Mass (gm)	Load (N)	MOR (MPa)	Comments	Description of Sample
111	384	3.77	2.24		stock powder, 10 vol. % rhoplex, 750C
112	320	3.14	1.87		" "
113	418	4.10	2.44		" "
114	328	3.22	1.92		"
115	256	2.51	1.49		"
116	328	3.22	1.92		"
117	358	3.51	2.09		"
118	439	4.31	2.56		"
119	414	4.06	2.42		"
120	354	3.47	2.07		"
121	451	4.42	2.63		"
122	389	3.82	2.27		"
			average= 2.16		

*Note: stock powder is Norton 7920 electronic grade alμmina, 30μm, 0.2% citric acid

Data from 4 point bending test 2-23-94

Sample	Mass (gm)	Load (N)	MOR (MPa)	Comments	Description of Sample
ACG1	539	5.29	3.15	ugly bars!	Rhoplex AC-604, co-dispersion
ACG2	555	5.44	3.24		10 -18 vol. % mixture
ACG3	520	5.10	3.04		old stock powder - 7920, 30um
ACG4	501	4.91	2.93		crosslinked @ 175C
ACG5	457	4.48	2.67		" "
ACG6	650	6.38	3.80		" "
			average= 3.14		
ACF3	230	2.26	1.34		Rhoplex AC-604, co-dispersion
ACF4	210	2.06	1.23		10 -18 vol. % mixture
ACF5	240	2.35	1.40		old stock powder - 7920, 30um
ACF6	235	2.31	1.37		fired @ 900C
ACF7	150	1.47	0.88		" "
			average= 1.24		

Data from 4 point bending test 3-13-94

Sample	Mass (gm)	Load (N)	MOR (MPa)	Comments	Description of Sample
123	174	1.71	1.02		Rhoplex AC-604, co-dispersion
124	240	2.35	1.40		2-18 vol. % mixture
125	213	2.09	1.24		old stock powder - 7920, 30um
126	249	2.44	1.45		crosslinked @ 175C
127	247	2.42	1.44		" "
128	230	2.26	1.34		" "
			average= 1.32		
129	346	3.39	2.02		Rhoplex AC-604, co-dispersion
130	460	4.51	2.69		2-18 vol. % mixture
131	379	3.72	2.21		old stock powder - 7920, 30um
132	378	3.71	2.21		fired @ 750C
133	397	3.89	2.32		" "
			average= 2.29		
134	610	5.98	3.56		Rhoplex AC-604, co-dispersion
135	644	6.32	3.76		2-18 vol. % mixture
136	634	6.22	3.70		old stock powder - 7920, 30um
137	531	5.21	3.10		fired @ 900C
138	711	6.97	4.15		" "
139	630	6.18	3.68		" "
			average= 3.66		

Data from 4 point bending test 3-13-94, continued

Sample	Mass (gm)	Load (N)	MOR (MPa)	Comments	Description of Sample
140	1290	12.65	7.53		Rhoplex AC-604, co-dispersion
141	1260	12.36	7.36		2-18 vol. % mixture
142	1327	13.02	7.75		old stock powder - 7920, 30um
143	1341	13.16	7.83		fired @ 1100C
144	1388	13.62	8.10		" "
			average= 7.71		

Data from 4 point bending test 3-19-94

Sample	Mass (gm)	Load (N)	MOR (MPa)	Comments	Description of Sample
	380	3.73	2.22		Ludox SK-B
	310	3.04	1.81		old stock powder - 7920, 30um
	380	3.73	2.22		dried @ 75C
	320	3.14	1.87		
	346	3.39	2.02		
	311	3.05	1.82		
			average= 1.99		
	437	4.29	2.55		Ludox SK-B
	496	4.87	2.90		old stock powder - 7920, 30um
	474	4.65	2.77		fired @ 750C
	438	4.30	2.56		
	410	4.02	2.39		
	410	4.02	2.39		
			average= 2.59		
	670	6.57	3.91		Ludox SK-B
	763	7.49	4.46		old stock powder - 7920, 30um
	664	6.51	3.88		fired @ 900C
	582	5.71	3.40		
	590	5.79	3.44		
	627	6.15	3.66		
			average= 3.79		
	3580	35.12	20.90		Ludox SK-B
	3870	37.96	22.60		old stock powder - 7920, 30um
	3930	38.55	22.95		fired @ 1100C
	3970	38.95	23.18		
			average= 22.41		

Data from 4 point bending test 3-19-94

Sample	Mass (gm)	Load (N)	MOR (MPa)	Comments	Description of Sample
	423	4.15	2.47		Rhoplex AC-604, co-dispersion
	400	3.92	2.34		5 -18 vol. % mixture
	387	3.80	2.26		old stock powder - 7920, 30um
	338	3.32	1.97		crosslinked @ 175C
	310	3.04	1.81		
	340	3.34	1.99		
			average= 2.14		
	570	5.59	3.33		Rhoplex AC-604, co-dispersion
	508	4.98	2.97		5 -18 vol. % mixture
	583	5.72	3.40		old stock powder - 7920, 30um
	425	4.17	2.48		fired @ 900C
	429	4.21	2.50		
	487	4.78	2.84		
			average= 2.92		
	601	5.90	3.51		Rhoplex AC-604, co-dispersion
	527	5.17	3.08		10 -18 vol. % mixture
	489	4.80	2.86		old stock powder - 7920, 30um
	615	6.03	3.59		crosslinked @ 175C
	559	5.48	3.26		
			average= 3.26		

493	4.84	3.33	Rhoplex AC-604, co-dispersion
436	4.28	2.97	10 -18 vol. % mixture
400	3.92	3.40	old stock powder - 7920, 30um
585	5.74	2.48	fired @ 900C
		average= 3.05	

C.2 Shrinkage Data

Date printed3/22/94
Material 7920 batch 013-94 size 28μm packing about 42% FSC
Binder Rhoplex HA-16 co-dispersion, 10-17 vol.%
Printing condmisted, 0.3% citric, 1.2 cc/min, rinsed, 30 layers printed

Bar	Bar no.	Wet		Diff	Error	Dried (75°C)		Diff	Error
		X1	X2			X1	X2		
0.1309	0.131.1	4.9946	5.1238	0.1292	-0.0017	5.0279	5.1577	0.1298	-0.0011
0.1309	0.131.2	4.9921	5.1218	0.1297	-0.0012	5.0258	5.1560	0.1302	-0.0007
0.1309	0.131.3	4.9878	5.1179	0.1301	-0.0008	5.0236	5.1530	0.1294	-0.0015
0.1309	0.131.4	5.5357	5.6653	0.1296	-0.0013	4.6729	4.8025	0.1296	-0.0013
0.1309	0.131.5	5.5310	5.6622	0.1312	0.0003	4.6698	4.8001	0.1303	-0.0006
0.1309	0.131.6	5.5296	5.6584	0.1288	-0.0021	4.6672	4.7975	0.1303	-0.0006
0.1309	0.131.7	5.8468	5.9771	0.1303	-0.0006	5.1452	5.2744	0.1292	-0.0017
0.1309	0.131.8	5.8425	5.9718	0.1293	-0.0016	5.1422	5.2717	0.1295	-0.0014
0.1309	0.131.9	5.8408	5.9695	0.1287	-0.0022	5.1411	5.2696	0.1285	-0.0024
0.1309	0.131.10	5.8377	5.9677	0.1300	-0.0009	5.1401	5.2700	0.1299	-0.0010
0.372	0.375.1	4.3736	4.7464	0.3728	0.0008	4.4067	4.7772	0.3705	-0.0015
0.372	0.375.2	4.3707	4.7432	0.3725	0.0005	4.4013	4.7729	0.3716	-0.0004
0.372	0.375.3	4.3670	4.7392	0.3722	0.0002	4.4031	4.7742	0.3711	-0.0009
0.372	0.375.4	4.9167	5.2901	0.3734	0.0014	4.0522	4.4244	0.3722	0.0002
0.372	0.375.5	4.9134	5.2861	0.3727	0.0007	4.0492	4.4212	0.3720	0.0000
0.372	0.375.6	4.9111	5.2829	0.3718	-0.0002	4.0471	4.4186	0.3715	-0.0005
0.372	0.375.7	5.2248	5.5894	0.3646	-0.0074	4.5218	4.8942	0.3724	0.0004
0.372	0.375.8	5.2224	5.5938	0.3714	-0.0006	4.5198	4.8919	0.3721	0.0001
0.372	0.375.9	5.2184	5.5903	0.3719	-0.0001	4.5180	4.8907	0.3727	0.0007
0.372	0.375.10	5.2119	5.5866	0.3747	0.0027	4.5164	4.8877	0.3713	-0.0007
0.7441	0.75.1	3.3831	4.1249	0.7418	-0.0023	3.4166	4.1556	0.7390	-0.0051
0.7441	0.75.2	3.3784	4.1209	0.7425	-0.0016	3.4131	4.1526	0.7395	-0.0046
0.7441	0.75.3	3.3754	4.1164	0.7410	-0.0031	3.4134	4.1525	0.7391	-0.0050
0.7441	0.75.4	3.9261	4.6683	0.7422	-0.0019	3.0635	3.8014	0.7379	-0.0062
0.7441	0.75.5	3.9216	4.6646	0.7430	-0.0011	3.0594	3.7981	0.7387	-0.0054
0.7441	0.75.6	3.9196	4.6626	0.7430	-0.0011	3.0560	3.7972	0.7412	-0.0029
0.7441	0.75.7	4.2342	4.9746	0.7404	-0.0037	3.5316	4.2729	0.7413	-0.0028
0.7441	0.75.8	4.2305	4.9717	0.7412	-0.0029	3.5301	4.2698	0.7397	-0.0044
0.7441	0.75.9	4.1850	4.9694	0.7844	0.0403	3.5280	4.2672	0.7392	-0.0049
0.7441	0.75.10	4.2241	4.9663	0.7422	-0.0019	3.5268	4.2664	0.7396	-0.0045
1.998	2.1	1.1320	3.1242	1.9922	-0.0058	1.1668	3.1545	1.9877	-0.0103
1.998	2.2	1.1285	3.1215	1.9930	-0.0050	1.1644	3.1525	1.9881	-0.0099
1.998	2.3	1.1256	3.1172	1.9916	-0.0064	1.1620	3.1487	1.9867	-0.0113
1.998	2.4	1.6759	3.6675	1.9916	-0.0064	0.8097	2.7984	1.9887	-0.0093
1.998	2.5	1.6675	3.6633	1.9958	-0.0022	0.8082	2.7969	1.9887	-0.0093
1.998	2.6	1.6656	3.6607	1.9951	-0.0029	0.8066	2.7950	1.9884	-0.0096
1.998	2.7	1.9839	3.9741	1.9902	-0.0078	1.2803	3.2696	1.9893	-0.0087
1.998	2.8	1.9818	3.9719	1.9901	-0.0079	1.2794	3.2663	1.9869	-0.0111
1.998	2.9	1.9729	3.9695	1.9966	-0.0014	1.2802	3.2668	1.9866	-0.0114
1.998	2.10	1.9744	3.9658	1.9914	-0.0066	1.2779	3.2642	1.9863	-0.0117
3.9961	4.1	1.1337	5.1239	3.9902	-0.0059	1.1703	5.1501	3.9798	-0.0163
3.9961	4.2	1.1319	5.1196	3.9877	-0.0084	1.1689	5.1475	3.9786	-0.0175
3.9961	4.3	1.1286	5.1183	3.9897	-0.0064	1.1651	5.1464	3.9813	-0.0148
3.9961	4.4	BROKEN				BROKEN			
3.9961	4.5	1.6687	5.6633	3.9946	-0.0015	0.8108	4.7925	3.9817	-0.0144
3.9961	4.6	1.6690	5.6588	3.9898	-0.0063	0.8080	4.7914	3.9834	-0.0127
3.9961	4.7	1.6689	5.6569	3.9880	-0.0081	0.8060	4.7878	3.9818	-0.0143

3.9961	4.8	1.9848	5.9720	3.9872	-0.0089	1.2816	5.2637	3.9821	-0.0140
3.9961	4.9	1.9748	5.9691	3.9943	-0.0018	1.2820	5.2627	3.9807	-0.0154
3.9961	4.10	1.9712	5.9658	3.9946	-0.0015	1.2804	5.2604	3.9800	-0.0161

Date printed3/22/94
Material 7920 batch 013-94 size 28μm packing about 42% FSC
Binder Rhoplex HA-16 co-dispersion, 10-17 vol.%
Printing condmisted, 0.3% citric, 1.2 cc/min, rinsed, 30 layers printed

X-linked(160°C)		Diff	Error	fired (900°C)		Diff	Error
X1	X2			X1	X2		
5.1736	5.3034	0.1298	-0.0011	5.6177	5.7477	0.1300	-0.0009
5.1717	5.3014	0.1297	-0.0012	5.6164	5.7454	0.1290	-0.0019
5.1701	5.2994	0.1293	-0.0016	5.6191	5.7479	0.1288	-0.0021
5.0878	5.2175	0.1297	-0.0012	5.6019	5.7317	0.1298	-0.0011
5.0854	5.2158	0.1304	-0.0005	5.5967	5.7266	0.1299	-0.0010
5.0852	5.2139	0.1287	-0.0022	5.5899	5.7189	0.1290	-0.0019
5.0973	5.2269	0.1296	-0.0013	5.7411	5.8705	0.1294	-0.0015
5.0949	5.2243	0.1294	-0.0015	5.6949	5.8257	0.1308	-0.0001
5.0948	5.2236	0.1288	-0.0021	5.6868	5.8153	0.1285	-0.0024
5.0950	5.2245	0.1295	-0.0014	5.6968	5.8267	0.1299	-0.0010
4.5522	4.9230	0.3708	-0.0012	4.9983	5.3694	0.3711	-0.0009
4.5479	4.9184	0.3705	-0.0015	4.9945	5.3648	0.3703	-0.0017
4.5496	4.9205	0.3709	-0.0011	4.9932	5.3633	0.3701	-0.0019
4.4678	4.8387	0.3709	-0.0011	4.9830	5.3542	0.3712	-0.0008
4.4657	4.8373	0.3716	-0.0004	4.9756	5.3465	0.3709	-0.0011
4.4636	4.8354	0.3718	-0.0002	4.9694	5.3410	0.3716	-0.0004
4.4732	4.8451	0.3719	-0.0001	5.1327	5.5058	0.3731	0.0011
4.4734	4.8448	0.3714	-0.0006	5.0736	5.4437	0.3701	-0.0019
4.4724	4.8441	0.3717	-0.0003	5.0667	5.4370	0.3703	-0.0017
4.4714	4.8437	0.3723	0.0003	5.0597	5.4285	0.3688	-0.0032
3.5618	4.3017	0.7399	-0.0042	4.0090	4.7481	0.7391	-0.0050
3.5585	4.2982	0.7397	-0.0044	4.0047	4.7445	0.7398	-0.0043
3.5594	4.2986	0.7392	-0.0049	4.0029	4.7434	0.7405	-0.0036
3.4783	4.2175	0.7392	-0.0049	3.9917	4.7304	0.7387	-0.0054
3.4744	4.2143	0.7399	-0.0042	3.9850	4.7240	0.7390	-0.0051
3.4724	4.2132	0.7408	-0.0033	3.9198	4.6582	0.7384	-0.0057
3.4837	4.2240	0.7403	-0.0038	4.1325	4.8731	0.7406	-0.0035
3.4815	4.2219	0.7404	-0.0037	4.0858	4.8246	0.7388	-0.0053
3.4810	4.2225	0.7415	-0.0026	4.0784	4.8168	0.7384	-0.0057
3.4818	4.2217	0.7399	-0.0042	4.0723	4.8118	0.7395	-0.0046
1.3150	3.2994	1.9844	-0.0136	1.7639	3.7446	1.9807	-0.0173
1.3128	3.2980	1.9852	-0.0128	1.7601	3.7449	1.9848	-0.0132
1.3124	3.2951	1.9827	-0.0153	1.7614	3.7418	1.9804	-0.0176
1.2296	3.2130	1.9834	-0.0146	1.7449	3.7285	1.9836	-0.0144
1.2269	3.2134	1.9865	-0.0115	1.7385	3.7238	1.9853	-0.0127
1.2255	3.2112	1.9857	-0.0123	1.7317	3.7150	1.9833	-0.0147
1.2341	3.2209	1.9868	-0.0112	1.9592	3.9451	1.9859	-0.0121
1.2348	3.2207	1.9859	-0.0121	1.9161	3.8994	1.9833	-0.0147
1.2340	3.2208	1.9868	-0.0112	1.8307	3.8173	1.9866	-0.0114
1.2333	3.2200	1.9867	-0.0113	1.8868	3.8717	1.9849	-0.0131
1.3156	5.2955	3.9799	-0.0162	1.7650	5.7413	3.9763	-0.0198
1.3184	5.2938	3.9754	-0.0207	1.7683	5.7400	3.9717	-0.0244
1.3141	5.2918	3.9777	-0.0184	1.7595	5.7368	3.9773	-0.0188
BROKEN				BROKEN			
1.2304	5.2085	3.9781	-0.0180	1.7400	5.7198	3.9798	-0.0163
1.2271	5.2069	3.9798	-0.0163	1.7369	5.7136	3.9767	-0.0194

1.2261	5.2052	3.9791	-0.0170	1.8399	5.8126	3.9727	-0.0234
1.2352	5.2160	3.9808	-0.0153	1.8955	5.8720	3.9765	-0.0196
1.2343	5.2158	3.9815	-0.0146	1.8354	5.8148	3.9794	-0.0167
1.2352	5.2149	3.9797	-0.0164	1.8304	5.8062	3.9758	-0.0203

Date 3/20/94
Material 7920 batch 013-94 size 28μm packing about 42% FSC
Binder Rhoplex HA-16 co-dispersion, 10-17 vol.%
Printing condmisted, 0.5% citric, 1.3 cc/min, rinsed, 30 layers printed

Bar	Bar no.	Dried (60°C)		Diff	Error	X-linked (160°C)		Diff	Error
		X1	X2			X1	X2		
0.1309	0.131.1	1.2001	1.3297	0.1296	-0.0013	4.4848	4.6145	0.1297	-0.0012
0.1309	0.131.1	1.2174	1.3465	0.1291	-0.0018	NOT APPLICABLE			
0.1309	0.131.2	1.2109	1.3400	0.1291	-0.0018	4.4280	4.5566	0.1286	-0.0023
0.1309	0.131.2	1.2086	1.3389	0.1303	-0.0006	NOT APPLICABLE			
0.1309	0.131.3	1.3157	1.4441	0.1284	-0.0025	4.4159	4.5448	0.1289	-0.0020
0.1309	0.131.3	1.3110	1.4399	0.1289	-0.0020	NOT APPLICABLE			
0.1309	0.131.4	4.5120	4.6422	0.1302	-0.0007	5.3870	5.5166	0.1296	-0.0013
0.1309	0.131.5	4.5129	4.6424	0.1295	-0.0014	5.3810	5.5103	0.1293	-0.0016
0.1309	0.131.6	4.5145	4.6439	0.1294	-0.0015	5.3767	5.5060	0.1293	-0.0016
0.1309	0.131.7	5.5993	5.7276	0.1283	-0.0026	5.1731	5.3016	0.1285	-0.0024
0.1309	0.131.8	5.5961	5.7251	0.1290	-0.0019	5.1724	5.3010	0.1286	-0.0023
0.1309	0.131.9	5.5934	5.7229	0.1295	-0.0014	5.1715	5.3002	0.1287	-0.0022
0.1309	0.131.10	5.5906	5.7200	0.1294	-0.0015	5.1710	5.2999	0.1289	-0.0020
0.372	0.375.1	BROKEN				BROKEN			
0.372	0.375.2	1.5883	1.9607	0.3724	0.0004	3.8659	4.2364	0.3705	-0.0015
0.372	0.375.2	1.5875	1.9585	0.3710	-0.0010	NOT APPLICABLE			
0.372	0.375.3	1.6055	1.9770	0.3715	-0.0005	3.8764	4.2487	0.3723	0.0003
0.372	0.375.3	1.6052	1.9761	0.3709	-0.0011	NOT APPLICABLE			
0.372	0.375.4	3.8910	4.2618	0.3708	-0.0012	4.7656	5.1370	0.3714	-0.0006
0.372	0.375.5	3.8900	4.2609	0.3709	-0.0011	4.7581	5.1298	0.3717	-0.0003
0.372	0.375.6	3.8922	4.2638	0.3716	-0.0004	4.7557	5.1266	0.3709	-0.0011
0.372	0.375.7	4.9780	5.3472	0.3692	-0.0028	4.5517	4.9229	0.3712	-0.0008
0.372	0.375.8	4.9750	5.3463	0.3713	-0.0007	4.5512	4.9220	0.3708	-0.0012
0.372	0.375.9	4.9716	5.3424	0.3708	-0.0012	4.5500	4.9209	0.3709	-0.0011
0.372	0.375.10	4.9698	5.3403	0.3705	-0.0015	4.5492	4.9209	0.3717	-0.0003
0.7441	0.75.1	2.2066	2.9472	0.7406	-0.0035	2.9046	3.6449	0.7403	-0.0038
0.7441	0.75.1	2.2066	2.9466	0.7400	-0.0041	NOT APPLICABLE			
0.7441	0.75.2	2.2088	2.9487	0.7399	-0.0042	2.9008	3.6409	0.7401	-0.0040
0.7441	0.75.2	2.2063	2.9469	0.7406	-0.0035	NOT APPLICABLE			
0.7441	0.75.3	2.2156	2.9568	0.7412	-0.0029	2.8978	3.6384	0.7406	-0.0035
0.7441	0.75.3	2.2137	2.9539	0.7402	-0.0039	NOT APPLICABLE			
0.7441	0.75.4	2.9003	3.6411	0.7408	-0.0033	3.7758	4.5162	0.7404	-0.0037
0.7441	0.75.5	2.9015	3.6418	0.7403	-0.0038	3.7691	4.5101	0.7410	-0.0031
0.7441	0.75.6	2.9026	3.6425	0.7399	-0.0042	3.7655	4.5059	0.7404	-0.0037
0.7441	0.75.7	3.9863	4.7273	0.7410	-0.0031	3.5617	4.3022	0.7405	-0.0036
0.7441	0.75.8	3.9841	4.7248	0.7407	-0.0034	3.5605	4.3020	0.7415	-0.0026
0.7441	0.75.9	3.9813	4.7218	0.7405	-0.0036	3.5594	4.2996	0.7402	-0.0039
0.7441	0.75.10	3.9792	4.7198	0.7406	-0.0035	3.5589	4.2997	0.7408	-0.0033
1.998	2.1	3.2063	5.1909	1.9846	-0.0134	0.6606	2.6454	1.9848	-0.0132
1.998	2.1	3.2055	5.1895	1.9840	-0.0140	NOT APPLICABLE			
1.998	2.2	3.2070	5.1925	1.9855	-0.0125	0.6579	2.6427	1.9848	-0.0132
1.998	2.2	3.2055	5.1906	1.9851	-0.0129	NOT APPLICABLE			
1.998	2.3	3.2187	5.2036	1.9849	-0.0131	0.6509	2.6352	1.9843	-0.0137
1.998	2.3	3.2163	5.2013	1.9850	-0.0130	NOT APPLICABLE			
1.998	2.4	0.6548	2.6403	1.9855	-0.0125	1.5294	3.5153	1.9859	-0.0121

1.998	2.5	0.6549	2.6420	1.9871	-0.0109	1.5234	3.5103	1.9869	-0.0111
1.998	2.6	0.6561	2.6421	1.9860	-0.0120	1.5183	3.5053	1.9870	-0.0110
1.998	2.7	1.7391	3.7255	1.9864	-0.0116	1.3134	3.3013	1.9879	-0.0101
1.998	2.8	1.7383	3.7249	1.9866	-0.0114	1.3144	3.3015	1.9871	-0.0109
1.998	2.9	1.7375	3.7236	1.9861	-0.0119	1.3161	3.3018	1.9857	-0.0123
1.998	2.10	BROKEN				BROKEN			
3.9961	4.1	1.2095	5.1887	3.9792	-0.0169	0.6613	4.6412	3.9799	-0.0162
3.9961	4.1	1.2089	5.1888	3.9799	-0.0162	NOT APPLICABLE			
3.9961	4.2	1.2096	5.1861	3.9765	-0.0196	BROKEN			
3.9961	4.2	1.2083	5.1853	3.9770	-0.0191	NOT APPLICABLE			
3.9961	4.3	1.2181	5.1941	3.9760	-0.0201	0.6561	4.6320	3.9759	-0.0202
3.9961	4.3	1.2169	5.1937	3.9768	-0.0193	NOT APPLICABLE			
3.9961	4.4	0.6565	4.6322	3.9757	-0.0204	1.5335	5.5100	3.9765	-0.0196
3.9961	4.5	0.6559	4.6343	3.9784	-0.0177	1.5277	5.5065	3.9788	-0.0173
3.9961	4.6	0.6573	4.6362	3.9789	-0.0172	1.5226	5.5019	3.9793	-0.0168
3.9961	4.7	BROKEN				BROKEN			
3.9961	4.8	1.7403	5.7208	3.9805	-0.0156	1.3155	5.2958	3.9803	-0.0158
3.9961	4.9	1.7393	5.7168	3.9775	-0.0186	1.3162	5.2949	3.9787	-0.0174
3.9961	4.10	1.7350	5.7142	3.9792	-0.0169	1.3140	5.2941	3.9801	-0.0160

Date 3/20/94
Material 7920 batch 013-94 size 28μm packing about 42% FSC
Binder Rhoplex HA-16 co-dispersion, 10-17 vol.%
Printing condmisted, 0.5% citric, 1.3 cc/min, rinsed, 30 layers printed

fired (900°C)		Diff	Error
X1	X2		
2.2826	2.4121	0.1295	-0.0014
NOT APPLICABLE			
2.2509	2.3789	0.1280	-0.0029
NOT APPLICABLE			
2.2280	2.3562	0.1282	-0.0027
NOT APPLICABLE			
2.5832	2.7128	0.1296	-0.0013
2.5862	2.7150	0.1288	-0.0021
2.5796	2.7088	0.1292	-0.0017
5.9970	6.1252	0.1282	-0.0027
5.9261	6.0552	0.1291	-0.0018
5.9221	6.0511	0.1290	-0.0019
5.9044	6.0329	0.1285	-0.0024
BROKEN			
1.6783	2.0490	0.3707	-0.0013
NOT APPLICABLE			
1.6778	2.0472	0.3694	-0.0026
NOT APPLICABLE			
1.9623	2.3329	0.3706	-0.0014
1.9585	2.3296	0.3711	-0.0009
1.9571	2.3281	0.3710	-0.0010
5.3028	5.6734	0.3706	-0.0014
5.3033	5.6732	0.3699	-0.0021
5.2978	5.6678	0.3700	-0.0020
5.2927	5.6641	0.3714	-0.0006
0.7176	1.4582	0.7406	-0.0035
NOT APPLICABLE			
0.7142	1.4536	0.7394	-0.0047
NOT APPLICABLE			
0.6910	1.4296	0.7386	-0.0055

NOT APPLICABLE
0.9728 1.7121 0.7393 -0.0048
0.9698 1.7089 0.7391 -0.0050
0.9678 1.7075 0.7397 -0.0044
4.3117 5.0512 0.7395 -0.0046
4.3128 5.0526 0.7398 -0.0043
4.3080 5.0485 0.7405 -0.0036
4.3077 5.0470 0.7393 -0.0048
-1.5233 0.4587 1.9820 -0.0160
NOT APPLICABLE
-1.5290 0.4546 1.9836 -0.0144
NOT APPLICABLE
-1.5332 0.4580 1.9912 -0.0068
NOT APPLICABLE
-1.2709 0.7127 1.9836 -0.0144
-1.2749 0.7102 1.9851 -0.0129
-1.2759 0.7084 1.9843 -0.0137
2.0712 4.0557 1.9845 -0.0135
2.0685 4.0532 1.9847 -0.0133
2.0680 4.0520 1.9840 -0.0140
BROKEN
-1.5223 2.4532 3.9755 -0.0206
NOT APPLICABLE
BROKEN
NOT APPLICABLE
-1.5211 2.4516 3.9727 -0.0234
NOT APPLICABLE
BROKEN
-1.2733 2.7035 3.9768 -0.0193
-1.2741 2.7011 3.9752 -0.0209
BROKEN
2.0713 6.0463 3.9750 -0.0211
2.0702 6.0446 3.9744 -0.0217
2.0672 6.0404 3.9732 -0.0229

Date 4/14/94
Material 7920 batch 013-94 size 28μm packing about 42% FSC
Binder Rhoplex HA-16 binder, 10 vol.% polymer solids, ammonia added
Printing condmisted, 0.5% citric, 1.2 cc/min, rinsed, 30 layers printed

Bar length	Bar no.	Wet		Diff	Error	Dried (60°C)		Diff	Error
		X1	X2			X1	X2		
3.9961	4.1	BROKEN				BROKEN			
1.998	2.1	5.8039	7.8030	1.9991	0.0011	3.6119	5.6103	1.9984	0.0004
0.7441	0.75.1	8.0567	8.8008	0.7441	0.0000	5.8645	6.6085	0.7440	-0.0001
0.372	0.375.1	9.0488	9.4217	0.3729	0.0009	6.8560	7.2284	0.3724	0.0004
0.1309	0.131.1	9.6803	9.8109	0.1306	-0.0003	6.0900	6.2201	0.1301	-0.0008
3.9961	4.2	5.8024	9.7984	3.9960	-0.0001	3.6096	7.6032	3.9936	-0.0025
1.998	2.2	5.8021	7.8010	1.9989	0.0009	3.6085	5.6062	1.9977	-0.0003
0.7441	0.75.2	8.0547	8.7995	0.7448	0.0007	5.8606	6.6047	0.7441	0.0000
0.372	0.375.2	9.0472	9.4201	0.3729	0.0009	6.8535	7.2255	0.3720	0.0000
0.1309	0.131.2	9.6672	9.7976	0.1304	-0.0005	7.4722	7.6021	0.1299	-0.0010
3.9961	4.3	5.8017	9.7961	3.9944	-0.0017	3.6069	7.5999	3.9930	-0.0031
1.998	2.3	5.8007	7.7996	1.9989	0.0009	3.6057	5.6033	1.9976	-0.0004
0.7441	0.75.3	8.0534	8.7968	0.7434	-0.0007	5.8577	6.6003	0.7426	-0.0015
0.372	0.375.3	9.0460	9.4192	0.3732	0.0012	6.8494	7.2226	0.3732	0.0012
0.1309	0.131.3	9.6659	9.7951	0.1292	-0.0017	7.4689	7.5986	0.1297	-0.0012

3.9961	4.4	5.8001	9.7951	3.9950	-0.0011	3.6035	7.5966	3.9931	-0.0030
1.998	2.4	5.8076	7.8056	1.9980	0.0000	3.6494	5.6468	1.9974	-0.0006
0.7441	0.75.4	8.0603	8.8032	0.7429	-0.0012	5.9020	6.6446	0.7426	-0.0015
0.372	0.375.4	9.0509	9.4249	0.3740	0.0020	6.8927	7.2658	0.3731	0.0011
0.1309	0.131.4	9.6716	9.8011	0.1295	-0.0014	7.5114	7.6416	0.1302	-0.0007
3.9961	4.5	5.8070	9.8020	3.9950	-0.0011	3.6462	7.6395	3.9933	-0.0028
1.998	2.5	5.8057	7.8044	1.9987	0.0007	3.6437	5.6414	1.9977	-0.0003
0.7441	0.75.5	8.0590	8.8029	0.7439	-0.0002	5.8961	6.6396	0.7435	-0.0006
0.372	0.375.5	9.0503	9.4235	0.3732	0.0012	6.8891	7.2602	0.3711	-0.0009
0.1309	0.131.5	9.6711	9.8020	0.1309	0.0000	7.5077	7.6382	0.1305	-0.0004
3.9961	4.6	5.8054	9.8004	3.9950	-0.0011	3.6407	7.6340	3.9933	-0.0028
1.998	2.6	5.8052	7.8042	1.9990	0.0010	3.6386	5.6365	1.9979	-0.0001
0.7441	0.75.6	8.0576	8.8015	0.7439	-0.0002	5.8906	6.6334	0.7428	-0.0013
0.372	0.375.6	9.0505	9.4222	0.3717	-0.0003	6.8835	7.2545	0.3710	-0.0010
0.1309	0.131.6	9.6704	9.8008	0.1304	-0.0005	7.5022	7.6330	0.1308	-0.0001
3.9961	4.7	5.8051	9.7994	3.9943	-0.0018	3.6359	7.6292	3.9933	-0.0028
1.998	2.7	5.8039	7.8035	1.9996	0.0016	3.6330	5.6317	1.9987	0.0007
0.7441	0.75.7	8.0568	8.8006	0.7438	-0.0003	5.8859	6.6281	0.7422	-0.0019
0.372	0.375.7	9.0479	9.4222	0.3743	0.0023	6.8769	7.2502	0.3733	0.0013
0.1309	0.131.7	9.6682	9.7984	0.1302	-0.0007	7.4953	7.6261	0.1308	-0.0001
3.9961	4.8	5.7794	9.7744	3.9950	-0.0011	bad measurement			
1.998	2.8	5.7778	7.7773	1.9995	0.0015	3.7125	5.7119	1.9994	0.0014
0.7441	0.75.8	8.0301	8.7753	0.7452	0.0011	5.9650	6.7098	0.7448	0.0007
0.372	0.375.8	9.0238	9.3958	0.3720	0.0000	6.9585	7.3308	0.3723	0.0003
0.1309	0.131.8	9.6420	9.7718	0.1298	-0.0011	7.5769	7.7078	0.1309	0.0000
3.9961	4.9	5.7760	9.7706	3.9946	-0.0015	3.7123	7.7060	3.9937	-0.0024
1.998	2.9	5.7735	7.7730	1.9995	0.0015	3.7110	5.7096	1.9986	0.0006
0.7441	0.75.9	8.0268	8.7704	0.7436	-0.0005	5.9637	6.7072	0.7435	-0.0006
0.372	0.375.9	9.0190	9.3926	0.3736	0.0016	6.9545	7.3300	0.3755	0.0035
0.1309	0.131.9	9.6385	9.7694	0.1309	0.0000	7.5745	7.7052	0.1307	-0.0002
3.9961	4.10	5.7716	9.7667	3.9951	-0.0010	3.7098	7.7036	3.9938	-0.0023
1.998	2.10	5.7694	7.7681	1.9987	0.0007	3.7081	5.7062	1.9981	0.0001
0.7441	0.75.10	8.0216	8.7683	0.7467	0.0026	5.9601	6.7050	0.7449	0.0008
0.372	0.375.10	9.0142	9.3860	0.3718	-0.0002	6.9516	7.3246	0.3730	0.0010
0.1309	0.131.10	9.6353	9.7660	0.1307	-0.0002	7.5727	7.7040	0.1313	0.0004

Date 4/14/94
Material 7920 batch 013-94 size 28μm packing about 42% FSC
Binder Rhoplex HA-16 binder, 10 vol.% polymer solids, ammonia added
Printing condmisted, 0.5% citric, 1.2 cc/min, rinsed, 30 layers printed

X-linked (160°C)		Diff	Error
X1	X2		
BROKEN			
5.6224	7.6207	1.9983	0.0003
7.8750	8.6162	0.7412	-0.0029
8.8647	9.2377	0.3730	0.0010
8.0900	8.2212	0.1312	0.0003
5.6203	9.6132	3.9929	-0.0032
5.6208	7.6180	1.9972	-0.0008
7.8722	8.6162	0.7440	-0.0001
8.8647	9.2376	0.3729	0.0009
9.4844	9.6151	0.1307	-0.0002
5.6210	9.6130	3.9920	-0.0041
5.6211	7.6186	1.9975	-0.0005
7.8728	8.6157	0.7429	-0.0012
8.8647	9.2371	0.3724	0.0004

9.4844	9.6144	0.1300	-0.0009
5.6209	9.6141	3.9932	-0.0029
6.9194	8.9161	1.9967	-0.0013
9.1714	9.9137	0.7423	-0.0018
10.1625	10.5346	0.3721	0.0001
10.7815	10.9126	0.1311	0.0002
6.9190	10.9114	3.9924	-0.0037
6.9183	8.9152	1.9969	-0.0011
9.1695	9.9129	0.7434	-0.0007
10.1617	10.5340	0.3723	0.0003
10.7802	10.9110	0.1308	-0.0001
6.9172	10.9097	3.9925	-0.0036
6.9172	8.9152	1.9980	0.0000
9.1687	9.9121	0.7434	-0.0007
10.1615	10.5336	0.3721	0.0001
10.7791	10.9097	0.1306	-0.0003
6.9162	10.9082	3.9920	-0.0041
6.9155	8.9138	1.9983	0.0003
9.1684	9.9117	0.7433	-0.0008
10.1584	10.5319	0.3735	0.0015
10.7772	10.9074	0.1302	-0.0007
4.2242	8.2179	3.9937	-0.0024
4.2229	6.2221	1.9992	0.0012
6.4752	7.2202	0.7450	0.0009
7.4687	7.8409	0.3722	0.0002
8.0869	8.2177	0.1308	-0.0001
4.2220	8.2154	3.9934	-0.0027
4.2201	6.2186	1.9985	0.0005
6.4726	7.2159	0.7433	-0.0008
7.4640	7.8384	0.3744	0.0024
8.0836	8.2142	0.1306	-0.0003
4.2186	8.2118	3.9932	-0.0029
4.2167	6.2150	1.9983	0.0003
6.4694	7.2140	0.7446	0.0005
7.4605	7.8334	0.3729	0.0009
8.0818	8.2122	0.1304	-0.0005

Date printed3/22/94
Material 7920 batch 013-94 size 28μm packing about 42% FSC
Binder Rhoplex HA-16 co-dispersion, 10-17 vol.%
Printing condmisted, 0.3% citric, 1.2 cc/min, rinsed, 30 layers printed

Bar	Bar no.		post-dipped, 2nd fired (900°C)			
			x1	x2	diff	error
3.9961	4.1	1	1.5817	5.5546	3.9729	-0.0232
1.998	2.1	1	1.5849	3.5651	1.9802	-0.0178
0.7441	0.75.1	1	3.6491	4.3869	0.7378	-0.0063
0.372	0.375.1	1	4.4660	4.8365	0.3705	-0.0015
0.1309	0.131.1	1	4.9184	5.0474	0.1290	-0.0019
3.9961	4.2	2	1.5868	5.5570	3.9702	-0.0259
1.998	2.2	2	1.5877	3.5697	1.9820	-0.0160
0.7441	0.75.2	2	3.6529	4.3913	0.7384	-0.0057
0.372	0.375.2	2	4.4719	4.8424	0.3705	-0.0015
0.1309	0.131.2	2	4.9248	5.0550	0.1302	-0.0007
3.9961	4.3	3	1.5916	5.5621	3.9705	-0.0256
1.998	2.3	3	1.5910	3.5707	1.9797	-0.0183
0.7441	0.75.3	3	3.6560	4.3938	0.7378	-0.0063

0.372	0.375.3	3	4.4742	4.8448	0.3706	-0.0014
0.1309	0.131.3	3	4.9270	5.0564	0.1294	-0.0015
3.9961	4.4	4	BROKEN			
1.998	2.4	4	1.5901	3.5709	1.9808	-0.0172
0.7441	0.75.4	4	3.6547	4.3938	0.7391	-0.0050
0.372	0.375.4	4	4.4732	4.8450	0.3718	-0.0002
0.1309	0.131.4	4	4.9239	5.0534	0.1295	-0.0014
3.9961	4.5	5	1.5890	5.5612	3.9722	-0.0239
1.998	2.5	5	1.5886	3.5718	1.9832	-0.0148
0.7441	0.75.5	5	3.6255	4.3632	0.7377	-0.0064
0.372	0.375.5	5	4.4436	4.8147	0.3711	-0.0009
0.1309	0.131.5	5	4.8954	5.0249	0.1295	-0.0014

Date printed3/22/94
Material 7920 batch 013-94 size 28μm packing about 42% FSC
Binder Rhoplex HA-16 co-dispersion, 10-17 vol.%
Printing condmisted, 0.3% citric, 1.2 cc/min, rinsed, 30 layers printed

Bar	Bar no.		control, 2nd fired (900°C)			
			x1	x2	diff	error
3.9961	4.6	6	1.5535	5.5299	3.9764	-0.0197
1.998	2.6	6	1.5497	3.5333	1.9836	-0.0144
0.7441	0.75.6	6	3.6144	4.3549	0.7405	-0.0036
0.372	0.375.6	6	4.4331	4.8038	0.3707	-0.0013
0.1309	0.131.6	6	4.8860	5.0169	0.1309	0.0000
3.9961	4.7	7	1.5475	5.5221	3.9746	-0.0215
1.998	2.7	7	1.5427	3.5277	1.9850	-0.0130
0.7441	0.75.7	7	3.6100	4.3494	0.7394	-0.0047
0.372	0.375.7	7	4.4272	4.7997	0.3725	0.0005
0.1309	0.131.7	7	4.8789	5.0080	0.1291	-0.0018
3.9961	4.8	8	1.5402	5.5164	3.9762	-0.0199
1.998	2.8	8	1.5382	3.5215	1.9833	-0.0147
0.7441	0.75.8	8	3.6043	4.3426	0.7383	-0.0058
0.372	0.375.8	8	4.4223	4.7939	0.3716	-0.0004
0.1309	0.131.8	8	4.8768	5.0072	0.1304	-0.0005
3.9961	4.9	9	1.9684	5.9468	3.9784	-0.0177
1.998	2.9	9	2.4755	4.4620	1.9865	-0.0115
0.7441	0.75.9	9	4.5424	5.2804	0.7380	-0.0061
0.372	0.375.9	9	5.3613	5.7338	0.3725	0.0005
0.1309	0.131.9	9	5.8118	5.9411	0.1293	-0.0016
3.9961	4.10	10	1.9543	5.9304	3.9761	-0.0200
1.998	2.10	10	2.4557	4.4414	1.9857	-0.0123
0.7441	0.75.10	10	4.5240	5.2624	0.7384	-0.0057
0.372	0.375.10	10	5.3456	5.7177	0.3721	0.0001
0.1309	0.131.10	10	5.7964	5.9260	0.1296	-0.0013

Date 3/20/94
Material 7920 batch 013-94 size 28μm packing about 42% FSC
Binder Rhoplex HA-16 co-dispersion, 10-17 vol.%
Printing condmisted, 0.5% citric, 1.3 cc/min, rinsed, 30 layers printed

Bar	Bar no.		post-dipped, 2nd fired (900°C)			
			x1	x2	diff	error
3.9961	4.1	1	BROKEN			
1.998	2.1	1	1.7564	3.7384	1.9820	-0.0160
0.7441	0.75.1	1	3.8216	4.5613	0.7397	-0.0044
0.372	0.375.1	1	BROKEN			
0.1309	0.131.1	1	4.6419	4.7715	0.1296	-0.0013
3.9961	4.2	2	BROKEN			
1.998	2.2	2	1.7644	3.7457	1.9813	-0.0167
0.7441	0.75.2	2	3.8263	4.5652	0.7389	-0.0052
0.372	0.375.2	2	4.6422	5.0124	0.3702	-0.0018
0.1309	0.131.2	2	5.0965	5.2256	0.1291	-0.0018
3.9961	4.3	3	1.7630	5.7337	3.9707	-0.0254
1.998	2.3	3	1.7619	3.7440	1.9821	-0.0159
0.7441	0.75.3	3	3.8238	4.5626	0.7388	-0.0053
0.372	0.375.3	3	4.6405	5.0119	0.3714	-0.0006
0.1309	0.131.3	3	5.0906	5.2192	0.1286	-0.0023
3.9961	4.4	4	BROKEN			
1.998	2.4	4	1.7603	3.7428	1.9825	-0.0155
0.7441	0.75.4	4	3.8226	4.5614	0.7388	-0.0053
0.372	0.375.4	4	4.6398	5.0110	0.3712	-0.0008
0.1309	0.131.4	4	5.0898	5.2185	0.1287	-0.0022
3.9961	4.5	5	1.7587	5.7310	3.9723	-0.0238
1.998	2.5	5	1.7563	3.7399	1.9836	-0.0144
0.7441	0.75.5	5	3.8203	4.5596	0.7393	-0.0048
0.372	0.375.5	5	4.6365	5.0075	0.3710	-0.0010
0.1309	0.131.5	5	5.0867	5.2161	0.1294	-0.0015

Date 3/20/94
Material 7920 batch 013-94 size 28μm packing about 42% FSC
Binder Rhoplex HA-16 co-dispersion, 10-17 vol.%
Printing condmisted, 0.5% citric, 1.3 cc/min, rinsed, 30 layers printed

Bar	Bar no.		control, 2nd fired (900°C)			
			x1	x2	diff	error
3.9961	4.6	6	1.7557	5.7308	3.9751	-0.0210
1.998	2.6	6	1.7528	3.7378	1.9850	-0.0130
0.7441	0.75.6	6	3.8239	4.5630	0.7391	-0.0050
0.372	0.375.6	6	4.6410	5.0124	0.3714	-0.0006
0.1309	0.131.6	6	5.0917	5.2210	0.1293	-0.0016
3.9961	4.7	7	BROKEN			
1.998	2.7	7	1.7582	3.7428	1.9846	-0.0134
0.7441	0.75.7	7	3.8245	4.5641	0.7396	-0.0045
0.372	0.375.7	7	4.6419	5.0130	0.3711	-0.0009
0.1309	0.131.7	7	5.0922	5.2204	0.1282	-0.0027
3.9961	4.8	8	1.7582	5.7338	3.9756	-0.0205
1.998	2.8	8	1.7572	3.7420	1.9848	-0.0132
0.7441	0.75.8	8	3.8230	4.5631	0.7401	-0.0040
0.372	0.375.8	8	4.6398	5.0105	0.3707	-0.0013
0.1309	0.131.8	8	5.0896	5.2185	0.1289	-0.0020
3.9961	4.9	9	1.7612	5.7358	3.9746	-0.0215

1.998	2.9	9	1.7515	3.7353	1.9838	-0.0142
0.7441	0.75.9	9	3.8141	4.5535	0.7394	-0.0047
0.372	0.375.9	9	4.6326	5.0034	0.3708	-0.0012
0.1309	0.131.9	9	5.0810	5.2100	0.1290	-0.0019
3.9961	4.10	10	BROKEN			
1.998	2.10	10	BROKEN			
0.7441	0.75.10	10	1.7475	2.4870	0.7395	-0.0046
0.372	0.375.10	10	2.5664	2.9366	0.3702	-0.0018
0.1309	0.131.10	10	3.0183	3.1473	0.1290	-0.0019

C.3 Warping Data

Silica plate #1, right side of powder bed, fired at 900°C

x1	y1	z1	x2	y2	z2	x3	y3	z3
0.1237	0.1186	-0.0922	0.1242	0.1192	-0.0920	0.1238	0.1188	-0.0878
0.8753	0.1175	-0.0964	0.8756	0.1180	-0.0960	0.8754	0.1175	-0.0921
1.6228	0.1139	-0.0970	1.6230	0.1143	-0.0968	1.6227	0.1141	-0.0929
2.3726	0.1198	-0.0976	2.3727	0.1200	-0.0969	2.3729	0.1200	-0.0934
3.1257	0.1123	-0.0938	3.1258	0.1125	-0.0929	3.1256	0.1123	-0.0896
0.1286	0.8675	-0.0977	0.1289	0.8678	-0.0977	0.1282	0.8676	-0.0934
0.8736	0.8707	-0.1014	0.8739	0.8707	-0.1013	0.8734	0.8714	-0.0971
1.6255	0.8716	-0.1028	1.6259	0.8722	-0.1023	1.6258	0.8718	-0.0986
2.3747	0.8719	-0.1009	2.3746	0.8722	-0.1005	2.3751	0.8724	-0.0968
3.1284	0.8709	-0.0972	3.1285	0.8711	-0.0967	3.1286	0.8710	-0.0932
0.1292	1.6180	-0.0965	0.1294	1.6178	-0.0968	0.1292	1.6178	-0.0921
0.8779	1.6214	-0.1012	0.8780	1.6208	-0.1017	0.8783	1.6217	-0.0972
1.6268	1.6197	-0.1025	1.6269	1.6198	-0.1026	1.6267	1.6196	-0.0990
2.3768	1.6196	-0.1011	2.3769	1.6200	-0.1012	2.3767	1.6198	-0.0972
3.1252	1.6216	-0.0965	3.1254	1.6215	-0.0959	3.1258	1.6217	-0.0930
0.1325	2.3692	-0.0965	0.1328	2.3692	-0.0967	0.1329	2.3696	-0.0921
0.8793	2.3675	-0.1009	0.8792	2.3671	-0.1012	0.8796	2.3672	-0.0966
1.6266	2.3709	-0.1013	1.6269	2.3701	-0.1012	1.6268	2.3708	-0.0969
2.3803	2.3688	-0.1004	2.3806	2.3687	-0.1004	2.3808	2.3684	-0.0963
3.1300	2.3699	-0.0973	3.1299	2.3706	-0.0971	3.1302	2.3700	-0.0927
0.1308	3.1177	-0.0950	0.1309	3.1171	-0.0954	0.1307	3.1172	-0.0907
0.8825	3.1205	-0.0988	0.8827	3.1199	0.0988	0.8825	3.1207	-0.0950
1.6312	3.1162	-0.0993	1.6315	3.1158	-0.0993	1.6317	3.1160	-0.0951
2.3806	3.1196	-0.0974	2.3809	3.1188	-0.0975	2.3808	3.1198	-0.0933
3.1304	3.1168	-0.0935	3.1303	3.1167	-0.0932	3.1308	3.1166	-0.0897

Silica plate #2, middle of powder bed, fired at 900°C

xavg	yavg	xdev	ydev	zavg
0.1252	0.1179	0.0002	0.0004	-0.0936
0.8765	0.1167	0.0001	0.0006	-0.0968
1.6235	0.1133	0.0003	0.0007	-0.0977
2.3734	0.1200	0.0001	0.0004	-0.0965
3.1267	0.1120	0.0002	0.0002	-0.0931
0.1295	0.8669	0.0002	0.0002	-0.0976
0.8747	0.8690	0.0002	0.0003	-0.1018
1.6270	0.8707	0.0002	0.0003	-0.1033
2.3758	0.8711	0.0002	0.0004	-0.1023
3.1298	0.8699	0.0001	0.0004	-0.0976
0.1301	1.6172	0.0001	0.0002	-0.0988
0.8792	1.6194	0.0001	0.0002	-0.1017
1.6279	1.6182	0.0002	0.0005	-0.1035
2.3779	1.6186	0.0001	0.0003	-0.1034
3.1269	1.6201	0.0002	0.0005	-0.1012
0.1337	2.3686	0.0002	0.0004	-0.0967
0.8805	2.3659	0.0003	0.0003	-0.1013
1.6277	2.3675	0.0002	0.0001	-0.1023
2.3817	2.3674	0.0001	0.0007	-0.1014

3.1315	2.3689	0.0003	0.0004	-0.0964
0.1318	3.1163	0.0003	0.0003	-0.0940
0.8836	3.1183	0.0002	0.0003	-0.0993
1.6325	3.1156	0.0002	0.0007	-0.0998
2.3822	3.1169	0.0002	0.0002	-0.0998
3.1319	3.1158	0.0002	0.0005	-0.0963

Silica plate #3, left side of powder bed, fired at 900°C

x	y	z	xdev	ydev	zdev
0.1255	0.1178	-0.0903	0.0005	0.0004	0.0005
0.8767	0.1170	-0.0945	0.0002	0.0004	0.0003
1.6238	0.1127	-0.0949	0.0001	0.0006	0.0003
2.3736	0.1194	-0.0950	0.0001	0.0003	0.0002
3.1266	0.1111	-0.0909	0.0003	0.0006	0.0003
0.1298	0.8667	-0.0939	0.0002	0.0002	0.0001
0.8748	0.8687	-0.0994	0.0001	0.0005	0.0002
1.6274	0.8682	-0.0997	0.0003	0.0004	0.0002
2.3759	0.8683	-0.0990	0.0002	0.0003	0.0002
3.1299	0.8669	-0.0961	0.0002	0.0003	0.0003
0.1305	1.6168	-0.0950	0.0002	0.0003	0.0002
0.8793	1.6187	-0.0999	0.0002	0.0003	0.0002
1.6279	1.6159	-0.0998	0.0002	0.0004	0.0002
2.3781	1.6158	-0.0985	0.0002	0.0003	0.0001
3.1268	1.6177	-0.0967	0.0002	0.0004	0.0005
0.1341	2.3685	-0.0939	0.0002	0.0003	0.0002
0.8808	2.3638	-0.0990	0.0002	0.0002	0.0002
1.6280	2.3673	-0.0991	0.0003	0.0003	0.0003
2.3818	2.3646	-0.0976	0.0001	0.0002	0.0002
3.1314	2.3663	-0.0928	0.0001	0.0004	0.0001
0.1321	3.1161	-0.0890	0.0001	0.0003	0.0002
0.8838	3.1168	-0.0937	0.0002	0.0004	0.0002
1.6327	3.1124	-0.0945	0.0002	0.0004	0.0003
2.3822	3.1161	-0.0938	0.0001	0.0004	0.0002
3.1319	3.1127	-0.0895	0.0003	0.0003	0.0002

TRIS Co-dispersion plate #1, right side of powder bed, crosslinked at 160°C

x1	y1	z1	z2	z3	zavg	zdev
0.1246	0.1166	-0.0937	-0.0936	-0.0936	-0.0936	0.0001
0.8765	0.1166	-0.0956	-0.0956	-0.0957	-0.0956	0.0001
1.6239	0.1122	-0.0958	-0.0959	-0.0958	-0.0958	0.0001
2.3734	0.1198	-0.0953	-0.0952	-0.0952	-0.0952	0.0001
3.1265	0.1109	-0.0921	-0.0920	-0.0921	-0.0921	0.0001
0.1298	0.8664	-0.0952	-0.0953	-0.0952	-0.0952	0.0001
0.8748	0.8686	-0.0978	-0.0979	-0.0978	-0.0978	0.0001
1.6271	0.8679	-0.0994	-0.0993	-0.0994	-0.0994	0.0001
2.3762	0.8684	-0.0976	-0.0976	-0.0975	-0.0976	0.0001
3.1302	0.8670	-0.0953	-0.0952	-0.0952	-0.0952	0.0001
0.1306	1.6168	-0.0947	-0.0945	-0.0946	-0.0946	0.0001
0.8792	1.6194	-0.0978	-0.0975	-0.0977	-0.0977	0.0002
1.6277	1.6159	-0.0986	-0.0987	-0.0987	-0.0987	0.0001
2.3782	1.6163	-0.0968	-0.0968	-0.0969	-0.0968	0.0001
3.1271	1.6177	-0.0930	-0.0928	-0.0930	-0.0929	0.0001

0.1337	2.3681	-0.0930	-0.0932	-0.0932	-0.0931	0.0001
0.8806	2.3638	-0.0948	-0.0948	-0.0948	-0.0948	0.0000
1.6278	2.3668	-0.0955	-0.0955	-0.0955	-0.0955	0.0000
2.3821	2.3654	-0.0951	-0.0951	-0.0951	-0.0951	0.0000
3.1316	2.3656	-0.0935	-0.0934	-0.0934	-0.0934	0.0001
0.1322	3.1160	-0.0948	-0.0949	-0.0947	-0.0948	0.0001
0.8838	3.1170	-0.0954	-0.0953	-0.0952	-0.0953	0.0001
1.6325	3.1126	-0.0947	-0.0947	-0.0948	-0.0947	0.0001
2.3823	3.1158	-0.0952	-0.0951	-0.0953	-0.0952	0.0001
3.1319	3.1124	-0.0947	-0.0948	-0.0945	-0.0947	0.0002

TRIS Co-dispersion plate #2, middle of powder bed, crosslinked at 160°C

x	y	z1	z2	z3	zavg
0.1246	0.1182	-0.0952	-0.0936	-0.0946	-0.0945
0.8766	0.1175	-0.0956	-0.0956	-0.0951	-0.0954
1.6236	0.1134	-0.0956	-0.0959	-0.0952	-0.0956
2.3732	0.1195	-0.0956	-0.0952	-0.0952	-0.0953
3.1267	0.1116	-0.0937	-0.092	-0.0935	-0.0931
0.1292	0.8671	-0.0961	-0.0953	-0.0958	-0.0957
0.8746	0.8687	-0.0993	-0.0979	-0.0988	-0.0987
1.6274	0.868	-0.0991	-0.0993	-0.0987	-0.099
2.3758	0.8684	-0.0983	-0.0976	-0.098	-0.098
3.1299	0.8675	-0.0934	-0.0952	-0.0934	-0.094
0.1301	1.6173	-0.0942	-0.0945	-0.0937	-0.0941
0.8791	1.6186	-0.0971	-0.0975	-0.0967	-0.0971
1.6276	1.6172	-0.0976	-0.0987	-0.0972	-0.0978
2.3778	1.6164	-0.0959	-0.0968	-0.0959	-0.0962
3.1268	1.6175	-0.0923	-0.0928	-0.0925	-0.0925
0.1336	2.3684	-0.0927	-0.0932	-0.092	-0.0926
0.8801	2.3666	-0.0935	-0.0948	-0.0934	-0.0939
1.6278	2.3668	-0.0958	-0.0955	-0.0955	-0.0956
2.382	2.3658	-0.0961	-0.0951	-0.096	-0.0957
3.1316	2.3662	-0.0917	-0.0934	-0.0918	-0.0923
0.1314	3.1165	-0.0922	-0.0949	-0.0918	-0.093
0.8833	3.117	-0.094	-0.0953	-0.0939	-0.0944
1.6323	3.1147	-0.0942	-0.0947	-0.0939	-0.0943
2.3823	3.1163	-0.0944	-0.0951	-0.0942	-0.0946
3.1319	3.1151	-0.0915	-0.0948	-0.0912	-0.0925

TRIS Co-dispersion plate #3, left side of powder bed, crosslinked at 160°C

x	y	z1	z2	z3	zavg
0.1258	0.1193	-0.0946	-0.0945	-0.0944	-0.0945
0.8758	0.1179	-0.0948	-0.0946	-0.0944	-0.0946
1.6232	0.1145	-0.0942	-0.094	-0.094	-0.0940667
2.373	0.1203	-0.0945	-0.0944	-0.0943	-0.0944
3.126	0.1126	-0.0933	-0.0935	-0.0933	-0.0933667
0.1289	0.8682	-0.0947	-0.0945	-0.0944	-0.0945333
0.8739	0.8696	-0.0979	-0.0975	-0.0975	-0.0976333
1.6261	0.8707	-0.0987	-0.0984	-0.0983	-0.0984667
2.3752	0.8717	-0.0984	-0.0983	-0.0982	-0.0983
3.1291	0.8708	-0.0954	-0.0951	-0.0951	-0.0952
0.1296	1.6184	-0.0927	-0.0926	-0.0924	-0.0925667

0.8783	1.6199	-0.0957	-0.0959	-0.096	-0.0958667
1.6269	1.6195	-0.0975	-0.0973	-0.0974	-0.0974
2.3773	1.6197	-0.0964	-0.0965	-0.0966	-0.0965
3.126	1.6209	-0.0946	-0.0946	-0.0945	-0.0945667
0.133	2.3699	-0.0911	-0.0912	-0.0911	-0.0911333
0.8796	2.3674	-0.0952	-0.0951	-0.0949	-0.0950667
1.6272	2.3687	-0.095	-0.0949	-0.0948	-0.0949
2.381	2.3692	-0.0945	-0.0944	-0.0946	-0.0945
3.1309	2.3702	-0.0928	-0.0927	-0.0927	-0.0927333
0.1312	3.1181	-0.0918	-0.0922	-0.0919	-0.0919667
0.883	3.1193	-0.0941	-0.0939	-0.0939	-0.0939667
1.6318	3.1162	-0.093	-0.0931	-0.0929	-0.093
2.3816	3.1177	-0.0925	-0.0923	-0.0924	-0.0924
3.1311	3.1168	-0.093	-0.0928	-0.0929	-0.0929

Ammonia Co-dispersion plate #1, right side of powder bed, crosslinked at 160°C

x	y	z1	z2	z3	zavg
0.1246	0.1176	-0.0957	-0.0952	-0.095	-0.0953
0.8767	0.1167	-0.0963	-0.0961	-0.0961	-0.0961667
1.6235	0.1129	-0.0955	-0.0952	-0.095	-0.0952333
2.3733	0.1193	-0.0952	-0.0948	-0.0945	-0.0948333
3.1267	0.1115	-0.0958	-0.0953	-0.0958	-0.0956333
0.1297	0.867	-0.0962	-0.0962	-0.0962	-0.0962
0.8749	0.8688	-0.0597	-0.0606	-0.0609	-0.09568
1.6274	0.8683	-0.0953	-0.0967	-0.0966	-0.0962
2.3758	0.8684	-0.096	-0.0963	-0.0962	-0.0961667
3.1299	0.8671	-0.0954	-0.0953	-0.0949	-0.0952
0.1303	1.6165	-0.0927	-0.0931	-0.0934	-0.0930667
0.8791	1.6189	-0.094	-0.0943	-0.0942	-0.0941667
1.6277	1.6159	-0.0941	-0.0942	-0.0943	-0.0942
2.3778	1.6156	-0.0938	-0.0935	-0.0935	-0.0936
3.1268	1.6176	-0.0936	-0.0935	-0.0935	-0.0935333
0.1339	2.3686	-0.0931	-0.0934	-0.0937	-0.0934
0.8808	2.3639	-0.0956	-0.0958	-0.0958	-0.0957333
1.6278	2.3672	-0.0936	-0.094	-0.0938	-0.0938
2.382	2.3653	-0.0939	-0.0938	-0.0938	-0.0938333
3.1317	2.3662	-0.0944	-0.0944	-0.0942	-0.0943333
0.1322	3.1159	-0.091	-0.0915	-0.0916	-0.0913667
0.8838	3.1171	-0.0934	-0.0935	-0.0934	-0.0934333
1.6322	3.1123	-0.0946	-0.0944	-0.0947	-0.0945667
2.3825	3.1159	-0.0907	-0.0918	-0.0919	-0.0914667
3.132	3.1126	-0.0944	-0.0946	-0.0946	-0.0945333

Ammonia Co-dispersion plate #3, left side of powder bed, crosslinked at 160°C

x	y	z1	z2	z3	zavg
0.1241	0.1175	-0.0958	-0.0956	-0.0956	-0.0956667
0.8754	0.1163	-0.0948	-0.0947	-0.0947	-0.0947333
1.6231	0.1128	-0.0953	-0.0957	-0.0955	-0.0955
2.3728	0.1189	-0.0958	-0.0959	-0.0961	-0.0959333
3.1257	0.1108	-0.0945	-0.0945	-0.0948	-0.0946
0.1286	0.8665	-0.0942	-0.0942	-0.0942	-0.0942

0.8736	0.8686	-0.0956	-0.096	-0.0959	-0.0958333
1.626	0.8681	-0.0966	-0.0966	-0.0966	-0.0966
2.375	0.8684	-0.097	-0.0967	-0.0966	-0.0967667
3.1289	0.8674	-0.0956	-0.0958	-0.0956	-0.0956667
0.1293	1.6168	-0.0917	-0.0918	-0.0916	-0.0917
0.8785	1.6196	-0.0938	-0.0943	-0.0941	-0.0940667
1.6267	1.6175	-0.0938	-0.0946	-0.0945	-0.0943
2.3773	1.6161	-0.0938	-0.0945	-0.0945	-0.0942667
3.126	1.618	-0.0927	-0.0927	-0.0928	-0.0927333
0.1331	2.3678	-0.0909	-0.0921	-0.0924	-0.0918
0.8796	2.3652	-0.0939	-0.0942	-0.0941	-0.0940667
1.6266	2.367	-0.0937	-0.0945	-0.0948	-0.0943333
2.3811	2.365	-0.0939	-0.0948	-0.0947	-0.0944667
3.1306	2.3663	-0.0924	-0.093	-0.093	-0.0928
0.1312	3.1158	-0.0906	-0.0909	-0.0908	-0.0907667
0.8832	3.1169	-0.0911	-0.0928	-0.0924	-0.0921
1.6316	3.1145	-0.0932	-0.0946	-0.0944	-0.0940667
2.3814	3.1159	-0.0943	-0.0945	-0.0942	-0.0943333
3.131	3.1136	-0.0927	-0.0941	-0.0939	-0.0935667

TRIS co-dispersion plate #1, right side of powder bed, fired at 900°C

x	y	z1	z2	z3	zavg
0.1249	0.1202	-0.0914	-0.0918	-0.092	-0.0917333
0.8767	0.1176	-0.0959	-0.0963	-0.0961	-0.0961
1.6239	0.1138	-0.097	-0.0969	-0.0965	-0.0968
2.3736	0.12	-0.0952	-0.0953	-0.0951	-0.0952
3.1268	0.1121	-0.0905	-0.0905	-0.0904	-0.0904667
0.1301	0.869	-0.0947	-0.0944	-0.094	-0.0943667
0.8748	0.8701	-0.1002	-0.0999	-0.0998	-0.0999667
1.6272	0.8692	-0.1009	-0.101	-0.1009	-0.1009333
2.3762	0.8691	-0.0986	-0.0986	-0.0982	-0.0984667
3.1298	0.8686	-0.0939	-0.0938	-0.0939	-0.0938667
0.1307	1.6186	-0.0925	-0.0923	-0.0926	-0.0924667
0.8793	1.6196	-0.0987	-0.1057	-0.1083	-0.1042333
1.6279	1.6174	-0.0998	-0.0994	-0.1004	-0.0998667
2.3779	1.6166	-0.0974	-0.0977	-0.0975	-0.0975333
3.1268	1.6193	-0.0923	-0.0927	-0.0927	-0.0925667
0.1342	2.3702	-0.0919	-0.0916	-0.0916	-0.0917
0.8804	2.3659	-0.0945	-0.0948	-0.0947	-0.0946667
1.6277	2.3681	-0.0955	-0.0966	-0.0967	-0.0962667
2.382	2.3662	-0.0949	-0.0957	-0.0957	-0.0954333
3.1314	2.3672	-0.0911	-0.0915	-0.0916	-0.0914
0.1324	3.1184	-0.0899	-0.09	-0.0904	-0.0901
0.8839	3.118	-0.0938	-0.094	-0.0935	-0.0937667
1.6327	3.1139	-0.093	-0.0927	-0.0927	-0.0928
2.3824	3.1174	-0.093	-0.0929	-0.0928	-0.0929
3.132	3.114	-0.0904	-0.0903	-0.0901	-0.0902667

TRIS co-dispersion plate #2, middle of powder bed, fired at 900°C

x	y	z1	z2	z3	zavg
0.1242	0.1201	-0.0916	-0.091	-0.0909	-0.0911667
0.8763	0.1183	-0.0947	-0.0943	-0.0943	-0.0944333
1.623	0.1146	-0.0963	-0.1138	-0.1141	-0.1080667
2.3731	0.1214	-0.096	-0.0957	-0.0961	-0.0959333
3.1261	0.1124	-0.0922	-0.0924	-0.0923	-0.0923
0.1293	0.8692	-0.0952	-0.095	-0.0947	-0.0949667
0.8744	0.8724	-0.1001	-0.1	-0.0998	-0.0999667
1.6264	0.8725	-0.1012	-0.1012	-0.101	-0.1011333
2.3756	0.8723	-0.0999	-0.1002	-0.1	-0.1000333
3.1296	0.8714	-0.0945	-0.0944	-0.0943	-0.0944
0.1301	1.6195	-0.094	-0.0942	-0.0943	-0.0941667
0.8785	1.6222	-0.0995	-0.0997	-0.0997	-0.0996333
1.6274	1.6199	-0.101	-0.1013	-0.1014	-0.1012333
2.3774	1.62	-0.0986	-0.099	-0.0987	-0.0987667
3.1266	1.6217	-0.0936	-0.0935	-0.0942	-0.0937667
0.1333	2.3706	-0.0921	-0.0919	-0.092	-0.092
0.8803	2.3676	-0.0956	-0.0971	-0.0967	-0.0964667
1.6273	2.3709	-0.0987	-0.099	-0.0989	-0.0988667
2.3814	2.369	-0.0979	-0.0979	-0.0979	-0.0979
3.1313	2.3708	-0.0924	-0.0926	-0.0926	-0.0925333
0.1316	3.1182	-0.0921	-0.0925	-0.0924	-0.0923333
0.8834	3.1213	-0.0954	-0.0959	-0.0957	-0.0956667
1.632	3.1164	-0.096	-0.096	-0.0957	-0.0959
2.3819	3.1201	-0.0968	-0.0972	-0.0972	-0.0970667
3.1314	3.1164	-0.0902	-0.0906	-0.091	-0.0906

TRIS co-dispersion plate #3, left side of powder bed, fired at 900°C

x	y	z1	z2	z3	zavg
0.1269	0.1204	-0.09	-0.0896	-0.0898	-0.0898
0.8769	0.118	-0.0923	-0.0921	-0.0919	-0.0921
1.6237	0.1144	-0.0938	-0.0932	-0.0931	-0.0933667
2.3735	0.1207	-0.0928	-0.0924	-0.0923	-0.0925
3.1268	0.1125	-0.0893	-0.0893	-0.0891	-0.0892333
0.1298	0.8693	-0.0917	-0.0915	-0.0913	-0.0915
0.8746	0.87	-0.0974	-0.0966	-0.0964	-0.0968
1.6271	0.871	-0.0985	-0.0982	-0.0981	-0.0982667
2.3763	0.8702	-0.0977	-0.0976	-0.0975	-0.0976
3.1301	0.8704	-0.0932	-0.093	-0.0929	-0.0930333
0.1304	1.6195	-0.0909	-0.0906	-0.0905	-0.0906667
0.879	1.6201	-0.0963	-0.0963	-0.0962	-0.0962667
1.6278	1.6192	-0.0986	-0.0991	-0.099	-0.0989
2.3782	1.6182	-0.0965	-0.0975	-0.0975	-0.0971667
3.127	1.6188	-0.0922	-0.0926	-0.0929	-0.0925667
0.1339	2.3705	-0.0899	-0.0899	-0.0898	-0.0898667
0.8804	2.3673	-0.096	-0.096	-0.0958	-0.0959333
1.6277	2.3683	-0.0972	-0.0968	-0.0968	-0.0969333
2.3819	2.3675	-0.096	-0.096	-0.0958	-0.0959333
3.1316	2.3682	-0.0928	-0.0931	-0.0929	-0.0929333
0.1318	3.1185	-0.09	-0.0906	-0.0906	-0.0904
0.884	3.1183	-0.0961	-0.0959	-0.0958	-0.0959333

1.6324	3.1162	-0.0948	-0.0946	-0.0947	-0.0947
2.3824	3.1182	-0.0954	-0.0953	-0.0951	-0.0952667
3.1322	3.1169	-0.0923	-0.0929	-0.0934	-0.0928667

Stock silica plate #1, right side of powder bed, fired at 900°C, measured on the top surface

z1	z2	z3	zavg	stdev	x	y
0.0222	0.0226	0.0224	0.0224	0.0002	0.1875	0.125
0.0194	0.0195	0.0195	0.0195	0.0001	0.9375	0.125
0.0192	0.019	0.019	0.0191	0.0001	1.6875	0.125
0.0192	0.0192	0.0192	0.0192	0	2.4375	0.125
0.021	0.0209	0.021	0.021	0.0001	3.0625	0.125
0.0214	0.0211	0.0211	0.0212	0.0002	0.1875	0.875
0.017	0.0172	0.0168	0.017	0.0002	0.9375	0.875
0.0163	0.0158	0.0158	0.016	0.0003	1.6875	0.875
0.0174	0.0171	0.017	0.0172	0.0002	2.4375	0.875
0.0201	0.0201	0.0198	0.02	0.0002	3.0625	0.875
0.0201	0.02	0.0198	0.02	0.0002	0.1875	1.625
0.0158	0.0158	0.0158	0.0158	0	0.9375	1.625
0.0156	0.0155	0.0155	0.0155	0.0001	1.6875	1.625
0.0162	0.0161	0.016	0.0161	0.0001	2.4375	1.625
0.0192	0.019	0.0188	0.019	0.0002	3.0625	1.625
0.0199	0.0193	0.0192	0.0195	0.0004	0.1875	2.375
0.0165	0.0161	0.0161	0.0162	0.0002	0.9375	2.375
0.0169	0.0166	0.0166	0.0167	0.0002	1.6875	2.375
0.0166	0.0163	0.0163	0.0164	0.0002	2.4375	2.375
0.0194	0.0192	0.019	0.0192	0.0002	3.0625	2.375
0.024	0.0238	0.0238	0.0239	0.0001	0.1875	3.125
0.0212	0.0208	0.0208	0.0209	0.0002	0.9375	3.125
0.02	0.0194	0.0193	0.0196	0.0004	1.6875	3.125
0.0212	0.0204	0.0207	0.0208	0.0004	2.4375	3.125
0.0228	0.0227	0.0226	0.0227	0.0001	3.0625	3.125

Stock silica plate #2, middle of powder bed, fired at 900°C, measured on the top surface

x	y	z1	z2	z3	zavg
0.1859	0.1266	0.0224	0.0225	0.0225	0.02246667
0.9377	0.1275	0.0183	0.0184	0.0186	0.01843333
1.6878	0.1279	0.0172	0.0173	0.0178	0.01743333
2.4377	0.1282	0.0185	0.0188	0.0188	0.0187
3.0622	0.1275	0.0215	0.0218	0.0218	0.0217
0.1873	0.8764	0.0205	0.0205	0.0205	0.0205
0.9379	0.8774	0.0159	0.016	0.016	0.01596667
1.6876	0.8775	0.0154	0.0154	0.0155	0.01543333
2.4378	0.8777	0.0158	0.0159	0.016	0.0159
3.0622	0.8775	0.0196	0.0195	0.0196	0.01956667
0.1873	1.6264	0.0197	0.0198	0.0198	0.01976667
0.9375	1.6271	0.0159	0.016	0.0162	0.01603333
1.6876	1.6276	0.0149	0.0151	0.0152	0.01506667
2.4377	1.6277	0.0154	0.015	0.0151	0.01516667
3.0621	1.6275	0.0189	0.019	0.0191	0.019
0.1873	2.3762	0.0202	0.02	0.0201	0.0201

0.9377	2.3774	0.0159	0.016	0.0161	0.016
1.6876	2.3774	0.0152	0.0152	0.0152	0.0152
2.4374	2.3779	0.0154	0.0152	0.0152	0.01526667
3.0624	2.3773	0.0186	0.0188	0.0189	0.01876667
0.1874	3.1262	0.0256	0.0256	0.0255	0.02556667
0.9377	3.1275	0.0213	0.0206	0.021	0.02096667
1.6877	3.1278	0.0195	0.0198	0.0188	0.01936667
2.4378	3.1272	0.02	0.0202	0.0202	0.02013333
3.0624	3.128	0.0234	0.0234	0.0232	0.02333333

Stock silica plate #3, left side of powder bed, fired at 900°C, measured on the top surface

x	y	z1	z2	z3	zavg
0.186	0.1258	0.0218	0.0224	0.0223	0.02216667
0.938	0.1278	0.0196	0.02	0.02	0.01986667
1.6874	0.1273	0.0192	0.0197	0.0197	0.01953333
2.438	0.1273	0.019	0.0194	0.0194	0.01926667
3.0626	0.1277	0.0227	0.0225	0.0227	0.02263333
0.1876	0.875	0.02	0.0197	0.0197	0.0198
0.9379	0.8771	0.0169	0.0168	0.0167	0.0168
1.6877	0.8776	0.0155	0.0159	0.016	0.0158
2.4378	0.8774	0.0174	0.0176	0.0177	0.01756667
3.0627	0.8775	0.0204	0.0209	0.0209	0.02073333
0.1873	1.6256	0.0192	0.0185	0.0184	0.0187
0.9377	1.6269	0.0156	0.0156	0.0157	0.01563333
1.6878	1.6273	0.0147	0.0146	0.0147	0.01466667
2.4381	1.6273	0.0161	0.0156	0.0155	0.01573333
3.0625	1.6273	0.0189	0.0192	0.0192	0.0191
0.1874	2.3754	0.0201	0.0197	0.0187	0.0195
0.9379	2.3769	0.0163	0.0159	0.0159	0.01603333
1.6877	2.3776	0.0162	0.0164	0.0166	0.0164
2.4379	2.3779	0.0164	0.0163	0.016	0.01623333
3.0623	2.3774	0.0195	0.0199	0.0199	0.01976667
0.1879	3.1252	0.0235	0.0232	0.023	0.02323333
0.938	3.1273	0.0218	0.0214	0.0207	0.0213
1.6877	3.1274	0.0197	0.0189	0.0185	0.01903333
2.4378	3.127	0.0215	0.0217	0.0216	0.0216
3.0625	3.1278	0.0248	0.0248	0.0246	0.02473333